Study on the application and mechanism of enhanced methane recovery from hydrate

Shi, Meng

Publication date:
2021

Document Version
Publisher's PDF, also known as Version of record

Study on the application and mechanism of enhanced methane recovery from hydrate

Meng Shi

Ph.D Thesis

2021

DTU Chemical Engineering
Department of Chemical and Biochemical Engineering

Study on the application and mechanism of enhanced methane recovery from hydrate

Meng Shi

Center for Energy Resources Engineering

Department of Chemical and Biochemical Engineering

Technical University of Denmark

Ph.D. thesis

February 2021

Supervisors Nicolas von Solms (DTU Chemical Engineering)

John M. Woodley (DTU Chemical Engineering)

DTU Chemical Engineering
Department of Chemical and Biochemical Engineering

Technical University of Denmark

Anker Engelundsvej 1

Building 101A

DK-2800, Kgs. Lyngby

Denmark

CVR-nr.30060946

Phone:(+45) 45 25 25 25

Email:dtu@dtu.dk

www.dtu.dk

Preface and Acknowledgments

This dissertation results from three years of research, from 2018 to 2021, conducted in the Center for Energy Resources Engineering (CERE) research center at the Department of Chemical & Biochemical Engineering, Technical University of Denmark (DTU), funded by DTU and China Scholarship Council. The PhD. project was supervised by

Main supervisor: Professor Nicolas von Solms (CERE, DTU)

Co-supervisor: Professor John M. Woodley (Process and Systems Engineering Centre, DTU)

I first became interested in the gas hydrate area while working on my master's project at South China University of Technology. Subsequently, I received a three-year exclusive learning experience in the Center for Energy Resources Engineering DTU. Nearing my Ph.D., I would like to extend my sincerest gratitude and appreciation to the people who gave me support and assistance throughout my Ph.D. study. My first acknowledgment goes to my supervisors Nicolas von Solms and John Woodley, for their continuous endorsement and guidance during this period. I have learned a lot from their abundant and valuable experiences and knowledge. Special thanks go to Prof. Nicolas von Solms for always offering me continuous support and encouragement on my work. Thanks for allowing me to investigate the ideas of my freedom, even though some of them were not mature and failed in the end.

Nevertheless, the process of this exploration gave me abundant experience and lessons for future work and life. I admire his enthusiasm and energy in the research and his kind, easygoing personality. It has been a fantastic experience to work under his guidance.

In addition to my supervisors, I am grateful to our lab technicians (Tran Thuong Dang, Duc Thuong Vu, Povl Valdemar Andersen, and Zacarias Tecle) for my experimental setups, troubleshooting, as well as departmental administration staff (Patricia Wagner, Anne Louise Biede, and Christian Ove Carlsson) for their full supports and a great help. Finally, I appreciate all the zealous and excellent CERE employees for their invaluable assistance.

I would like to thank my parents for their love and understanding throughout my life, without which I would not have made it this far in life. I will never be able to repay them for their continuous financial and spiritual support.

This thesis is submitted as partial fulfillment of the Doctorate (Ph.D.) degree requirements at Technical University of Denmark.

February 2021

Meng Shi

Abstract

Energy is a key element for human survival and development. The current dominant primary energy sources worldwide are natural gas, oil, and coal, the supply of which is dwindling and causing environmental problems. Highly efficient and clean energy sources are of great importance for sustainable development. Natural gas hydrates, the main component of which is methane, have received growing attention in the global energy system due to their abundance in nature and CO_2 neutrality, if properly extracted with CO_2 injection, compared to conventional fossil fuels. Although discovered in 1883, extensive research was only initiated during the last 50 years by scientists from the micro to macro scales. Major gas hydrates exploitation methods include chemical injection, thermal stimulation, pressure reduction, and CO_2 replacement. Each method has advantages and disadvantages, but the depressurization and CO_2 replacement methods show relative superiority compared to the others. The combination of depressurization and CO_2 replacement shows a higher recovery rate and efficiency. At the present research stage, the replacement gas employed in the laboratory studies varies from pure CO_2 (either in liquid or gaseous form) to simulated flue gas (a CO_2 and N_2 gas mixture). Limited studies on hydrate production with the injection of air, which is cheap and abundant, have been conducted. Many factors of the swapping recovery process have been considered, but the hydrate decomposition mechanism behind these factors is complex and challenging to elucidate.

To investigate the effects of certain factors on the depressurization production process, three groups of spherical methane hydrate samples with variant diameters of 11mm, 17mm, and 22mm were prepared to simulate hydrate particles macroscopically. Each sample group has approximately the same overall volume of 8980 mm^3. Hydrate decomposition starts with an initial pressure of 6.1 to 6.4 MPa and ends at a final constant pressure between 1.6 MPa and 2.4 MPa. The results show that the effect of depressurization is significant on the methane recovery ratio, while the effect of the surface-area-to-mass ratio is less significant. During the hydrate decomposition process, the methane production rate increases with increasing operating pressure and surface-area-to-mass ratio. The methane decomposition is jointly governed by two processes: 1) the dissociation process, in which methane molecules leave the hydrate cage, which is controlled by the pressure difference between the equilibrium pressure and the system pressure; and 2) the gas diffusion process, in which

methane molecules travel from the hydrate surface through the ice layer. The experiments show that the gas production process can be divided into three main periods: excess gas release, fast hydrate production, and slow hydrate production. The production rate at low operation pressure is rapid due to the initially prevailing pressure driving force control, whereas gas diffusion with ice coverage on various pellet sizes becomes more dominant at higher operating pressure. In addition, the experimental results indicate that hydrate decomposition is time-dependent. Initial ice nucleation and conglomeration play an important role in the hydrate decomposition rate.

Based on the depressurization investigation, a series of experiments were conducted aiming to obtain a new method for improved recovery by the combination of the depressurization and gas replacement methods, in which air/CO_2-enriched air was injected into an artificial multilayer hydrate sediment at pressures ranging from 8.5 to 18.7 MPa. The recovery efficiency was investigated using a method combining three-stage depressurization assisted with CO_2-enriched air injection. The initial production pressure was found to have a positive effect on the recovery of methane via injecting of air, with an opposite influence via injecting CO_2-enriched air. Compared with injecting air, injecting CO_2-enriched air promotes the performance of gas hydrate production with up to a 74.4 % recovery ratio. A novel multilayer hydrate cap mechanism is therefore proposed to describe the improved efficiency during the replacement-depressurization process for the first time. The multilayer hydrate cap and its composition are largely dependent on the initial condition of injected gas, thereby causing limited recovery efficiency. The results obtained from this study are beneficial for the future optimization of operating conditions to maximize efficiency and develop planning for natural gas hydrate resources.

To further explain the experimental results and study the mechanism of methane hydrate decomposition behavior, a molecular dynamics simulation method was performed under one-step and multi-step depressurization processes with NVT ensemble. The influence of temperature was also examined. The effect of hydrate structural properties on the decomposition process was theoretically investigated, including configuration, potential energy, the radial distribution function (RDF), the F_4 order parameter, mean square displacement (MSD), and the diffusion coefficient. MSDs and RDFs showed similar behaviors in line with increasing temperature, which can reduce hydrate stability. A sudden

decrease in potential energy was observed for one-step depressurization during simulation times ranging from 1.5 ns to 3 ns. The F_4 order parameter confirmed the tendency for the regeneration of hydrates during this period. The diffusion coefficient can also be improved by an increase in temperature. Multi-step depressurization compensates for energy loss by including the released methane molecules dissolved in the liquid water phase, thus breaking the tendency for hydrate reformation during decomposition. The application of multi-step depressurization in molecular simulation can provide significant insights for on-field hydrate resource exploitation and help to understand the mechanisms behind hydrate production at the molecular scale.

Dansk resumé

Energi er altid et centralt element for menneskelig overlevelse og udvikling. De nuværende dominerende primære energikilder på verdensplan er naturgas, olie og kul, hvis forsyning svinder og forårsager miljøproblemer. Meget effektive og rene energikilder er af stor betydning for en bæredygtig udvikling. Naturgashydrater, hvis hovedkomponent er metan, har fået voksende opmærksomhed i det globale energisystem på grund af deres overflod i naturen og CO_2 -neutralitet, hvis de udvindes korrekt med CO_2 -injektion, sammenlignet med konventionelle fossile brændstoffer. Selvom det blev opdaget i 1883, blev omfattende forskning kun igangsat i løbet af de sidste 50 år af forskere fra mikro- til makroskalaerne. Store udnyttelsesmetoder for gashydrater omfatter kemisk injektion, termisk stimulering, trykreduktion og CO_2 -udskiftning. Hver metode har både fordele og ulemper, og trykfalds- og CO_2 -udskiftningsmetoderne viser relativ overlegenhed i forhold til de andre. Kombinationen af trykaflastning og CO_2 -udskiftning viser en højere genopretningshastighed og effektivitet. På det nuværende forskningsstadium varierer den erstatningsgas, der anvendes i laboratorieundersøgelserne, fra ren CO_2 (enten i flydende eller gasform) til simuleret røggas (en CO_2- og N_2 -gasblanding). Begrænsede undersøgelser af hydratproduktion med indsprøjtning af luft, som er billig og rigelig i naturen, er blevet gennemført. Mange faktorer ved udskiftningsprocessen er blevet overvejet, men hydratnedbrydningsmekanismen bag disse faktorer er kompleks og udfordrende at belyse.

For at undersøge visse faktorers virkninger på trykaflastningsproduktionsprocessen blev tre grupper af sfæriske metanhydratprøver med variantdiametre på 11 mm, 18 mm og 22 mm forberedt til at simulere hydratpartikler makroskopisk. Hver prøvegruppe har omtrent det samme samlede volumen på 8980 mm^3. Hydratnedbrydning starter med et indledende tryk på 6.1 til 6.4 MPa og slutter ved et endeligt konstant tryk mellem 1.6 MPa og 2.4 MPa. Resultaterne viser, at effekten af trykaflastning er signifikant på metanindvindingsforholdet, mens effekten af forholdet mellem overfladeareal og masse er mindre signifikant. Under hydratnedbrydningsprocessen øges metanproduktionshastigheden med stigende driftstryk og overflade-areal-til-masseforhold. Metannedbrydningen styres i fællesskab af to processer: 1) dissociationsprocessen, hvor metanmolekyler forlader hydratburet, som styres af trykforskellen mellem ligevægtstrykket og systemtrykket; og 2) gasdiffusionsprocessen, hvor methanmolekyler bevæger sig fra hydratoverfladen gennem islaget. Eksperimenterne

viser, at gasproduktionsprocessen kan opdeles i tre hovedperioder: overskydende gasudslip, hurtig hydratproduktion og langsom hydratproduktion. Produktionshastigheden ved lavt driftstryk er hurtig på grund af den oprindeligt gældende trykdrevskontrol, hvorimod gasdiffusion med isdækning på forskellige pelletstørrelser bliver mere dominerende ved højere driftstryk. Desuden indikerer de eksperimentelle resultater, at hydratnedbrydning er tidsafhængig. Indledende iskerning og konglomeration spiller en vigtig rolle i hydratnedbrydningshastigheden.

Baseret på afprøvningsundersøgelsen blev der udført en række forsøg med det formål at opnå en ny metode til forbedret genvinding ved kombinationen af tryk- og gasudskiftningsmetoderne, hvor luft/CO_2-beriget luft blev injiceret i et kunstigt flerlagshydrat-sediment ved tryk fra 8,5 til 18,7 MPa. Genopretningseffektiviteten blev undersøgt ved hjælp af en metode, der kombinerer tretrins trykaflastning assisteret med CO_2-beriget luftindsprøjtning. Det oprindelige produktionstryk viste sig at have en positiv effekt på genvindingen af metan via indsprøjtning af luft, med en modsat påvirkning via indsprøjtning af CO_2-beriget luft. Sammenlignet med indsprøjtning af luft fremmer indsprøjtning af CO_2-beriget luft udførelsen af gashydratproduktion med op til 74,4 % genvindingsforhold. En ny flerlagshydratdækselmekanisme foreslås derfor for første gang at beskrive den forbedrede effektivitet under udskiftning-trykfaldsprocessen. Flerlagshydratdækslet og dets sammensætning er i høj grad afhængige af den indledende tilstand af injiceret gas og forårsager derved begrænset genvindingseffektivitet. Resultaterne fra denne undersøgelse er gavnlige for den fremtidige optimering af driftsbetingelser for at maksimere effektiviteten og udvikle planlægning af naturgashydratressourcer.

For yderligere at forklare de eksperimentelle resultater og studere mekanismen for metanhydratnedbrydningsadfærd blev molekylærdynamiksimuleringsmetoden udført under et-trins og flertrins depressuriseringsprocesser med NVT-ensemble ved hjælp af molekylære dynamiksimuleringer. Temperaturens indflydelse blev også undersøgt. Effekten af hydratstrukturelle egenskaber på nedbrydningsprocessen blev teoretisk undersøgt, herunder konfiguration, potentiel energi, den radiale fordelingsfunktion (RDF), F_4 -ordensparameteren, middelværdi -forskydning (MSD) og diffusionskoefficienten. MSD'er og RDF'er viste lignende adfærd i takt med stigende temperatur, hvilket kan reducere hydratstabilitet. Et pludseligt fald i potentiel energi blev observeret for tryksætning i et trin

under simuleringstider fra 1,5 ns til 3 ns. F_4 -ordensparameteren bekræftede tendensen til regenerering af hydrater i denne periode. Diffusionskoefficienten kan også forbedres ved en temperaturstigning. Multi-trins trykaflastning kompenserer for energitab ved at inkludere de frigivne methanmolekyler opløst i flydende vandfasen og dermed bryde tendensen til hydratreformation under nedbrydning. Anvendelsen af flertrins trykaflastning i molekylær simulering kan give væsentlig indsigt i udnyttelse af hydratressourcer på marken og hjælpe med at forstå mekanismerne bag hydratproduktion på molekylær skala.

Contents

List of Figures

List of Tables

List of Abbreviations

NGHs: Natural gas hydrates;

sI: Structure I;

sII: Structure II;

sH: Structure H;

SNG: Solidified Natural Gas;

THF: Tetrahydrofuran;

CP: Cyclopentane;

CH: Cyclohexane;

NMR: Nuclear Magnetic Resonance;

MD: Molecular Dynamics;

SPC/E: The Extended Simple Point Charge;

LJ: Lennard-Jones;

TraPPE: Transferable Potentials for Phase Equilibria;

SPC: Simple point charge;

g(r):The radial distribution function;

NVT: The canonical ensemble;

NPT: The isothermal-isobaric ensemble;

NVE: The microcanonical ensemble;

OPLS-AA: Optimized Potentials for Liquid Simulations−all atoms;

PME: The Particle Mesh Ewald technique;

TIP3P/4P/5P: Transferable Intermolecular Potential 3/4/5−sit water models;

D: The self-diffusion coefficient;

MSD: The mean square displacement;

Nomenclature

1 Introduction

Natural gas hydrate (NGH) reservoirs are distributed worldwide and contain a significant amount of natural gas. Research and development projects have aimed at efficient and economic recovery of CH_4 from hydrate reservoirs in recent decades. Conventional technologies include depressurization, thermal stimulation, chemical injection, and CO_2 injection, each of which has unique advantages for specific reservoirs.

Many factors that influence the CH_4 recovery process have been considered. A common process used in all production technologies is hydrate decomposition. At the present stage, the theories behind hydrate decomposition are complex and some key aspects need to be elucidated and systematically studied. One of the challenging factors in investigating hydrate decomposition kinetics is quantifying the decomposition rate, which is of fundamental importance to advancing our understandings of gas hydrate production. The conventional macroscopic measurement method used to investigate hydrates can be inaccurate and difficult if the hydrate sample species are small and bound water or ice is present, as they make kinetics modeling a complex task. More fundamental studies are thus needed to measure the time-dependence of hydrate decomposition. Applying kinetic models to predict laboratory experimental results is still problematic

The replacement gas used in the laboratory study varied from pure CO_2 (either in liquid or gaseous form) [1,2], to simulated flue gas (CO_2 and N_2 gas mixture) [3]. In 2014, Kang et al. [4] proposed that NGH can be extracted from permeable subsea sediments using air which, because of its easy accessibility and abundance, has the greatest advantages for use in actual NGH exploitation, a process that is accompanied by the release of methane (through the decomposition of NGH) as well as CH_4-air replacement. The potential for using air as a component in producing methane from hydrate is thus attractive.

Although there has been abundant experimental and theoretical research on hydrate dissociation and exploitation, there are still many details within the dissociation process that need to be further explored through experimental and simulation work. Novel methods are required to enhance the performance of conventional production processes. Moreover, the hydrate decomposition mechanism needs to be fully understood for future industrial applications.

1.1. Project objectives

This Ph.D. project aims at improving current understandings of the methane extraction process from hydrates, which is a complex combination of molecular dissociation and gas diffusion. Specifically, this work focuses on the effects of depressurization, CO_2 injection, and their combination in hydrate production during multi-step depressurization:

- Understanding the influence of particle size on the performance of hydrate production by depressurization process and its kinetics.
- Enhancement of methane recovery and CO_2 storage by the combination of multi-stage depressurization assisted with CO_2-enriched air injection.
- Qualitative understanding of the mechanisms of depressurization on hydrate decomposition by molecular simulation.

1.2. Structure of the thesis

Including the introduction, this thesis is divided into six chapters.

Chapter 1: Introduction

Introduction of project objectives and structure of this thesis.

Chapter 2: Background

This chapter provides an overview of the current research on methane hydrate exploitation from theoretical, experimental, and simulation aspects. Research from laboratory and molecular simulation on hydrate decomposition is presented. Current

techniques for methane hydrate decomposition driven by depressurization and CO_2 injection are introduced.

Chapter 3: Macroscopic study on the production of hydrate spheres below the freezing point of water

This chapter describes the experimental study of the influence of particle size on hydrate production performance by system. Experimental setups and procedures for hydrate sample formation and hydrate decomposition by depressurization are described, and experimental results on hydrate production rates with various hydrate sphere diameters are presented. An ice layer shielding mechanism for hydrate decomposition under depressurization conditions is analyzed based on experimental findings, and a kinetic hydrate decomposition model is proposed.

Chapter 4: An experimental study on improved production performance by depressurization combined with CO_2-enriched air injection

This chapter summarizes the experimental results of the influence of injecting air and CO_2-enriched air with a three-stage depressurization process on methane hydrate production. The details of the experimental setup and procedure for hydrate formation and recovery are reported. Results on methane recovery ratio variation over time during the depressurization process are presented for the above-mentioned operation conditions. A novel multilayer hydrate cap attenuation mechanism for explaining the production behavior via injected gas combined with depressurization is proposed.

Chapter 5: A molecular simulation of the methane hydrate decomposition multi-step depressurization

To further explain the enhanced hydrate production performance by the stepwise depressurization process demonstrated in Chapter 4, this chapter presents the molecular simulation of the methane hydrate decomposition process by system depressurization using molecular dynamics simulations. In the model, system depressurization is achieved by a vacuum removal approach. For both one-step depressurization and multi-step depressurization processes, the variation of hydrate configuration, potential energy, radial

distribution function (RDF), F_4 order parameter, mean square displacement (MSD), and the diffusion coefficient are examined.

Chapter 6: Concluding remarks and future work

In this chapter, a summary of the main conclusions from this Ph.D. thesis and suggestions for future work is presented.

2 Background

This chapter provides an overview of the fundamental theory of clathrate gas hydrate, gas hydrate applications, the status of current gas hydrate investigations, and gas hydrate exploitation methods. With the dramatic growth of the global economy, energy consumption remains dynamic and continues to increase in most countries. Energy supply and demand are still key economic factors, and human thirst for new energy sources is increasing. Being aware of the basic characteristics of energy sources, as well as the fundamentals of energy sources, is key to their efficient use.

Large amounts of NGH resources exist in permafrost and offshore in continental margin zones. It is estimated that the global reserves of natural gas hydrates are in the range of 14 to 34, 000 trillion cubic feet for permafrost areas, and from 3,100 to 7,600,000 trillion cubic meters for oceanic sediments [1,2]. The natural gas stored in hydrate form is equivalent to at least half of the total offshore oil and gas resources. There is, therefore, great potential to exploit this resource economically and efficiently. However, gas hydrates have limited potential for exploitation partly due to a lack of understanding of their basic characteristics.

2.1. Background of clathrate hydrate

2.1.1. Clathrate hydrate development

Gas hydrates (GHs) are non-stoichiometric crystalline compounds formed by guest molecules and hydrogen-bonded water molecules over a wide range of pressures and temperatures [3]. These guest molecules can include lower hydrocarbons, Freons, and some organic solvents, which interact with host water molecules via Van der Waals forces. GHs resemble ice and NGHs can burn. thus they are sometimes called "flammable ice" [4]. The development of GHs extends back to 1810 when chlorine was identified as an element

by Humphry Davy [5], a chemist from Cornwall, England. [6] He found that mixing chlorine and water under low temperatures can result in solid crystals. In the early 1820s, the first documented discovery of chlorine clathrate hydrate was issued by John Faraday [7], after which other types of clathrates were discovered [8]. In the mid-1930s, GHs attracted practical interest when they were found to block gas supply and cause emergencies in pipelines operating in Alaska [9]. Since then, research has aimed at prevent GH formation in oil and gas pipelines. The use of chemical additives (such as methanol, monoethylene glycol, and tetrapentylammonium bromide) is the most common measure to prevent hydrate formation during oil and gas transportation. This resulted in the explosive growth of the number of publications concerning kinetic GH inhibitors, thermodynamic inhibitors, and antiagglomerate GH inhibitors [10–12]. Kinetic GH inhibitors are used at low dosage (less than 1 wt%) and are required to be economically and environmentally friendly, while thermodynamic inhibitors are needed at high concentration (up to 50 wt% in the aqueous phase) for preventing the combination of free water molecules and gas. Antiagglomerate GH inhibitors prevent the agglomeration of small hydrate particles from forming bigger clusters. Thus, GH particles remain dispersed in the hydrocarbon phase and this slurry does not plug the pipeline [13]. A combination of antiagglomerates and kinetics inhibitors are also used as hydrate inhibitors.

In the early 1950s, scientific research focused on a theoretical description of clathrates up until 1958, when Van de Waals and Platteeeuw [14] developed a thermodynamic model of GHs based on a model proposed by Barrer and Stuart [15]. This model was subsequently widely applied to the prediction of GH thermodynamic properties. In the 1960s, the existence of GHs in nature was proven in the Messoyakha gas field in western Siberia [16,17]. and geologists and chemists began to study GHs in natural conditions. The development of hydrates transferred from a scientific curiosity to an aspect of energy resource exploration. In 1999, Ripmeester [18] discovered structure H hydrate in seafloor deposits and activities in gas production have expanded since then. There is a wide distribution of NGH reservoirs from the South China Sea, the Indian Ocean, and the Sea of Japan (seafloor on continental slopes, in deep seas and lakes) to the permafrost regions of Siberia, Alaska, and the Mackenzie Delta. Field tests have been carried out in both terrestrial permafrost regions and marine regions. Major production has been conducted in the Alaska North Slope, Mount Elbert [19], the Messoyakha hydrate gas field in western Siberia [20], the Mackenzie Delta,

the QTPP (Qinghai-Tibet plateau permafrost) [19], and the Shenhu [21], and Nankai Trough [13]. Several significant field trials on gas production from hydrate reservoirs and their features are shown in Figure 2.1. As can be seen in the figure, so far, only the Mallik field test used thermal stimulation technology, while most other fields have used the depressurization method. In addition, the volume of production has increased over time, while tests have not lasted more than six days, except for the CO_2–CH_4 tests in Alaska and Shenhu. Long-term production is hindered by the management of sand and water, as well as the low permeability of the deposits. Future field trials will need to evaluate higher production volumes and prolonged continuous production processes to reach a commercial production scale.

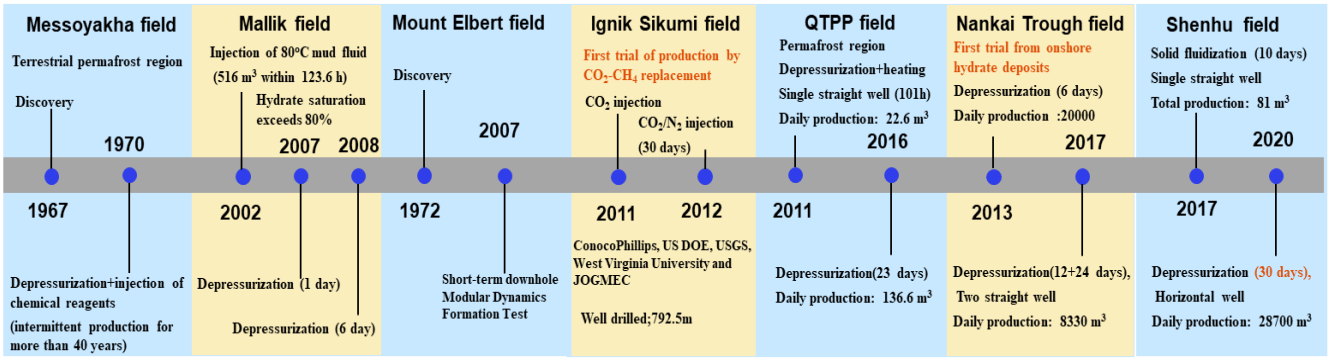

Figure 2.1 Milestones in natural gas hydrate resources exploitation.

As the recovery undisturbed natural methane hydrates is difficult due to their rapid decomposition under ambient conditions, several researchers have attempted to recreate the natural environment of GHs in sedimentary matrices via laboratory experiments, which leads to a set of idealized microstructural models as shown in (a) cementation, (b) encrustation, (c) matrix-supporting, and (d) pore-filling. It is believed that types (a), (b), and (c) NGHs exist in offshore India and Korea, where hydrates commonly appear in fine-grained mud or on the surface of the seafloor. The pore-filling type, as shown in (d), has been found in the Eastern Nankai Trough offshore Japan and the South China Sea [22,23]. The existence of these various types of NGHs presents more challenges to NGH exploration.

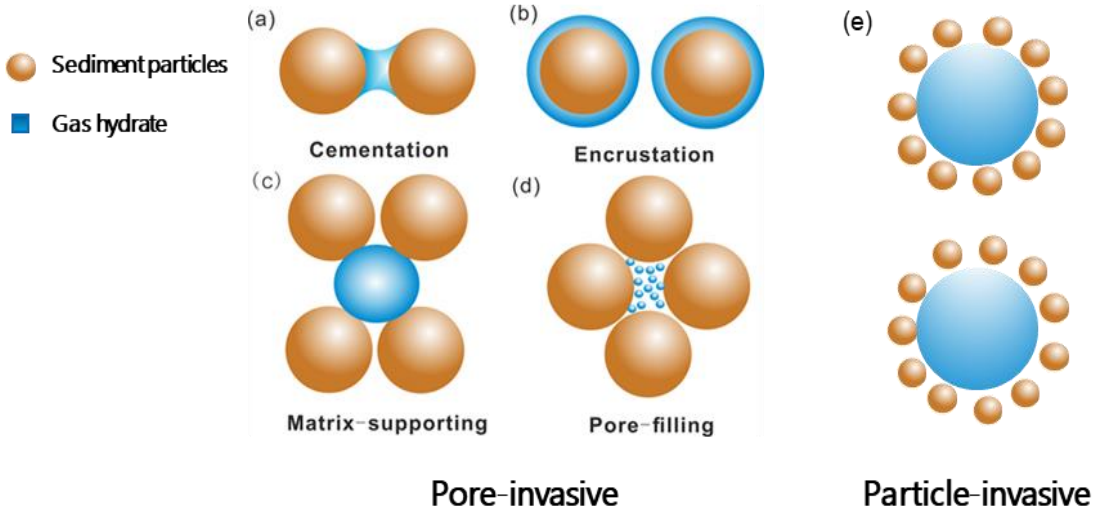

Figure 2.2 Various habits of how hydrate might be located in the sedimentary matrix. Pore-invasive: (a) Cementation, (b) Encrustation, (c) Matrix-supporting, (d) Pore-filling; (e) Particle-invasive

2.1.2. Clathrate hydrate fundamentals

GH consists of water molecules as the host and gas molecules as the guest. The water molecules form polyhedral cavities with different sizes and shapes through hydrogen bonds, where the cavity acts as an effective gas molecule trapper by absorbing guest gas molecules inside. One cage can generally only hold one guest molecule. The interaction between the water molecular cage and the guest gas is subjected to Van der Waals force, thus providing thermodynamic stability to hydrate crystals [24]. Clathrate hydrate cage lattices with different spatial structures are formed by polyhedrons as a basic structure from water molecules connecting the vertex or surface. There are mainly three types of clathrate hydrate structure from the arrangement characteristics of water molecules: structure I (sI), structure II (sII), and structure H (sH). With a few important exceptions, the structural feature common to all clathrate hydrates is the pentagonal dodecahedron 5^{12} of water molecules. It has 12 regular pentagonal faces, 20 vertices, and 30 edges. As a unit of water structure, each vertex is the site of an oxygen atom and each edge an O-H···O bond. Both sI and sII hydrates have cubic crystal structures, while sH hydrate has a hexagonal crystal structure [25]. All these hydrate structures are composed of two or more types of water cages packed within the crystal lattice. The structure of these three types of hydrate is shown in Figure 2.3.

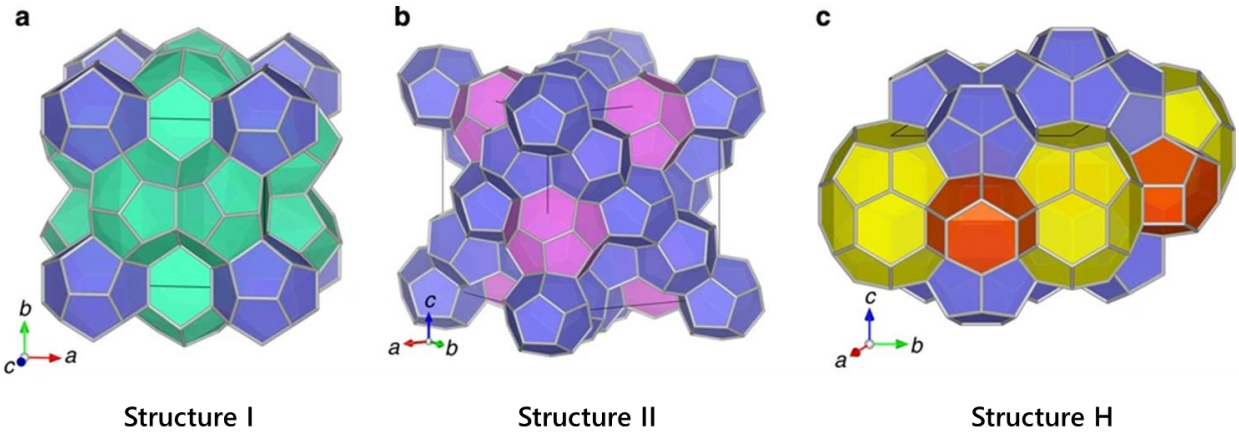

Figure 2.3 Simple schematic of common unit crystal structures of the clathrate hydrates, (a) structure I (b) structure II and (c) structure H [26].

2.1.3. Application of clathrate hydrate

Although hydrate formation in the petroleum and gas industry has negative implications, it can also be beneficial. In recent years, there have been numerous examples of clathrate hydrates being used in applications such as energy storage, water desalination/treatment, gas separation from flue gas streams, and the concentration of dilute solutions, water desalination/treatment, gas separation from flue gas streams, and the concentration of dilute solutions [27,28]. Figure 2.4 illustrates some specific applications of GH technologies. Concerning the applications of GH, numerous studies on clathrate hydrate have been conducted by research groups all over the world, focusing on the investigation of one or a few specific perspectives.

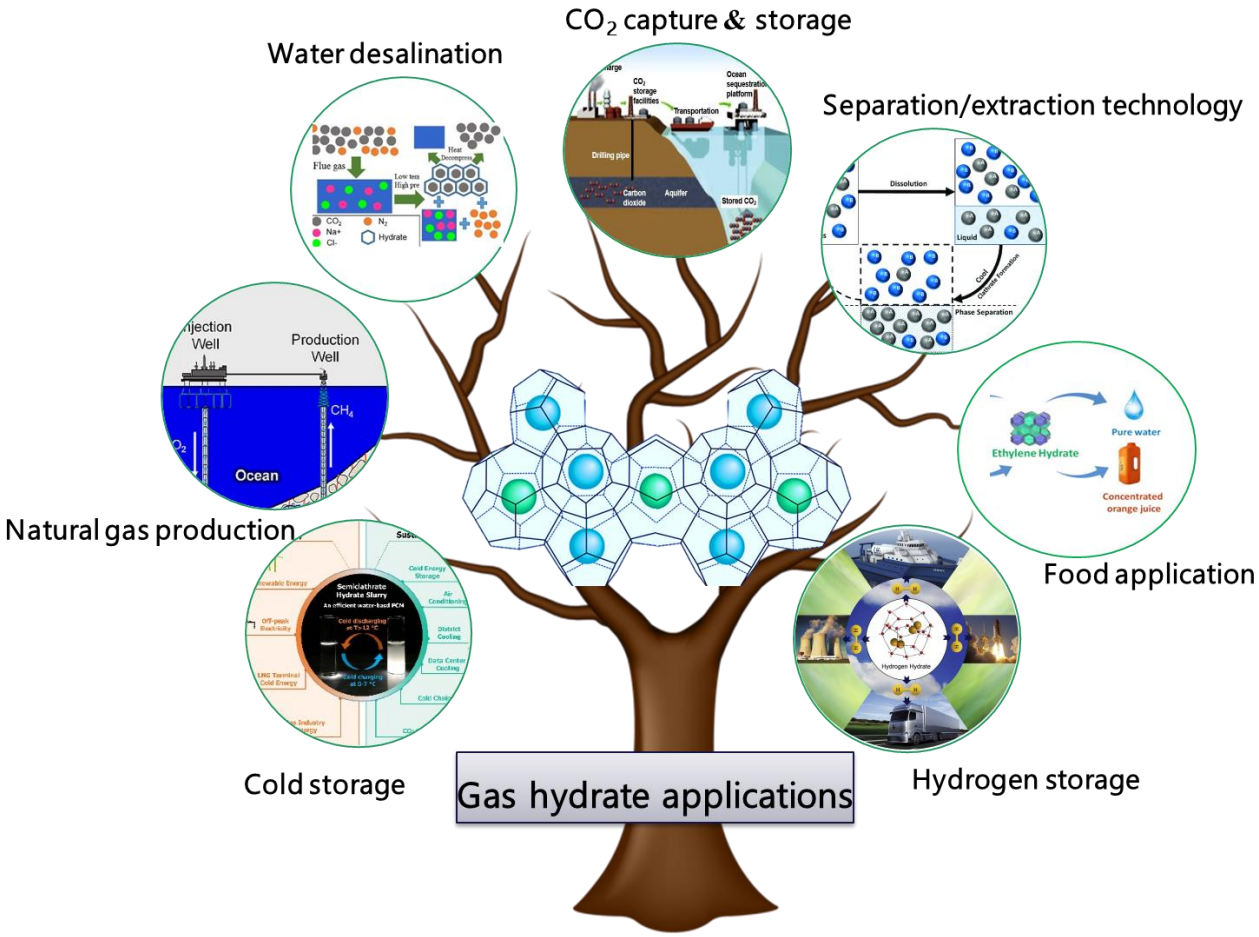

Figure 2.4 Gas hydrate application technologies based on hydrate' physical and thermodynamic characteristics.

2.1.3.1. Hydrate-based energy storage and transportation

GHs can serve as effective energy storage and transportation media due to hydrate properties. The main energy storage technologies are natural gas storage, hydrogen storage, and cold storage. CH_4 hydrate can be used as an effective technology for natural gas storage and transportation. The key advantage of storage CH_4 as a hydrate is high energy density as 150–170 m^3 of gas can be stored in 1 m^3 of solid GHs Besides, this technology is safer and more cost-effective when compared to liquefied natural gas technology [29,30]. The hydrate-based natural gas storage concept was first put forward by Benesh, who synthesized NGH at 283 K and 3.5 MPa. Methane hydrate can be stable above zero degrees °C due to the hydrate self-preservation effect An overview of the process chain of solidified natural gas (SNG) is depicted in Figure 2.5. It consists of four steps: hydrate formation, dewatering, pelletizing, and cooling and depressurizing to reach the required

storage temperatures (248 K and 1 atm). The objectives of studies on NGH storage are to either increase volumetric storage capacity, form rapidly, or store in moderate conditions. Nevertheless, it seems that the slow formation rate of NGH is a major issue hindering industrial applications of hydrate-based gas storage and transportation [31]. [31]. Enhanced methods for rapid hydrate formation have been developed, including water spray, promoter injection, and gas bubble injection. Shuqi et al. [32] systematically evaluated multiple parameters of the gas hydrate formation process in the spraying and ejector-type loop reactors. Based on their results, additive types had the most significant effect on formation performance, followed by the structure of the reactor. Tetrahydrofuran (THF) and cyclopentane (CP) acting as promoters have reported excellent performance for methane hydrate formation. In the past two decades, many researchers also used a variety of surfactants to promote GH formation, among which sodium dodecyl sulfate (SDS) was the most popular. Du et al. [33] reported 5 kmol of methane gas/m^3 of water using 0.2 wt% SDS at 15.0 MPa and 274.2 K. A study by Liu et al. [34] reported methane was taken up by 8.76 kmol/m^3 of water starting at 9.5 MPa and 273 K over 60 minutes by using 0.5 wt% l-leucine amino acid as a kinetic promoter. The literature [35–38] has also reported enhanced kinetics when porous materials are used, but the use of porous materials is less practical as they lower storage capacity per volume and present significant pelletizing challenges. Accordingly, surfactants enhance the formation of hydrates more than porous materials. Certain chemical additives and surfactants may be able to accelerate hydrate formation and increase storage capability. Even though surfactants can be affected by foam generation during hydrate dissociation, based on their effectiveness in promoting hydrate-based technologies, they remain one of the most effective promoters for industrial applications.

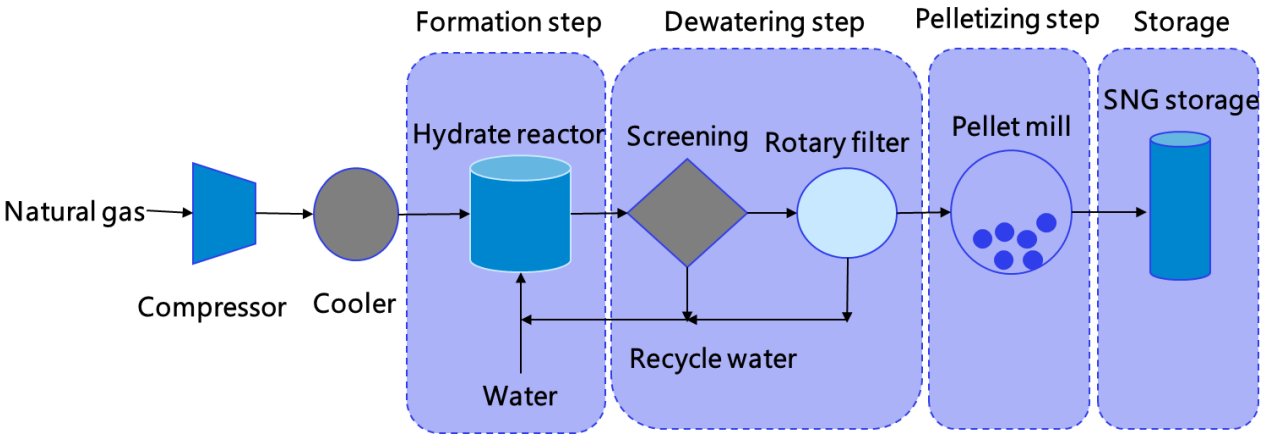

Figure 2.5 Illustration of the process chain of SNG technology.

Hydrogen is regarded as the most promising alternative to fossil fuels due to its being environmentally friendly and having a high energy density. Hydrate-based H_2 storage is an appealing technology after CH_4 storage by hydrate has proven to be reliable. This technique, however, presents a major challenge due to the high pressures required for its operation (200 MPa at 273 K). Despite this, studies have shown that the inclusion of another guest molecule, namely a promoter, can be useful to store hydrogen at a lower pressure, but this reduces the hydrogen storage capacity in hydrates [39]. Another major challenge for this storage method is the relatively slow rate of hydrate formation. Hence, further research has been devoted to modifying the requisite conditions through hydrate-based H_2 storage. According to one study, adding THF into water can reduce the hydrogen hydrate formation pressure from 200 MPa to 100 MPa at ambient temperatures. Furthermore, it was shown that the required pressure to form a binary H_2/CH_4 hydrate can be drastically lowered from 6.5 MPa to 0.3 MPa in the presence of 6 mol% of THF [40]. Semi-clathrate hydrates have also been important in the development of this area. While the addition of promotors, such as THF, can moderate the required conditions for hydrate formation, the required pressure still may be too high for some applications. As an alternative, semi-clathrate hydrates can also be considered [41,42].

2.1.3.2. Gas separation and CO_2 capture

As a result of rapid industrialization and population growth, the energy needs of humanity have continuously grown, and fossil fuels such as coal, oil, and natural gas have met these needs to date [43,44]. A number of comprehensive studies demonstrate the harmful effects

of large amounts of carbon dioxide, carbon monoxide, and hydrogen sulfide is emitted into the atmosphere every year As a result of burning fossil fuels. During the past few decades, concerns have grown regarding the effects of increased concentrations of these gases in the atmosphere and their contribution to global warming. Therefore, separation of these gases from their corresponding gas mixtures has generated great interest and a number of research studies recently. Hydrate-based separation approach have been investigated extensively among research groups [45–49]. Figure 2.6 illustrates a simple schematic of mechanism of hydrated-based gas separation taking CO_2 separation from mixture as an example. Hydrate based gas separation of CO_2 is due to the difference in chemical potential between CO_2 and other gases in the hydrate cages. The CO_2 hydrate are formed from a mixture of other gases, thus CO_2 in enriched when CO_2 hydrate decomposition.

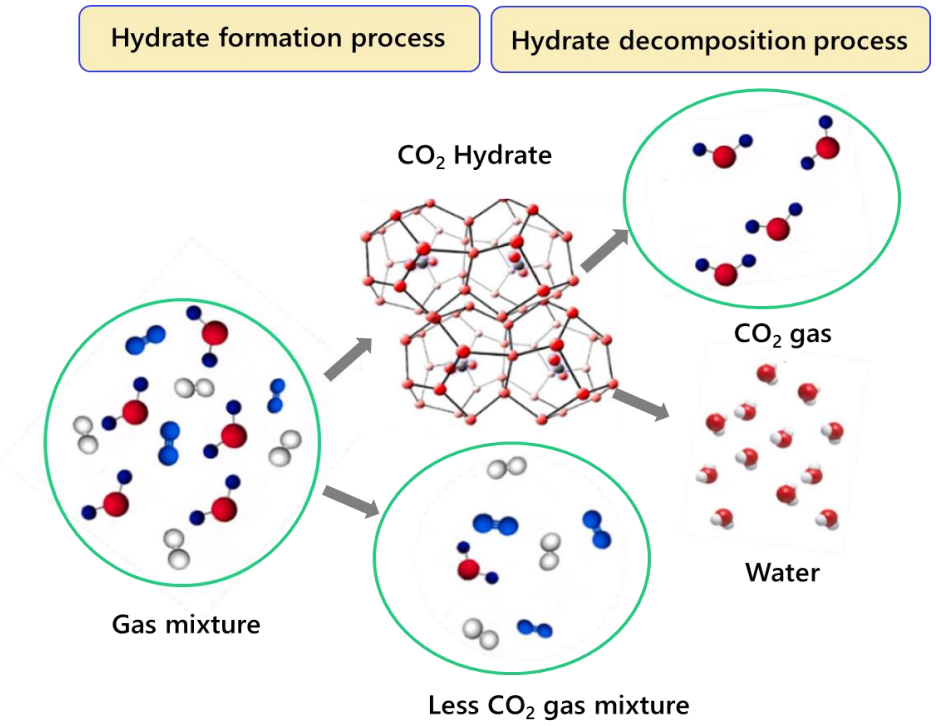

Figure 2.6 Simple schematic of mechanism of hydrated-based gas separation, an example for CO_2 capture.

2.1.3.3. Hydrate-based water treatment

Water treatment can be applied with gas hydrate technology by separating the hydrate cages from bine solution at temperature higher than water freezing temperature [50]. Fresh water is achieved after the hydrates melting and the guest component can be reused. A

number of researchers have been studying hydrate-based water treatment. CP [51], cyclohexane (CH), and CO_2 have been used as guest molecules [52]. However, CP and CH are toxic and highly volatile, they must be removed separately after decomposition of hydrate, whereas the cost of refrigeration and compressing CO_2 are high. In addition, hydrate formation has slower kinetics. It is critical to find hydrate formers that improve hydration kinetics and reduce the energy requirements.

2.2. Recovery of methane from natural gas hydrate

There have been successful efforts to recover methane gas from GH fields both in deep submarine and permafrost regions. In 2002, thermal stimulation was used to produce methane in the permafrost zones of the Canada Arctic off the Mackenzie [53], followed by the successful NGH exploitation by depressurization conducted by the Japan Oil, Gas, and Metals National (JOGMEC) and Natural Resources Canada (NRCan) in 2007 [54]. The landmark concept of CO_2 exchange as a production mechanism was put into practice by Japan Oil, JOGMEC, and ConocoPhilips in 2008 [55]. However, these NGH exploitations only proceeded in the short term. Most of the challenges come from the complex characteristics of the NGH system related to gas decomposition and mass/heat transfer processes that are not fully understood. Therefore, laboratory investigation for economical and efficient NGH recovery from field trials in the long term has been a key goal for researchers.

The most common occurrence of methane hydrate is in marine sediments and permafrost at specific temperatures and pressures. Decomposition of NGH resources and exploitation is a process in which methane molecules are released from water cages due to unstable thermodynamic conditions. Solid-state CH_4 hydrate decomposes into gas phase CH_4 and liquid phase water during this process. The production methods proposed are based on the hydrate thermodynamic characteristics illustrated in Figure 2.7, mainly including depressurization, thermal stimulation, and the chemical potential driven method (chemical injection and CO_2 replacement). This section describes the progress of research in each of the three major types of recovery methods and some important findings.

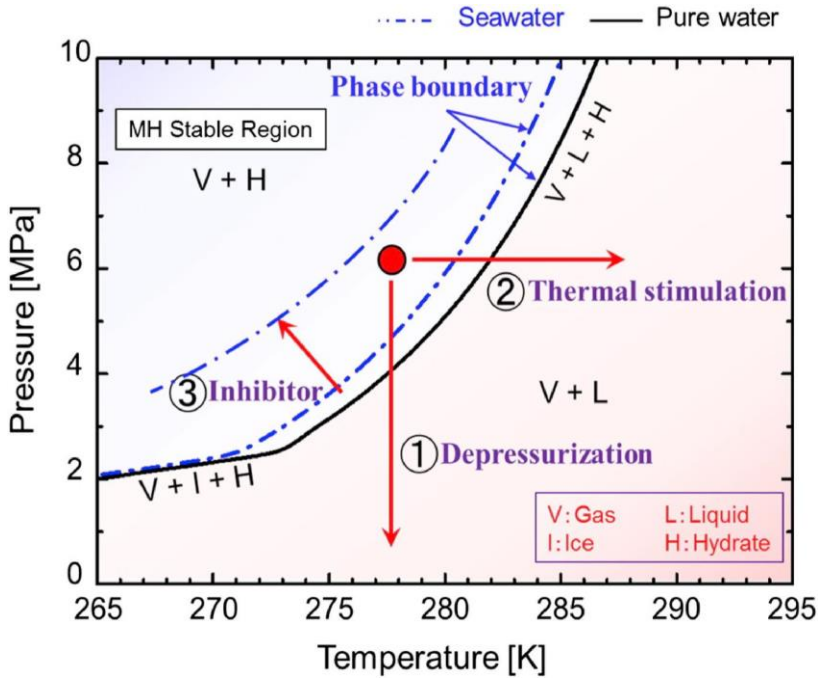

Figure 2.7 Illustration of commonly proposed NGHs recovery methods.(1 CH_4 hydrate production by depressurization approaches; 2 Thermal stimulation approach; 3 Chemical injection method) [56].

2.2.1. NGHs recovery driven by depressurization

As presented in Figure 2.7, natural gas production from GH reservoirs driven by depressurization is based on established mechanisms that lower pressure conditions to hydrate equilibrium pressure at specific temperatures. As a matter of field test, depressurization is a method of gas generation that dissociates NGHs by reducing the pressure in the wellbore drilled through hydrate-bearing sediments. Depressurization was the first natural gas exploitation method performed in an actual hydrate field.

The conceptual mechanism of NGH expoitation by depressurization is illustrated in Figure 2.8. It should be noted that the local temperature will continuously drop during NGHs decomposition, and the with a dissociation enthalpy of 53.9 kJ/mol [57]. The decomposition of NGHs might halt once the local temperature drops to the equilibrium temperature under a certain pressure. Therefore, this method has been investigated extensively by researchers. Holder and Angert [58] used an experimental methodology to investigate the impact of factors such as gas composition, porous medium, and additives on gas production, to better understand the hydrate decomposition process by depressurization. Goel et al. [59]

used experimental methodology to investigate the impact of factors such as gas composition, porous medium, and additive on gas production, to better understand the hydrate decomposition process by depressurization. Goel et al. [60] modified a model to estimate the efficiency of hydrate decomposition in a porous medium by using a radial diffusivity equation, in which the gas−mass balance in a gas hydrate well was analytically solved. The depressurization method was also studied by Kono et al. to examine the hydrate decomposition rate, who concluded that decomposition rate was controlled by the porous sediment parameters [61]. Zhao et al. [62] analyzed and compared the impact of the sensible heat of the reservoir and ambient heat over the gas generation process. Their results showed that the gas production rate is affected by the production pressure. The above-mentioned research indicates that a combination of theoretical models with systematic experiments is important for increasing methane recovery during NGH exploitation.

Table 2.1 Summary of experimental studies on gas hydrate decomposition by depressurization.

Reference	System	Purpose	Pressure	Temperature
Circone, Susan, et al. [63]	Granular ice and pressurized CH_4	Decomposition evolution	0.1 MPa	272 K and 289 K
Kono, Hisashi O., et al. [61]	Methane hydrate	Kinetic dissociation rate equation order of the reaction	6.8–13.6 MPa	273.5 K
Tang, Liang-Guang, et al. [64]	Methane hydrate	Hydrate dissociation kinetics dissociation constant of the order of 104 mol m^{-2} Pa^{-1} s^{-1}	0.1 MPa, 0.93 MPa and 1.93 MPa	273–275 K
Haligva, Cef, et al. [65]	Methane hydrate in silica sand bed	Size of the laboratory sample dependence on the rate of methane recovery	2.3 MPa and 3.1 MPa	277 K
Oyama, Hiroyuki, et al. [66]	Methane hydrate	Heat transfer was the dominant factor of gas production	0.2 MPa to 8.4 MP	285–286 K
Li, Bo, et al. [67]	Methane hydrate in quartz sand	Gas production behaviors and the hydrate dissociation kinetics under depressurization in porous media	4.5–5.6 MPa	281.15 K

When hydrate dissociation is driven by depressurization, temperature change becomes an important factor, particularly after water freezing, which delays the process [68]. In the

reservoir, the hydrate will first decompose due to the absorption of sensible heat. Therefore, different stages of hydrate decomposition were usually observed during the experiments by depressurization. This is confirmed by Halgva et al. [68] who studied the decomposition of methane hydrate by depressurization. In the first time period from 0 to 0.5 h, the hydrate decomposition rate was strongly dependent on the bed size of the hydrates, but the rate decreased during the second period from 0.5 to 1.0 h. Their experiments showed that freezing also occurred.

Methane can be economically and sustainably produced through depressurization if adequate heat transfer and energy are provided. Along with NGH decomposition, the NGH saturation decreases, and the effective permeability increases, further causing the enlarging of the regions with lower pressure. Thus, the sustainability of gas production by depressurization depends on the diffusion of pressure, the NGH saturation, and the effective permeability of the NGH reservoirs.

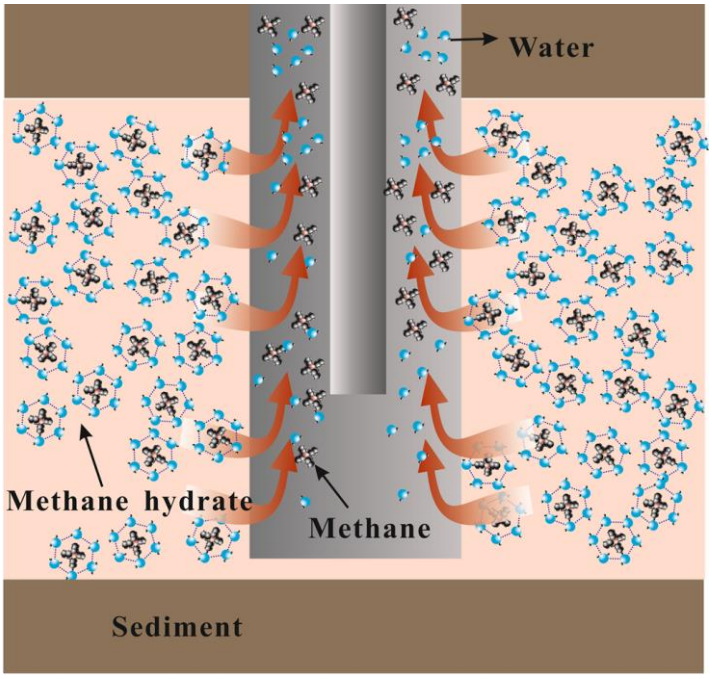

Figure 2.8 Natural gas hydrate dissociation and exploitation technologies are driven by depressurization (Modified after reference [19]).

2.2.2. Thermal stimulation and chemical injection method

The underlying concept of thermal stimulation is straightforward: GHs are heated until the temperature local to them is considerably higher than what they are likely to become stable under. A gas trapped inside the water cages is released when hydrate decomposes and flows through the wellbore where it is recovered. Wellbore heating or point-source heating is externally supplied. Laboratory activities to produce methane using thermal stimulation and some specific heat delivery techniques are discussed below.

The chemical injection method is to inject thermodynamic hydrate inhibitors or kinetic inhibitors, such as brine, alcohols, or glycols, into the hydrate reservoir to dissociate the hydrate and produce natural gas. This shifts the hydrate equilibrium curve toward the high-pressure and low-temperature region. With a small shift in the equilibrium curve, significant hydrate dissociation may not be achieved. The economic and environmental prospects are their drawbacks, making it less likely to be used widely. In addition, there are practical limitations to the infectivity of inhibitors into low permeable hydrate reservoirs.

Compared to inhibitor injection or thermal stimulation, depressurization seems to be the most economical gas hydrate production method. However, it takes more time than inhibitor injection and thermal stimulation to decompose GHs.

2.2.3. Gas replacement recovery method

The thermal stimulation method may increase overall efficiency and production rates compared to the depressurization method, but it may weaken the seafloor and potentially release methane as a side effect. The recently proposed replacement method for methane decomposition has attracted the attention of many researchers. This method involves injecting gas into the NGH reservoir to replace the methane gas. In most cases, CO_2 is the predominant guest gas to take the place of methane molecules in GHs. Simulated flue gas (a mixture of CO_2 and N_2), and air have recently been used in laboratory studies for replacement.

Injection of CO_2 gas could be captured as hydrate buried in the seafloor, which has the merit of producing methane and reducing the greenhouse effect, or even eliminating water production. This is because the water released from the methane decomposition process is

absorbed by carbon dioxide hydrate, and carbon dioxide hydrate can replace methane hydrate to maintain the mechanical strength of the sediment. Meanwhile, it is also a promising method to maintain the mechanical stability of sediments by filling the pore space, thereby expanding the recoverable geological environment and reducing clogging. Figure 2.9 shows NGH exploitation using CO_2 injection in hydrate reservoir. The gas replacement method, its benefits, and current research progress are examined in the following section.

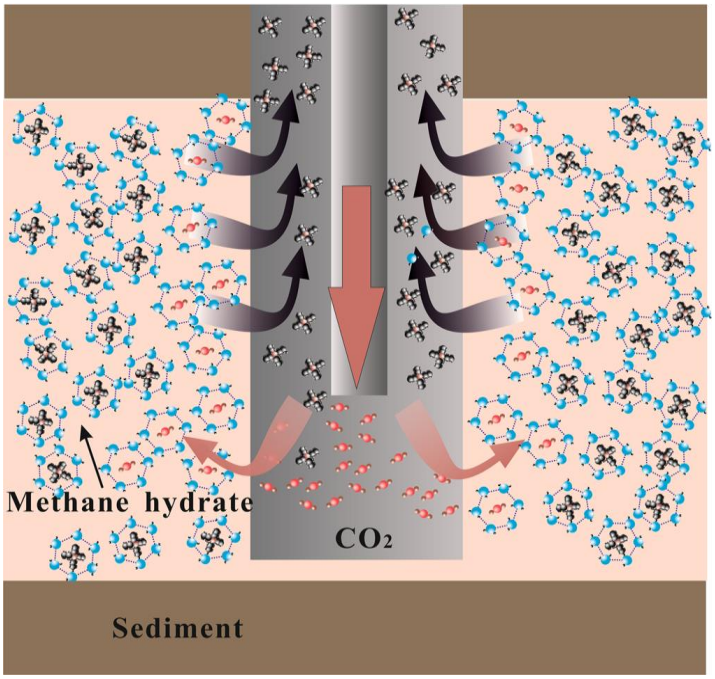

Figure 2.9 Natural gas hydrate exploitation technologies by CO_2 replacement (Modified after reference [19]).

CH_4 and CO_2 usually form gas hydrate as guest molecules in structure I. CO_2 has a molecular diameter of 5.12 Å, which is larger than CH_4. CO_2 molecules can be substituted for guest CH_4 molecules in hydrates under appropriate conditions, resulting in another type of hydrate. As early as the 1980s, the idea of using CO_2 to extract hydrates of natural gas was pro CH_4 and CO_2 usually form gas hydrate as guest molecules in structure I. CO_2 has a molecular diameter of 5.12 Å, which is larger than CH_4. CO_2 molecules can be substituted for guest CH_4 molecules in hydrates under appropriate conditions, resulting in another type of hydrate. As early as the 1980s, the idea of using CO_2 to extract hydrates of natural gas was proposed [69], in which CO_2 can be used to remove methane from hydrate reservoirs and CO_2 can also be sequestered. Ideally, the process of energy production can be carbon

neutral if the amount of CO_2 captured equals the amount of CH_4 extracted. It can also be spontaneously sustained since the amount of heat released by the formation of CO_2 hydrate (-57.98 kJ/mol) is greater than the amount of heat absorbed by the breakdown of CH_4 hydrate (54.49 kJ/mol) [70]. Yezdimer et al. [71] reported the Gibbs free energy of -12 kJ/mol during the substitution of CH_4 hydrate with CO_2 through the molecular dynamics simulation method, indicating that this exchange process is thermodynamically feasible.

The basic theory of this approach follows the difference in phase equilibrium that exists between methane hydrate and carbon dioxide hydrate. At lower temperatures (<283 K), CO_2 hydrate is more stable than methane hydrate [72]. CH_4 and CO_2 usually form gas hydrate as guest molecules in structure I (sI). CO_2 has a molecular diameter of 5.12 Å, which is larger than CH_4. The CO_2 molecules can be substituted for CH_4 molecules in hydrates under appropriate conditions, resulting in another type of gas hydrate; the conceptual mechanism is represent in Figure 2.10 [73]. The figure explained two mechanisms of the increased replacement efficiency. Figure 2.10 (a) suggests that the initial hydrate (sII) goes through an isostructural conversion into the structure II (sII) in a scenario where the CH_4-CO_2 exchange was enhanced with an increase in CO_2 injection pressure. The other mechanism in Figure 2.10 (b) is that the transition of initial sII into the sI along with an isostructural conversion into the sII under a lower CO_2 injection pressure.

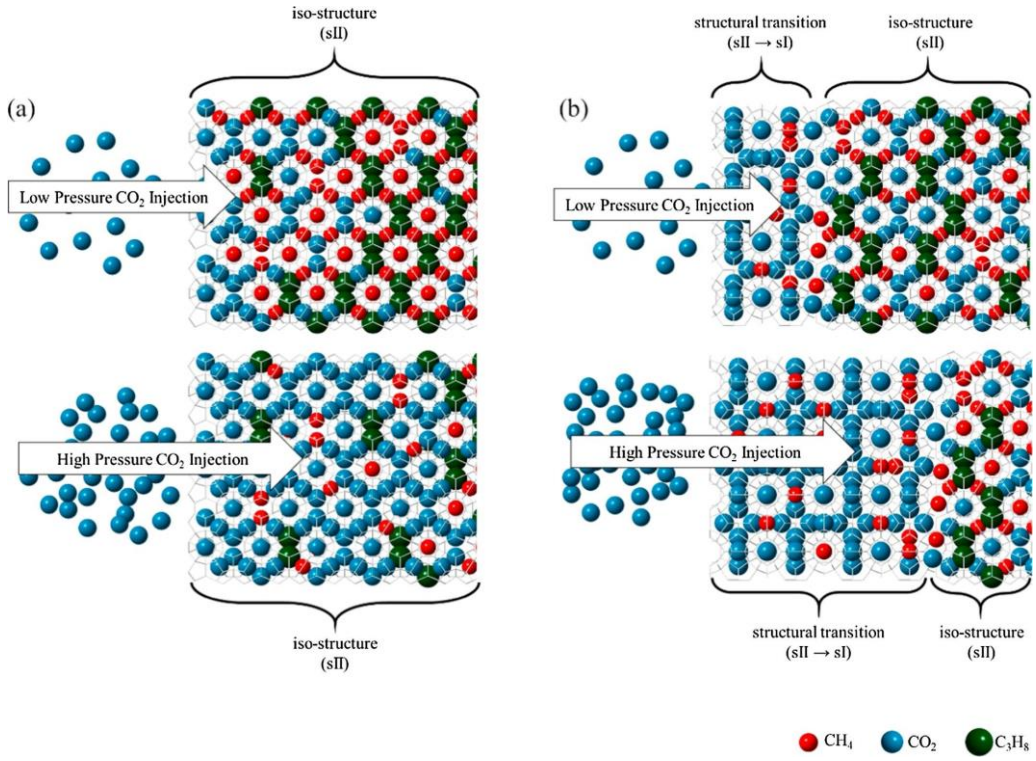

Figure 2.10 Conceptual mechanism of replacement scenarios. (a) sII hydrate converted into the sI hydrate under low CO_2 injection pressure; (b) transition of sII hydrate into sI hydrate along with an isostructural conversion into the sII hydrate [73] .

Experimental Investigations have confirmed that CO_2 molecules prefer to be in the hydrate phase at 280 K in a CH_4-CO_2 mixed hydrate system. The composition variation should be taken into account for the NGH recovery process. Composition in the vapor phase plays a significant role in the stability of NGHs. The increase in the proportion of long-chain hydrocarbons (e.g., propane) enhances the stability of hydrates. The phase equilibrium curves of a hydrate mixture of carbon dioxide hydrate and 99.5 mol % methane and 0.5 mol% propane are illustrated by Bishnoi et al. [74]. The sII hydrate has higher stability compared with the hydrate formed from pure methane in the presence of propane with even a low concentration. The stability of carbon dioxide hydrate is only slightly stronger than that of the mixed hydrate at temperatures below 283 K. In this case, the difference in phase equilibrium is not good evidence for the driving force of the CO_2/CH_4 replacement process. Schicks et al. [75] studied CH_4-C_3H_8 mixed hydrate with the replacement of CO_2 employing Raman, powder X-ray diffraction. They found that the process can proceed within 10 h. They also conducted a study of the replacement in the opposite direction. i.e., the replacement of CO_2 hydrate with hydrocarbon gas, and found that the direction of the replacement reaction

depends on the composition of the gas phase. The results of the study show good evidence that the driving force for a replacement process is not only related to the difference in thermodynamic stability but also the chemical imbalance in the composition of the gas and hydrate phases. This implies in NGH recovery by CO_2 that the replacement of CO_2 molecules in gas hydrates can form a more stable, CO_2-rich hydrate phase.

2.2.4. Depressurization combined method

As each of the recovery techniques described above has limitations, there is an agreement among gas producers that combining techniques can increase the effectiveness of gas recovery. The combined methods have been simulated and experimenally studied in order to overcome the limitations and disadvantages of single method, for example, depressurization and thermal stimulation combination [76–79], depressurization and gas replacement combination. Depressurization and chemical injection combination method is usually utilized through the pipline from risk of hydrate reformation [80,81].

For safe and effective exploitation of gas hydrates, it is necessary to investigate the effectiveness of various combined exploitation methods. Bin Wang et al. [79] experimentally evaluated heat injection and depressurization method indicated this mothod can effectively promote gas production from hydrate reservoir. The results indicate that the gas generation after ice generation can be divided into five stages: (1) a free gas release, (2) hydrate dissociation along the equilibrium curve driven by the reservoir sensible heat, (3) hydrate dissociation driven by the exothermic ice generation reaction, (4) ice melting and hydrate dissociation under ambient heat transfer, and (5) hydrate dissociation under ambient heat transfer. Li et al. [78] proposed injecting hot brine after depressurization to achieve a higher energy efficiency than a single injection of hot brine. The mathematical models developed by Bai et al. [76] showed that flooding method combined depressurization produced more gas for a longer period of time than when exploitation was performed separately. Moreover, the combined depressurization-thermal stimulation method has obvious advantages over single depressurization or thermal stimulation in terms of energy efficiency, gas production, and gas utilization levels. Combined methods can effectively suppress ice formation and hydrate reformation, thus preventing the formation of ice. Thus, depressurization accompanied by external heat enables hydrate dissociation and prevents hydrate

reformation. The inhibitor injection method is used to prevent hydrate reformation after decomposition through depressurization or thermal stimulation [80,81]. It is challenging to inject hot fluid into hydrate reservoirs due to the high pressure present; therefore, thermal stimulation is an additional method to be used after depressurization. Ahn et al.investigated the effect of a combined method consisting of hot brine injection and depressurization on preventing hydrate reformation [82]. They showed that hot brine injection after depressurization inhibited hydrate reformation more effectively than the two methods applied concurrently, or by using a single hot brine injection. In other words, under appropriate exploitation conditions, hydrate reformation can be prevented without additional energy. Zhou et al. [82] introduced the concept of combining depressurization and CO_2 replacement. Zhao et al. [83] studied this combined method and found that higher percentages of CH_4 can be produced, and more injected CO_2 can be captured in the hydrate phase.

To summarize, the future tendency of the exploration of GH will be a combination of multiple exploitation technologies and multiscale theoretical investigation, as shown in Figure 2.11. However, research is still in the theoretical stage, and further research should be carried out in terms of replacement location and efficiency in the future. In addition, the combination of depressurization and replacement has not been extensively investigated.

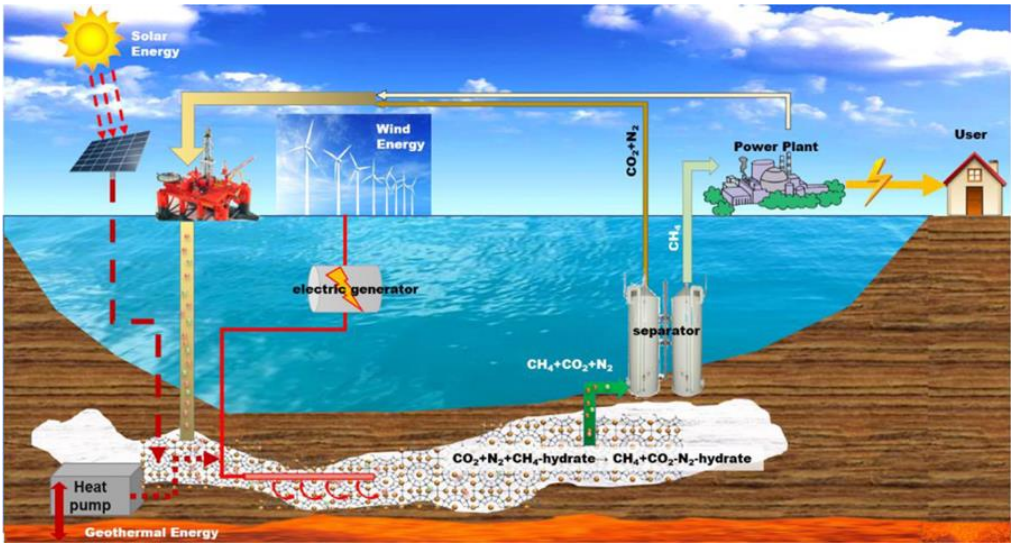

Figure 2.11 Conceptual of future multi-combined system for gas hydrate exploitation [26].

2.3. Methane hydrate recovery kinetics and mechanisms

So far, the thermodynamic equilibrium conditions of common gas components have mostly been established [3]. The formation and decomposition kinetics studies of gas hydrate are relevant to the exploitation of vast NGH resources and other hydrate-based technologies, including energy storage and transportation, gas mixture separation, and water treatment. Consequently, much literature is available on the study of decomposition rates and kinetic models. Furthermore, the underlying formation and decomposition mechanisms of GHs are important to understand hydrate system behaviors, one which perhaps can be controlled. The definitive formation and decomposition mechanisms of the GH exploitation process have not been clarified. To investigate the kinetics and mechanisms of hydrate systems, many computational and experimental works ranging from the macroscopic to the microscopic scales have been conducted. In the past few decades, many significant analytical methods have been employed for qualitative and quantitively study of hydrate systems, such as X-ray diffraction (XRD), neutron diffraction, and Raman and X-ray computed tomography [84–87]. Nonetheless, the much smaller length scales and shorter timescales—nanometers and nanoseconds, respectively—in which the hydrates behave present experimental difficulties in most molecular-level studies. Molecular dynamics (MD) simulations hence increasingly display merits in the understanding of the molecular mechanisms of hydrate systems.

Methane decomposition kinetics and mechanism studies have been extensively conducted and reveal a number of interesting characteristics, which are reviewed in the following sections.

2.3.1. Methane hydrate decomposition kinetics

The decomposition kinetics of hydrates are important in the gas generation process and production strategy. Methane hydrate decomposition kinetics has been developed in recent decades, with numerous studies revealing the hydrate decomposition kinetics influence factors of pressure, temperature, and phases contact area.

Pressure and temperature reduction can both trigger GH decomposition. An investigation of the kinetics of methane hydrate decomposition in loess was carried out by Jiang et al.

[88] in a temperature control mode. They revealed that the higher the dissociation temperature, the faster the hydrate decomposition rate. Mekala et al. [89] also demonstrated the distinctive decomposition behavior of methane hydrate and explained that the decomposition rates are faster in pure water than in seawater due to the inhibition effect caused by the presence of salts. This decomposition was stimulated by thermal at constant pressure.

The most classic hydrate decomposition model was proposed by Kim et al [90] who investigated methane hydrate decomposition kinetics and include the parameters by equation (2-1), a kinetics expression with fugacity difference ($f_{eq} - f_s$) between hydrate equilibrium pressure and that on solid hydrate phase as driving force.

$$\frac{dn}{dt} = -K_d A(f_{eq} - f_s) \tag{2-1}$$

where *A* is an important factor for the surface area between bulk fluid and hydrate phases. Subsequently, works focusing on particle size were also conducted by this group. Studies on decomposition kinetics tend to focus on hydrate dissociation above the ice point. However, temperature drops during hydrate decomposition and ice would appear on conditions of subzero or near zero. A related investigation by Liang et al. indicates that the thickness of the ice layer should be included in the kinetics model, which was thus formulated as:

$$\frac{dn}{dt} = \frac{D}{L} A(f_{eq} - f_s) \tag{2-2}$$

With the aid of high-pressure differential scanning calorimetry, it is shown that the shielding effect of the ice layer occurs under low pressure. The diffusion of the guest gas through hexagonal ice on the surface layer should be an important factor in understanding the shielding effect of the ice layer.[91].

In-situ Raman spectroscopy is a good analytical tool for real-time variation of gas hydrate, andKomai et al [92] integrated Raman intensity (*I*) for an elapsed time *t* for powdered methane hydrate with diameters ranging 100–250 μm. The kinetics model was given by.

$$3(1 - I(t)2/3) - 2(1 - I(t)) = \phi \frac{6Dt}{r_0^2} \quad (2\text{-}3)$$

where ϕ is a dimensionless parameter derived from driving force and particle size r_0 is included in the model, which makes it more suitable for real-world situations.

From the development of the model, we can see those multiple mechanisms and their coupling effects are essential for understanding the decomposition of GHs. One essential factor in the experimental analysis is particle size, which greatly affects hydrate decomposition kinetics.

2.3.2. Application of molecular dynamics simulation in gas hydrate decomposition

Implementation in the industrial exploration of NGH resources still faces many challenges in scientific and technological advancements, and the corresponding definitive mechanisms are poorly understood. Therefore, there have been many investigations aiming at comprehending the molecular-level details of GH formation and decomposition processes, particularly under natural conditions. These understandings can lead to improved control over the future industrial exploitation of NGH reservoirs. As a connection between macro-experimental phenomena and microstructural features, MD simulation can provide scientific micro-theoretical explanations for macro-experimental phenomena, analyze macro-experiments more deeply and thoroughly, and fundamentally explain the experimental phenomena. In addition, MD simulation is of theoretical significance to the economic aspect of the experimental works, which can greatly reduce the efforts of experimental work and reduce errors from experiments, hence saving a lot of experimental time. As a consequence, applying MD simulations is attractive as an effective methodology of microscopic research and has become an indispensable research tool in the hydrates research area [93–97].

Figure 2.12 is a summary of the literature published on the study of hydrates through MD simulation methodologies over the past two decades, which mainly focus on the structure of hydrates, the growth and decomposition of hydrates, hydrate separation, and hydrate inhibitors. However, there are few simulations on hydrate replacement and production. Many findings of simulations studies are reviewed here, including important mechanistic features and different perspectives on hydrate behaviors. Various methodologies are also reviewed for the visualization and characterization of hydrate systems.

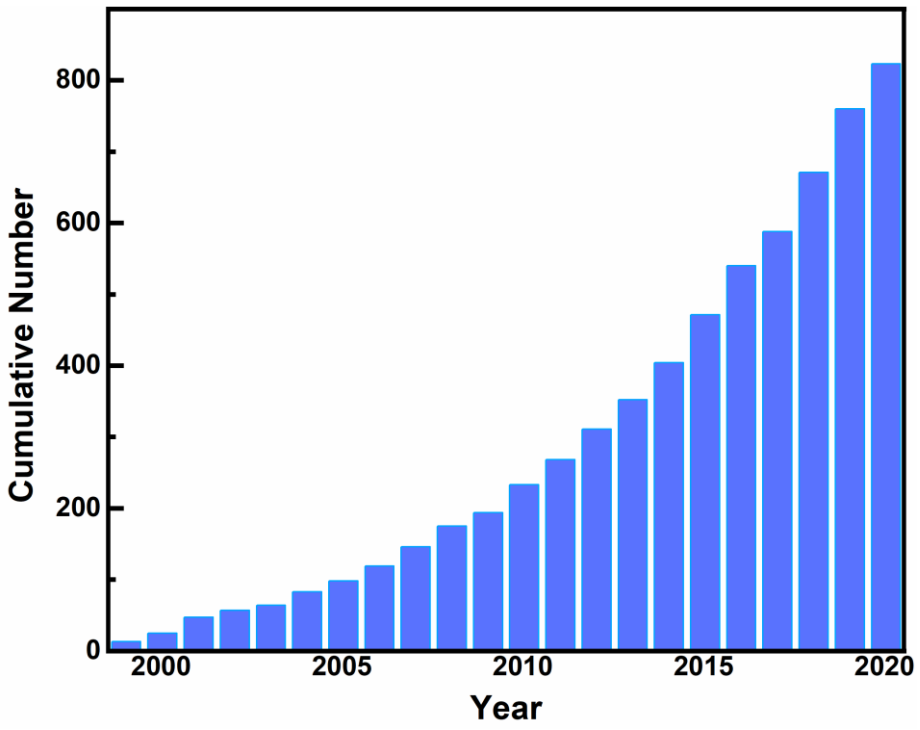

Figure 2.12 Cumulative number of publications regarding molecular simulation on clathrate hydrate over the past 20 years (summarized from web of science).

The mechanism investigation of clathrate hydrate decomposition is mainly based on experiments and simulations. The experimental study is focused on the decomposition behavior and morphology change through microscopic, modern technology such as Raman and nuclear magnetic resonance (NMR) to detect the structure of hydrate. From the perspective of simulations, the most commonly used methodologies by researchers are quantum calculations, Monte Carlo simulations, and MD simulations, which can explain hydrate decomposition mechanisms at the molecular scale. Since the formation and decomposition process of clathrate hydrate is a rare event and occurs very fast on a microsecond time scale, a large set of MD trajectories can be generated to display these processes. The main idea of MD simulation is solving the Newtonian equation of motion and calculating all atom coordinates to determine the force on each atom, which is derived from the sum of all potentials of the system. Then, atoms move as driven by these forces. The forces are obtained from classical equations of motion for all particles in all molecules [98]. Furthermore, new positions, velocities, or properties of interest are generated.

At present, there are three commonly used algorithms to solve the Newtonian equation of motion, namely the Verlet algorithm [99], the leapfrog algorithm [100], and the velocity-

Verlet algorithm [101]. The MD simulation programs mainly include TINKER, NAMD, CHARM, GROMACS, LAMMPS, and DL_POLY [102–105]. Different water force field models have been used during simulation, expressed as the LJ potential function combined with electrostatic interaction. The simple point charge (SPC) potential function assumes that water molecules are rigid [106–108]. TIP4P potential function is built on SPC potential function by adding virtual atoms with charge but no mass to describe hydrogen bonds [109]. TIP4P/Ice, TIP4P/2005, and TIP4P-EW are the three main water models often used in the clathrate hydrate simulation, which require a longer simulation time and memory than the SPC water model. Different conclusions have been drawn concerning these water models. Some studies represent variation in thermodynamic and physical properties found when introducing different water models [108,110,111]. Choudhary et al. [112] compared these water models and noticed that TIP4P/Ice and TIP4P/2005 both over-predict the melting point compared to experimental results, while TIP4P and SPC/E show a melting point between 265 K and 270 K. However, the results from Vikesh et al. [113] show similar behavior for both SPC/E and TIP4P models. As a result, a more appropriate water model under thermodynamic conditions needs to be investigated. Besides the LJ potential function, other popular models are OPLS-AA (Optimal Parameterization for the Liquid State) [114], the TraPPE (transferable potentials for phase equilibria) [115], and the united-atom model (UA) [116], commonly used to calculate the potential parameters for methane.

The main ensembles used in MD simulation are microcanonical ensemble (NVE), canonical ensemble (NVT, means that it has a certain number of particles (N), volume (V), and temperature (T) ensemble), and isobaric-isothermal Ensemble (NPT, means that it has a certain number of particles (N), pressure (P), and temperature (T)). MD simulations have been conducted at constant temperature conditions with NPT [107,117–119], NVT [120,121] or NVE ensembles [113,122]. In NPT or NVT ensembles simulations, the heat effect during this process is removed with a thermostat coupling. Mass transfer has been assumed to be an important factor in determining gas hydrates behaviors while heat transfer is less important. Using such an approach Nucleation is somewhat justified because it is a slow process It appears to be a relatively slow process.

After English et al. [110] have reported that NPT simulations have limitation in describing gas hydrate decomposition process. Ripmeester et al. [123] have performed MD simulations

of methane hydrates using NVE ensemble. According to their findings, hydrate decompostion consumes a lot of energy and the transfer of heat play a crucial role in the molecular mechanism and decomposition rate.

There are a few studies on hydrate decomposition using MD simulation with various complex systems and influencing factors [124–127]. In addition, attempts at applying MD simulation to the memory effect have been reported. This phenomenon shortens the induction time required in a system having no prior experience of hydrate formation. Most research has concluded that decomposition happens first at the outside of the hydrate phase [128]. Because it is difficult to reduce the pressure of the hydrate system to realize the hydrate decomposition process, there are few reports on the decomposition mechanism simulated by MD. The MD simulation results of hydrate decomposition at different temperatures show that the decomposition rate is closely related to temperature, and the higher the temperature is, the faster the decomposition rate will be. The gas swapping method can not only realize carbon dioxide storage but also hydrate mining without damaging the geological structure of the reservoir. The mechanism of GH formation is a fundamental scientific question. The decomposition of hydrates is subject to different hypotheses, but experimental studies cannot currently confirm them due to the nanometer scale at which it occurs.

Rodger et al. [129] accomplished simulation of the methane hydrate-methane gas interface by MD method. They found an increase in both ice-like and water-like structures at interface after hydrate decomposition, thus concluded that the memory effect in hydrate nucleation is not related to metastable structure of hydrate.

Ding et al. [97] found that the hydrate cell size during decomposition is due to the diffusion of the guest molecules. Myshakin [130] simulated the relationship between cage occupancy and hydrate decomposition rates and showed that the existence of an empty cage reduces the hydrate crystal stability, making it much easier to break down into hydrate residual rings. They also observed that methane molecules and residual rings in the liquid phase can reform hydrates, demonstrating the memory effect of the hydrate structure.

The simulation results of Sarupria et al. [131] on the effect of cage-specific occupancy on the rate of decomposition of carbon dioxide hydrate further suggest that the speed of hydrate

decomposition is not only affected by the total cage occupancy of hydrates, but also by the type of empty cage and the surrounding hydrate structure. The simulation results of Sarupria et al. [131] on the effect of cage-to-share specific occupancy ratio on the rate of decomposition of carbon dioxide hydrates further suggest that the speed of hydrate decomposition is not only affected by the total cage-occupancy rate of hydrates, but also by the type of empty cage and surrounding hydrate structure. Furthermore, MD simulations were conducted to investigate the microscopic mechanism of sI methane hydrate dissociation via depressurization [132]. To simulate depressurization, a vacuum removal system was used, in which methane is continuously removed from the surface of the hydrate layer.

2.4. Summary of literature study and future guidelines

Although many research results have shown the possibility of methane production by CO_2 replacement, the complex theory behind the replacement process is still unclear and needs to be further explored. The challenges to understanding the replacement process, mostly related to the kinetics of hydrate generation and the decomposition process, are summarized and outlined as follows.

1. There are only limited investigations on kinetic studies of methane gas decomposition and the replacement of CO_2. Although many studies have reported methane recovery rates, these results have not provided a good indication of whether methane is produced due to methane hydrate self-decomposition or by CO_2 replacement. Therefore, the key question is how to determine the rate of methane hydrate decomposition in the presence of replacement gas (CO_2, simulated flue gas or air).

3. There is a lack of studies on the kinetics of hydrate regeneration caused by the replacement process. More research data are needed to further analyze the influence of hydrate regeneration in the replacement process in porous media, the permeability of the accumulation, and the impact of the nature of the sediment itself on CO_2 sequestration.

2. To fully understand clathrate hydrate behaviors, it is necessary to combine the multiple-scale studies of macroscopic hydrate systems. This requires a deeper understanding of the mechanism by which the hydrate decomposition and replacement process occur. Although

microscopic observations and MD studies have provided some insight into the immigration or recombination of water during the replacement process, current microscopic observations and MD studies have not provided a good understanding of whether the original hydrate decomposes before the replacement process begins.

5. Research on hydrate decomposition and replacement with various gas media is required. At present, the simulated sediment media used in laboratory research on gas replacement includes CO_2, simulated flue gas (a mixture of CO_2 and N_2), and air. The injection of air for methane extraction has its advantages and potential due to its the generous accessibility and wide existence. However, the CH_4 recovery rate from replacement methods needs to be further improved, and the reaction rate between CH_4 and injection gas has become a hindrance to the hydrate exploitation strategy. The low reaction rates have been a bottleneck for the further development of methane exploitation. On the other hand, it is a necessity to understand the underlying mechanisms behind methane production and develop a novel method for an enhanced performance methane gas extraction.

6. Extensive theoretical studies using MD calculation at molecular level are required to better understanding the complex phenomena of gas hydrate decomposition. When enough research data is obtained, it is necessary to develop a suitable numerical simulation model for hydrate decomposition to determine the optimal well gas replacement and exploitation strategy.

a. References

[1] Singh P, Hazarika K. Methane Hydrate: Fuel of the Future-A Literature Review n.d.

[2] Kvenvolden KA. Gas hydrates—geological perspective and global change. Rev Geophys 1993;31:173–87. doi:https://doi.org/10.1029/93RG00268.

[3] Sloan Jr ED, Koh CA. Clathrate hydrates of natural gases. CRC press; 2007.

[4] Suess E, Bohrmann G, Greinert J, Lausch E. Flammable ice. Sci Am 1999;281:76–83.

[5] Siegfried R. Humphry Davy and the elementary nature of chlorine. J Chem Educ 1959;36:568.

[6] Pauling L, Marsh RE. The structure of chlorine hydrate. Proc Natl Acad Sci U S A 1952;38:112.

[7] Faraday M, Davy H. XIV. On fluid chlorine. Philos Trans R Soc London 1823;113:160–5.

doi:10.1098/rstl.1823.0016.

[8] Faraday M. XVII. On the condensation of several gases into liquids. Philos Trans R Soc London 1823:189–98.

[9] Hammerschmidt EG. Formation of gas hydrates in natural gas transmission lines. Ind Eng Chem 1934;26:851–5.

[10] Daraboina N, Pachitsas S, von Solms N. Natural gas hydrate formation and inhibition in gas/crude oil/aqueous systems. Fuel 2015;148:186–90.

[11] Daraboina N, Malmos C, von Solms N. Synergistic kinetic inhibition of natural gas hydrate formation. Fuel 2013;108:749–57.

[12] Perfeldt CM, Chua PC, Daraboina N, Friis D, Kristiansen E, Ramløv H, et al. Inhibition of gas hydrate nucleation and growth: efficacy of an antifreeze protein from the longhorn beetle Rhagium mordax. Energy & Fuels 2014;28:3666–72.

[13] Jones N. Gas-hydrate tests to begin in Alaska. Nat News 2012.

[14] Platteeuw JC, Van Der Waals JH. Thermodynamic properties of gas hydrates. Mol Phys 2010;1:91–6. doi:10.1080/00268975800100111.

[15] Barrer RM, Stuart WI. Non-stoicheiometric clathrate compounds of water. Proc R Soc London Ser A Math Phys Sci 1957;243:172–89. doi:10.1098/rspa.1957.0213.

[16] Makogon YF. Peculiarities a gas-field development in permafrost. Nedra, Moscow 1966:1–17.

[17] Makogon YF. A gas hydrate formation in the gas saturated layers under low temperature. Gas Ind 1965;5:14–5.

[18] Ripmeester JA, Tse JS, Ratcliffe CI, Powell BM. A new clathrate hydrate structure. Nature 1987;325:135–6. doi:10.1038/325135a0.

[19] Hunter RB, Collett TS, Boswell R, Anderson BJ, Digert SA, Pospisil G, et al. Mount Elbert Gas Hydrate Stratigraphic Test Well, Alaska North Slope: Overview of scientific and technical program. Mar Pet Geol 2011;28:295–310. doi:10.1016/J.MARPETGEO.2010.02.015.

[20] Makogon YF, Holditch SA, Makogon TY. Natural gas-hydrates—A potential energy source for the 21st Century. J Pet Sci Eng 2007;56:14–31.

[21] Zhu Y, Wang P, Pang S, Zhang S, Xiao R. A Review of the Resource and Test Production of Natural Gas Hydrates in China. Energy & Fuels 2021.

[22] Ito T, Komatsu Y, Fujii T, Suzuki K, Egawa K, Nakatsuka Y, et al. Lithological features of hydrate-bearing sediments and their relationship with gas hydrate saturation in the eastern Nankai Trough, Japan. Mar Pet Geol 2015;66:368–78.

[23] Zhu Y, Zhang Y, Wen H, Lu Z, Jia Z, Li Y, et al. Gas hydrates in the Qilian mountain permafrost, Qinghai, Northwest China. Acta Geol Sin Ed 2010;84:1–10.

[24] Sloan ED. Fundamental principles and applications of natural gas hydrates. Nature 2003;426:353–9. doi:10.1038/nature02135.

[25] Udachin KA, Ratcliffe CI, Ripmeester JA. Single Crystal Diffraction Studies of Structure I, II

and H Hydrates: Structure, Cage Occupancy and Composition. J Supramol Chem 2002;2:405–8. doi:https://doi.org/10.1016/S1472-7862(03)00049-2.

[26] Momma K, Ikeda T, Nishikubo K, Takahashi N, Honma C, Takada M, et al. New silica clathrate minerals that are isostructural with natural gas hydrates. Nat Commun 2011;2:196. doi:10.1038/ncomms1196.

[27] Yin Z, Zheng J, Kim H, Seo Y, Linga P. Hydrates for cold energy storage and transport: A review. Adv Appl Energy 2021;2:100022. doi:10.1016/J.ADAPEN.2021.100022.

[28] Babu P, Nambiar A, He T, Karimi IA, Lee JD, Englezos P, et al. A review of clathrate hydrate based desalination to strengthen energy–water nexus. ACS Sustain Chem Eng 2018;6:8093–107.

[29] Di Profio P, Arca S, Germani R, Savelli G. Novel Nanostructured Media for Gas Storage and Transport: Clathrate Hydrates of Methane and Hydrogen. J Fuel Cell Sci Technol 2006;4:49–55. doi:10.1115/1.2393304.

[30] Gudmundsson JS, Graff OF, Kvaerner A. Hydrate non-pipeline technology for transport of natural gas. 22nd World Gas Conf. Tokyo, Citeseer; 2003, p. 1–5.

[31] Nashed O, Partoon B, Lal B, Sabil KM, Shariff AM. Review the impact of nanoparticles on the thermodynamics and kinetics of gas hydrate formation. J Nat Gas Sci Eng 2018;55:452–65.

[32] Fang S, Zhang X, Zhang J, Chang C, Li P, Bai J. Evaluation on the natural gas hydrate formation process. Chinese J Chem Eng 2020;28:881–8. doi:10.1016/J.CJCHE.2019.12.021.

[33] Wang F, Jia Z-Z, Luo S-J, Fu S-F, Wang L, Shi X-S, et al. Effects of different anionic surfactants on methane hydrate formation. Chem Eng Sci 2015;137:896–903.

[34] Liu Y, Chen B, Chen Y, Zhang S, Guo W, Cai Y, et al. Methane storage in a hydrated form as promoted by leucines for possible application to natural gas transportation and storage. Energy Technol 2015;3:815–9.

[35] Prasad PSR, Sowjanya Y, Dhanunjana Chari V. Enhancement in methane storage capacity in gas hydrates formed in hollow silica. J Phys Chem C 2014;118:7759–64.

[36] Pasieka J, Coulombe S, Servio P. Investigating the effects of hydrophobic and hydrophilic multi-wall carbon nanotubes on methane hydrate growth kinetics. Chem Eng Sci 2013;104:998–1002.

[37] Yang L, Fan S, Wang Y, Lang X, Xie D. Accelerated formation of methane hydrate in aluminum foam. Ind Eng Chem Res 2011;50:11563–9.

[38] Casco ME, Silvestre-Albero J, Ramírez-Cuesta AJ, Rey F, Jordá JL, Bansode A, et al. Methane hydrate formation in confined nanospace can surpass nature. Nat Commun 2015;6:1–8.

[39] Karimi AA, Dolotko O, Dalmazzone D. Hydrate phase equilibria data and hydrogen storage capacity measurement of the system H2+ tetrabutylammonium hydroxide+ H2O. Fluid Phase Equilib 2014;361:175–80.

[40] Ozaki M, Tomura S, Ohmura R, Mori YH. Comparative study of large-scale hydrogen storage technologies: Is hydrate-based storage at advantage over existing technologies? Int J Hydrogen Energy 2014;39:3327–41.

[41] Chapoy A, Anderson R, Tohidi B. Low-pressure molecular hydrogen storage in semi-clathrate hydrates of quaternary ammonium compounds. J Am Chem Soc 2007;129:746–7.

[42] Gholinezhad J, Chapoy A, Tohidi B. Separation and capture of carbon dioxide from CO2/H2 syngas mixture using semi-clathrate hydrates. Chem Eng Res Des 2011;89:1747–51.

[43] Hall C, Tharakan P, Hallock J, Cleveland C, Jefferson M. Hydrocarbons and the evolution of human culture. Nature 2003;426:318–22.

[44] Chatti I, Delahaye A, Fournaison L, Petitet J-P. Benefits and drawbacks of clathrate hydrates: a review of their areas of interest. Energy Convers Manag 2005;46:1333–43.

[45] Mohammadi AH, Eslamimanesh A, Belandria V, Richon D. Phase Equilibria of Semiclathrate Hydrates of CO2, N2, CH4, or H2 + Tetra-n-butylammonium Bromide Aqueous Solution. J Chem Eng Data 2011;56:3855–65. doi:10.1021/je2005159.

[46] Tajima H, Yamasaki A, Kiyono F. Energy consumption estimation for greenhouse gas separation processes by clathrate hydrate formation. Energy 2004;29:1713–29.

[47] Zhang J, Yedlapalli P, Lee JW. Thermodynamic analysis of hydrate-based pre-combustion capture of CO2. Chem Eng Sci 2009;64:4732–6.

[48] Bruusgaard H, Beltrán JG, Servio P. Solubility measurements for the CH4+ CO2+ H2O system under hydrate–liquid–vapor equilibrium. Fluid Phase Equilib 2010;296:106–9.

[49] Linga P, Kumar R, Englezos P. The clathrate hydrate process for post and pre-combustion capture of carbon dioxide. J Hazard Mater 2007;149:625–9.

[50] Chong ZR, He T, Babu P, Zheng J, Linga P. Economic evaluation of energy efficient hydrate based desalination utilizing cold energy from liquefied natural gas (LNG). Desalination 2019;463:69–80.

[51] Ho-Van S, Bouillot B, Douzet J, Babakhani SM, Herri J-M. Implementing cyclopentane hydrates phase equilibrium data and simulations in brine solutions. Ind Eng Chem Res 2018;57:14774–83.

[52] Cha J-H, Seol Y. Increasing gas hydrate formation temperature for desalination of high salinity produced water with secondary guests. ACS Sustain Chem Eng 2013;1:1218–24.

[53] Majorowicz JA, Osadetz KG. Gas hydrate distribution and volume in Canada. Am Assoc Pet Geol Bull 2001;85:1211–30.

[54] Numasawa M, Yamamoto K, Yasuda M, Fujii T, Fujii K, Dallimore SR, et al. Objectives and operation overview of the 2007 JOGMEC/NRCAN/AURORA Mallik 2L-38 gas hydrate production test 2008.

[55] Schoderbek D, Farrell H, Howard J, Raterman K, Silpngarmlert S, Martin K, et al. ConocoPhillips Gas Hydrate Production Test Final Technical Report. Prep by Conoc Co United States Dep Energy, Natl Energy Technol Lab 2013:Medium: ED; Size: 204 p.

[56] Chen L, Yamada H, Kanda Y, Okajima J, Komiya A, Maruyama S. Investigation on the dissociation flow of methane hydrate cores: numerical modeling and experimental verification. Chem Eng Sci 2017;163:31–43.

[57] Sun S, Zhao J, Yu D. Dissociation enthalpy of methane hydrate in salt solution. Fluid Phase Equilib 2018;456:92–7. doi:10.1016/J.FLUID.2017.10.013.

[58] Holder GD, Angert PF. Simulation of gas production from a reservoir containing both gas hydrates and free natural gas. SPE Annu. Tech. Conf. Exhib., Society of Petroleum Engineers; 1982.

[59] Sun C-Y, Chen G-J. Methane hydrate dissociation above 0°C and below 0°C. Fluid Phase Equilib 2006;242:123–8. doi:https://doi.org/10.1016/j.fluid.2006.01.025.

[60] Goel N, Wiggins M, Shah S. Analytical modeling of gas recovery from in situ hydrates dissociation. J Pet Sci Eng 2001;29:115–27. doi:10.1016/S0920-4105(01)00094-8.

[61] Kono HO, Narasimhan S, Song F, Smith DH. Synthesis of methane gas hydrate in porous sediments and its dissociation by depressurizing. Powder Technol 2002;122:239–46.

[62] Zhao J, Zhu Z, Song Y, Liu W, Zhang Y, Wang D. Analyzing the process of gas production for natural gas hydrate using depressurization. Appl Energy 2015;142:125–34. doi:https://doi.org/10.1016/j.apenergy.2014.12.071.

[63] Circone S, Stern LA, Kirby SH, Pinkston JC, Durham WB. Methane hydrate dissociation rates at 0.1 MPa and temperatures above 272 K. Ann N Y Acad Sci 2000;912:544–55.

[64] Tang L-G, Li X-S, Feng Z-P, Li G, Fan S-S. Control Mechanisms for Gas Hydrate Production by Depressurization in Different Scale Hydrate Reservoirs. Energy & Fuels 2007;21:227–33. doi:10.1021/ef0601869.

[65] Haligva C, Linga P, A. Ripmeester J, Englezos P. Recovery of Methane from a Variable-Volume Bed of Silica Sand/Hydrate by Depressurization. Energy & Fuels 2010;24:2947–55. doi:10.1021/ef901220m.

[66] Oyama H, Konno Y, Masuda Y, Narita H. Dependence of depressurization-induced dissociation of methane hydrate bearing laboratory cores on heat transfer. Energy & Fuels 2009;23:4995–5002.

[67] Li B, Li X-S, Li G, Feng J-C, Wang Y. Depressurization induced gas production from hydrate deposits with low gas saturation in a pilot-scale hydrate simulator. Appl Energy 2014;129:274–86.

[68] Yousif MH, Abass HH, Selim MS, Sloan ED. Experimental and theoretical investigation of methane-gas-hydrate dissociation in porous media. SPE Reserv Eng 1991;6:69–76.

[69] Collett TS. Energy resource potential of natural gas hydrates. Am Assoc Pet Geol Bull 2002;86:1971–92.

[70] Behi H, Ghanbarpour M, Behi M. Investigation of PCM-assisted heat pipe for electronic cooling. Appl Therm Eng 2017;127:1132–42.

[71] Yezdimer EM, Cummings PT, Chialvo AA. Determination of the Gibbs Free Energy of Gas Replacement in SI Clathrate Hydrates by Molecular Simulation. J Phys Chem A 2002;106:7982–7. doi:10.1021/jp020795r.

[72] Zhao J, Zhang L, Chen X, Fu Z, Liu Y, Song Y. Experimental Study of Conditions for Methane Hydrate Productivity by the CO2 Swap Method. Energy & Fuels 2015;29:6887–95. doi:10.1021/acs.energyfuels.5b00913.

[73] Lee Y, Choi W, Shin K, Seo Y. CH4-CO2 replacement occurring in sII natural gas hydrates for CH4 recovery and CO2 sequestration. Energy Convers Manag 2017;150:356–64. doi:10.1016/J.ENCONMAN.2017.08.023.

[74] Bishnoi PR, Dholabhai PD. Equilibrium conditions for hydrate formation for a ternary mixture of methane, propane and carbon dioxide, and a natural gas mixture in the presence of electrolytes and methanol. Fluid Phase Equilib 1999;158:821–7.

[75] Schicks JM, Spangenberg E, Giese R, Steinhauer B, Klump J, Luzi M. New approaches for the production of hydrocarbons from hydrate bearing sediments. Energies 2011;4:151–72.

[76] Bai Y, Li Q. Simulation of gas production from hydrate reservoir by the combination of warm water flooding and depressurization. Sci China Technol Sci 2010;53:2469–76.

[77] Falser S, Uchida S, Palmer AC, Soga K, Tan TS. Increased gas production from hydrates by combining depressurization with heating of the wellbore. Energy & Fuels 2012;26:6259–67.

[78] LI S, CHEN Y, ZHANG W, XIA X. Experimental study of natural gas hydrate dissociation in porous media by thermal stimulation and depressurization. J Exp Mech 2011;2.

[79] Wang B, Dong H, Liu Y, Lv X, Liu Y, Zhao J, et al. Evaluation of thermal stimulation on gas production from depressurized methane hydrate deposits☆. Appl Energy 2018;227:710–8.

[80] Kim J, Chang D, Park KH, Seo Y. Risk Management of Hydrate Reformation Using Synergistic Inhibition During Methane Hydrate Production. 28th Int. Ocean Polar Eng. Conf., OnePetro; 2018.

[81] Kim J, Kim H, hoon Sohn Y, Chang D, Seo Y, Kang S-P. Prevention of methane hydrate re-formation in transport pipeline using thermodynamic and kinetic hydrate inhibitors. J Pet Sci Eng 2017;154:114–25.

[82] Ahn T, Kang JM, Lee J, Park C. Experimental investigation of methane hydrate reformation under dissociation process. Ninet. Int. Offshore Polar Eng. Conf., OnePetro; 2009.

[83] Zhao J, Zhang L, Chen X, Zhang Y, Liu Y, Song Y. Combined replacement and depressurization methane hydrate recovery method. Energy Explor Exploit 2016;34:129–39. doi:10.1177/0144598715623676.

[84] Zeng F, Guo J, Ma S, Chen Z. 3D observations of the hydraulic fracturing process for a model non-cemented horizontal well under true triaxial conditions using an X-ray CT imaging technique. J Nat Gas Sci Eng 2018;52:128–40. doi:10.1016/J.JNGSE.2018.01.033.

[85] Zhong J-R, Sun Y-F, Li W-Z, Xie Y, Chen G-J, Sun C-Y, et al. Structural transition range of methane-ethane gas hydrates during decomposition below ice point. Appl Energy 2019;250:873–81.

[86] Chen C, Li X, Chen Z, Yan K, Zhang Y, Xu C. Raman Spectroscopic Analysis on the Hydrate Formed in the Hydrate-Based Flue Gas Separation Process in Presence of Sulfur Dioxide and Tetra-n-butyl Ammonium Bromide. Spectrosc Lett 2015;48:499–505.

[87] Xu C-G, Cai J, Lin F, Chen Z-Y, Li X-S. Raman analysis on methane production from natural gas hydrate by carbon dioxide–methane replacement. Energy 2015;79:111–6. doi:10.1016/J.ENERGY.2014.10.068.

[88] Jiang G, Wu Q, Zhan J. Experimental studies of the formation and dissociation of methane hydrate in loess. J Nat Gas Chem 2010;19:217–23. doi:10.1016/S1003-9953(09)60067-0.

[89] Mekala P, Babu P, Sangwai JS, Linga P. Formation and dissociation kinetics of methane hydrates in seawater and silica sand. Energy & Fuels 2014;28:2708–16.

[90] Kim HC, Bishnoi PR, Heidemann RA, Rizvi SSH. Kinetics of methane hydrate decomposition. Chem Eng Sci 1987;42:1645–53.

[91] Falenty A, Kuhs WF. “Self-Preservation” of CO2 Gas Hydrates Surface Microstructure and Ice Perfection. J Phys Chem B 2009;113:15975–88.

[92] Komai T, Kang S-P, Yoon J-H, Yamamoto Y, Kawamura T, Ohtake M. In situ Raman spectroscopy investigation of the dissociation of methane hydrate at temperatures just below the ice point. J Phys Chem B 2004;108:8062–8.

[93] Peng JW, Schiffer CA, Xu P, van Gunsteren WF, Ernst RR. Investigations of peptide hydration using NMR and molecular dynamics simulations: A study of effects of water on the conformation and dynamics of antamanide. J Biomol NMR 1996;8:453–76. doi:10.1007/BF00228147.

[94] Kondori J, James L, Zendehboudi S. Molecular scale modeling approach to evaluate stability and dissociation of methane and carbon dioxide hydrates. J Mol Liq 2020;297:111503.

[95] Kumar A, Veluswamy HP, Linga P, Kumar R. Molecular level investigations and stability analysis of mixed methane-tetrahydrofuran hydrates: Implications to energy storage. Fuel 2019;236:1505–11.

[96] Tuckerman M. Statistical mechanics: theory and molecular simulation. Oxford university press; 2010.

[97] Ding LY, Geng CY, Zhao YH, Wen H. Molecular dynamics simulation on the dissociation process of methane hydrates. Mol Simul 2007;33:1005–16. doi:10.1080/08927020701528524.

[98] Orsi M. Molecular dynamics simulation of humic substances. Chem Biol Technol Agric 2014;1:1–14.

[99] Verlet L. Computer" experiments" on classical fluids. I. Thermodynamical properties of Lennard-Jones molecules. Phys Rev 1967;159:98.

[100] Hockney RW. The potential calculation and some applications. Methods Comput Phys 1970;9:136.

[101] Gear CW. Numerical initial value problems in ordinary differential equations. Prentice-Hall Ser Autom Comput 1971.

[102] Brooks BR, Bruccoleri RE, Olafson BD, States DJ, Swaminathan S a, Karplus M. CHARMM: a program for macromolecular energy, minimization, and dynamics calculations. J Comput Chem 1983;4:187–217.

[103] Hess B, Kutzner C, van der Spoel D, Lindahl E. GROMACS 4: Algorithms for Highly Efficient, Load-Balanced, and Scalable Molecular Simulation. J Chem Theory Comput 2008;4:435–47. doi:10.1021/ct700301q.

[104] Plimpton S. Fast parallel algorithms for short-range molecular dynamics. J Comput Phys 1995;117:1–19.

[105] Todorov IT, Smith W, Trachenko K, Dove MT. DL_POLY_3: new dimensions in molecular dynamics simulations via massive parallelism. J Mater Chem 2006;16:1911–8.

[106] Li J, Liang ZJ, Wang ZL. Characterization of microscopic nature of methane hydrate

decomposition by different molecular models. CIESC J 2020;71:955–64.

[107] Walsh MR, Koh CA, Sloan ED, Sum AK, Wu DT. Microsecond Simulations of Spontaneous Methane Hydrate Nucleation and Growth. Science (80-) 2009;326:1095 LP – 1098. doi:10.1126/science.1174010.

[108] Choudhary N, Chakrabarty S, Roy S, Kumar R. A comparison of different water models for melting point calculation of methane hydrate using molecular dynamics simulations. Chem Phys 2019;516:6–14. doi:10.1016/J.CHEMPHYS.2018.08.036.

[109] Huggins DJ. Correlations in liquid water for the TIP3P-Ewald, TIP4P-2005, TIP5P-Ewald, and SWM4-NDP models. J Chem Phys 2012;136:64518.

[110] English NJ, Phelan GM. Molecular dynamics study of thermal-driven methane hydrate dissociation. J Chem Phys 2009;131:74704. doi:10.1063/1.3211089.

[111] Alavi S, Thompson DL. Molecular dynamics studies of melting and some liquid-state properties of 1-ethyl-3-methylimidazolium hexafluorophosphate [emim][PF6]. J Chem Phys 2005;122:154704. doi:10.1063/1.1880932.

[112] Sloan ED. The Colorado School of Mines hydrate prediction program CSMHYD. Cent Hydrate Res Color Sch Mines 1996.

[113] Singh Baghel V, Kumar R, Roy S. Heat Transfer Calculations for Decomposition of Structure I Methane Hydrates by Molecular Dynamics Simulation. J Phys Chem C 2013;117:12172–82. doi:10.1021/jp4023772.

[114] MacKerell Jr AD, Bashford D, Bellott M, Dunbrack Jr RL, Evanseck JD, Field MJ, et al. All-atom empirical potential for molecular modeling and dynamics studies of proteins. J Phys Chem B 1998;102:3586–616.

[115] Martin MG, Siepmann JI. Transferable potentials for phase equilibria. 1. United-atom description of n-alkanes. J Phys Chem B 1998;102:2569–77.

[116] Guillot B, Guissani Y, Bratos S. A computer-simulation study of hydrophobic hydration of rare gases and of methane. I. Thermodynamic and structural properties. J Chem Phys 1991;95:3643–8.

[117] Jacobson LC, Hujo W, Molinero V. Nucleation pathways of clathrate hydrates: effect of guest size and solubility. J Phys Chem B 2010;114:13796–807.

[118] Matsumoto M. Four-body cooperativity in hydrophonic association of methane. J Phys Chem Lett 2010;1:1552–6.

[119] Nguyen AH, Jacobson LC, Molinero V. Structure of the clathrate/solution interface and mechanism of cross-nucleation of clathrate hydrates. J Phys Chem C 2012;116:19828–38.

[120] Walsh MR, Rainey JD, Lafond PG, Park D-H, Beckham GT, Jones MD, et al. The cages, dynamics, and structuring of incipient methane clathrate hydrates. Phys Chem Chem Phys 2011;13:19951–9.

[121] Walsh MR, Beckham GT, Koh CA, Sloan ED, Wu DT, Sum AK. Methane hydrate nucleation rates from molecular dynamics simulations: Effects of aqueous methane concentration, interfacial curvature, and system size. J Phys Chem C 2011;115:21241–8.

[122] Bagherzadeh SA, Alavi S, Ripmeester JA, Englezos P. Evolution of methane during gas

hydrate dissociation. Fluid Phase Equilib 2013;358:114–20. doi:10.1016/j.fluid.2013.08.017.

[123] Alavi S, Ripmeester JA. Nonequilibrium adiabatic molecular dynamics simulations of methane clathrate hydrate decomposition. J Chem Phys 2010;132:144703.

[124] Luis DP, García-González A, Saint-Martin H. A theoretical study of the hydration of methane, from the aqueous solution to the sI hydrate-liquid water-gas coexistence. Int J Mol Sci 2016;17:378.

[125] Michalis VK, Costandy J, Tsimpanogiannis IN, Stubos AK, Economou IG. Prediction of the phase equilibria of methane hydrates using the direct phase coexistence methodology. J Chem Phys 2015;142:44501.

[126] Yagasaki T, Matsumoto M, Andoh Y, Okazaki S, Tanaka H. Dissociation of methane hydrate in aqueous NaCl solutions. J Phys Chem B 2014;118:11797–804.

[127] Míguez JM, Conde MM, Torré JP, Blas FJ, Piñeiro MM, Vega C. Molecular dynamics simulation of CO2 hydrates: Prediction of three phase coexistence line. J Chem Phys 2015;142. doi:10.1063/1.4916119.

[128] BÁEZ LA, CLANCY P. Computer Simulation of the Crystal Growth and Dissolution of Natural Gas Hydratesa. Ann N Y Acad Sci 1994;715:177–86. doi:https://doi.org/10.1111/j.1749-6632.1994.tb38833.x.

[129] RODGER PM. Methane Hydrate: Melting and Memory. Ann N Y Acad Sci 2000;912:474–82. doi:https://doi.org/10.1111/j.1749-6632.2000.tb06802.x.

[130] Myshakin EM, Jiang H, Warzinski RP, Jordan KD. Molecular dynamics simulations of methane hydrate decomposition. J Phys Chem A 2009;113:1913–21.

[131] Sarupria S, G. Debenedetti P. Molecular Dynamics Study of Carbon Dioxide Hydrate Dissociation. J Phys Chem A 2011;115:6102–11. doi:10.1021/jp110868t.

[132] Yan K, Li X, Chen Z, Li B, Xu C. Molecular dynamics simulation of methane hydrate dissociation by depressurisation. Mol Simul 2013;39:251–60. doi:10.1080/08927022.2012.718437.

[133] Clarke MA, Bishnoi PR. Determination of the intrinsic rate constant and activation energy of CO2 gas hydrate decomposition using in-situ particle size analysis. Chem Eng Sci 2004;59:2983–93. doi:10.1016/j.ces.2004.04.030.

3 Macroscopic study of the decomposition of hydrate spheres below the freezing point of water

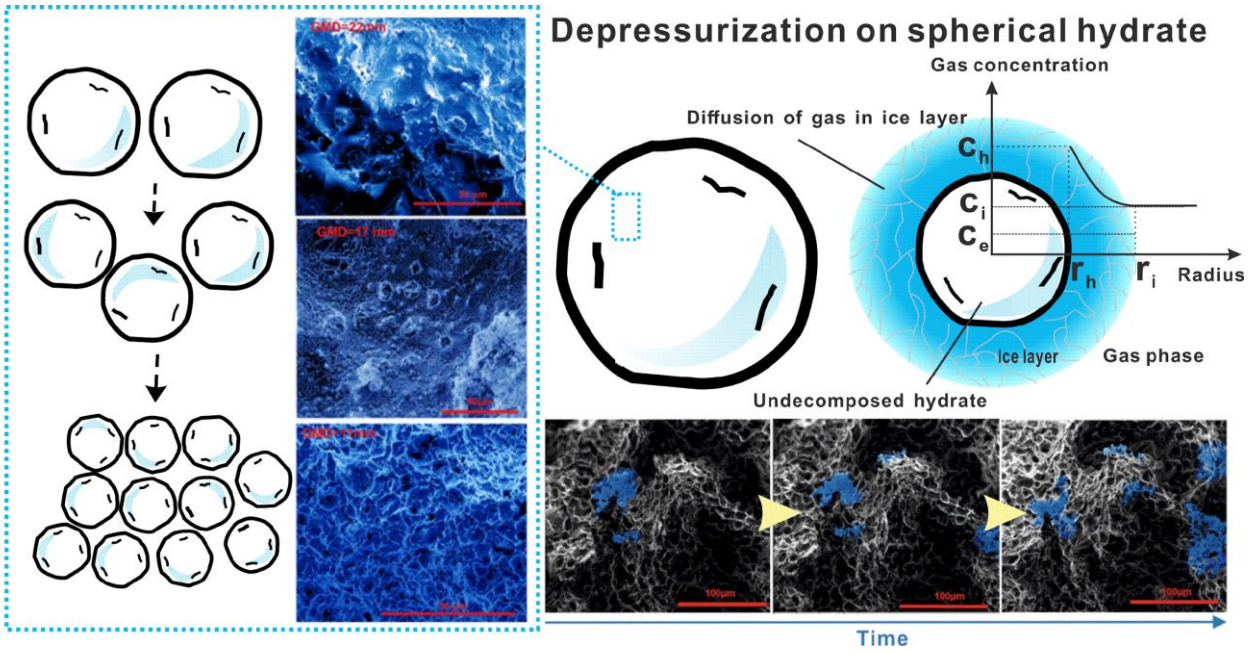

Highlights

1. The effect of the surface-area-to-mass ratio of hydrate samples on decomposition behavior is experimentally investigated.
2. Decomposition kinetics and gas diffusion jointly govern the hydrate decomposition reaction. The dominant process depends on the production pressure and pellet size.
3. A randomly distributed ice-layer shielding mechanism considering the influence of surface-area-to-mass ratio is proposed.

Abstract:

Depressurization is a promising technique for extracting gas contained within natural gas hydrate sediment. Most researchers agree that the gas production behavior found in hydrate-bearing sediments is an interfacial decomposition process. A better understanding of the kinetics of hydrate decomposition below the freezing point of water is essential to reliably predict the potential natural gas production from hydrate reservoirs. Due to the accumulation feature of gas hydrates, determining the surface area and volume of hydrate particles is always a challenging undertaking.

To investigate the effects of particle diameter, or surface-area-to mass ratio, on the depressurization decomposition process, approximately spherical methane hydrate samples with 11 mm, 18 mm, and 22 mm diameters were prepared to represent hydrate particles macroscopically. Experimental hydrate decomposition by depressurization was then carried out and the methane recovery ratio and gas production rate were measured. The results show that the effect of pressure is significant on the production percentage compared with the surface-area-to-mass ratio. With regards to production rates during decomposition, the extent of influence of production pressure is consistent with the surface-area-to-mass ratio. The driving forces of pressure difference and gas diffusion jointly govern the decomposition reaction. A cryogenic scanning electron microscopy (SEM) image of hydrate samples suggests that a hydrate larger in diameter has a smoother surface, which in turn could make it difficult for the ice cluster to attach to the hydrate surface. Ice clusters initially formed on the hydrate surface move, so a randomly distributed ice-layer shielding mechanism with different surface-area-to-mass ratios is proposed. Furthermore, no bound water was found to exist between pellets during production which could be deemed reliable for establishing the decomposition model.

3.1. Introduction

Energy is essential for achieving not only economic, social, and environmental goals but also for sustainable human development. The global energy system currently faces many challenges, including environmental issues such as climate change and the pollution of air and water. Another challenge concerns higher levels of consumption, restrictions on access, and energy security. For this challenge, the discovery of shale gas marked a considerable

shift in the global energy framework away from traditional coal fuel, but another hydrocarbon resource, natural gas hydrates (NGHs), has the potential to do even more. Natural gas hydrates are naturally occurring ice-like solids that are made of water molecules (as a cage-forming host) and gas molecules (as guests) [1]. Natural gas hydrate is globally abundant beneath the permafrost region, at depths ranging from about 130 to 2000 m, along ocean continental shelves, ranging from 100 to 1100 m in depth [2]. More than 99% of natural hydrates are methane-based, which motivated researchers to consider them as a potential energy source.

In recent years, two main hydrate research areas have surged in popularity, namely the fundamentals of hydrates, related to hydrate crystal structures and properties [3–6], thermodynamics and kinetics of hydrate formation and decomposition is much more challenging to investigate rested on a comparatively sound thermodynamic foundation. For the purpose of methane exploitation, another area has concentrated mainly on techniques to economically and safely produce natural gas from NGH reservoirs [7,8]. The application of hydrates is also popular in energy recovery, CO_2 capture and storage, gas separation, water desalination, gas storage and transport, refrigeration, etc. [9–11]. More recently, a variety of methods have received considerable attention for natural gas exploration from hydrates [12–14], among which the most widely used, namely depressurization, which decreases system pressure below that required for hydrate formation at a given temperature, is regarded as the most efficient [15–17]. The production of the hydrate via depressurization requires a hydrate decomposition process that releases gaseous methane and water in the hydrate as products. The overall process involves two steps: the initial destruction of the hydrate host lattice on the surface of the hydrate and the desorption of guest gas from the surface [18]. Reasonable conclusions have been drawn that the decomposition rate of hydrate is related to its dissociation process, which is controlled by the pressure difference between the hydrate equilibrium pressure and the solid hydrate pressure, as well as the diffusion process where the released gas-phase methane molecules travel from the solid hydrate surface to a neighboring ice layer. One of the challenging aspects in investigating hydrate decomposition kinetics is quantifying the decomposition rate, which is of fundamental importance to advance our understanding of gas hydrate production. The conventional macroscopic measurement method used to investigate hydrates can be inaccurate and difficult if the hydrate sample species are small and bound

water or ice are present between hydrate particles, leading to a deviated estimation of particle sphericity. As they make kinetics modeling a complex task, more fundamental studies are thus needed to measure the time-dependence of hydrate decomposition more accurately.

The mechanisms for hydrate dissociation are different depending on whether the temperature is above or below 0 °C. Many researchers have investigated hydrate decomposition characteristics below the ice melting point in laboratory systems in an effort to understand decomposition morphologies and the gas hydrate mechanism [19,20]. Stern et al. [20], for instance, conducted methane hydrate (MH) decomposition under 0.1 MPa, at temperatures ranging from 193 to 290 K, and found that the decomposition rate at a temperature of 242-271 K was lower than the theoretical value – a phenomenon explained as a “self-preservation effect”. This self-preservation effect has a potential application for the successful retrieval of natural gas hydrate or hydrate-bearing sediments from remote settings, as well as for the temporary low-pressure transport and storage of natural gas. The decomposition of gas below the water freezing temperature, and its simulation, is much more complex, and currently, there are no reliable calculation methods. Many researchers have proposed different hydrate dissociation patterns for hydrates at temperatures $T < 0$ °C [21-23], but these models are based on the hypothesis of uniform spherical hydrate particles. Clarke and Bishnoi et al. [24] proposed a model that included particle sphericity and shape factors, but it remains challenging to apply to hydrate particles in the real world. These effects should be part of an effective dissociation model of methane hydrate.

All of the dissociation models mentioned above are based on a regular geometrical spherical hydrate core and assume that all hydrate particles have the same geometrical diameter prior to dissociation. A more accurate measurement was performed by Clarke and Bishnoi [133] with a particle-size analyzer, and a similar dissociation correlation with a particle-size analyzer and a similar dissociation correlation was proposed. These dissociation models are based on the concept that the driving force for dissociation is a fugacity difference from the equilibrium state. Sean et al. [25] suggested a new dissociation model (hereafter the SSYK model) in which hydrate dissociation is driven by the difference in Gibbs free energy between the hydrate phase and the ambient aqueous phase. The advantage of the SSYK model is that it applies to decomposition by reducing gas

concentration in water. Various factors have an impact on the hydrate dissociation rate, such as temperature, pressure, and surface area of hydrate particles, and different geometric porosity parameters [26-28]. Even a slight change in the granule diameter (about 10%) can significantly affect the dissociation rate because it is related nonlinearly to the initial diameter of a particle. Li et al. [29] also modeled hydrate dissociation kinetics under the assumptions of the negligible influence of bound water and considering the hydrates are homogeneously distributed with identical diameter.

In this study, we illustrate our findings on how the macroscopic size of MH affects its decomposition. The study was designed to synthesize spherical methane hydrates of three different sizes, varying from 11 to 22 mm. The isothermal decomposition of methane hydrate is considered at a subzero temperature to examine the ice-shielding mechanism involved in hydrate decomposition. Decomposition kinetic data were obtained using the depressurizing method for different methane hydrate pellet sizes and characterized by cryogenic SEM. As a result of this work, we solved the difficulty in maintaining the uniform size and distribution of hydrate pellets during experiments. In addition, a hydrate decomposition mechanism considering hydrate size was proposed.

3.2. Experimental section

3.2.1. Materials and apparatus

The work for this study consists of setups for hydrate sample preparation and depressurization, respectively. For all hydrate formation, ultra-high purity (>99.99%) methane and distilled water were used. A schematic of the apparatus employed for spherical hydrate sample preparation is shown in Figure 3.1. It consists of a high-pressure crystallizer, a cryostat, methane gas supply, pressure and temperature sensors, a pressure regulator and a data acquisition computer. Spherical hydrate samples were analyzed using a cryogenic electron microscope (Quanta FEG 200 ESEM, voltage: 5kV).

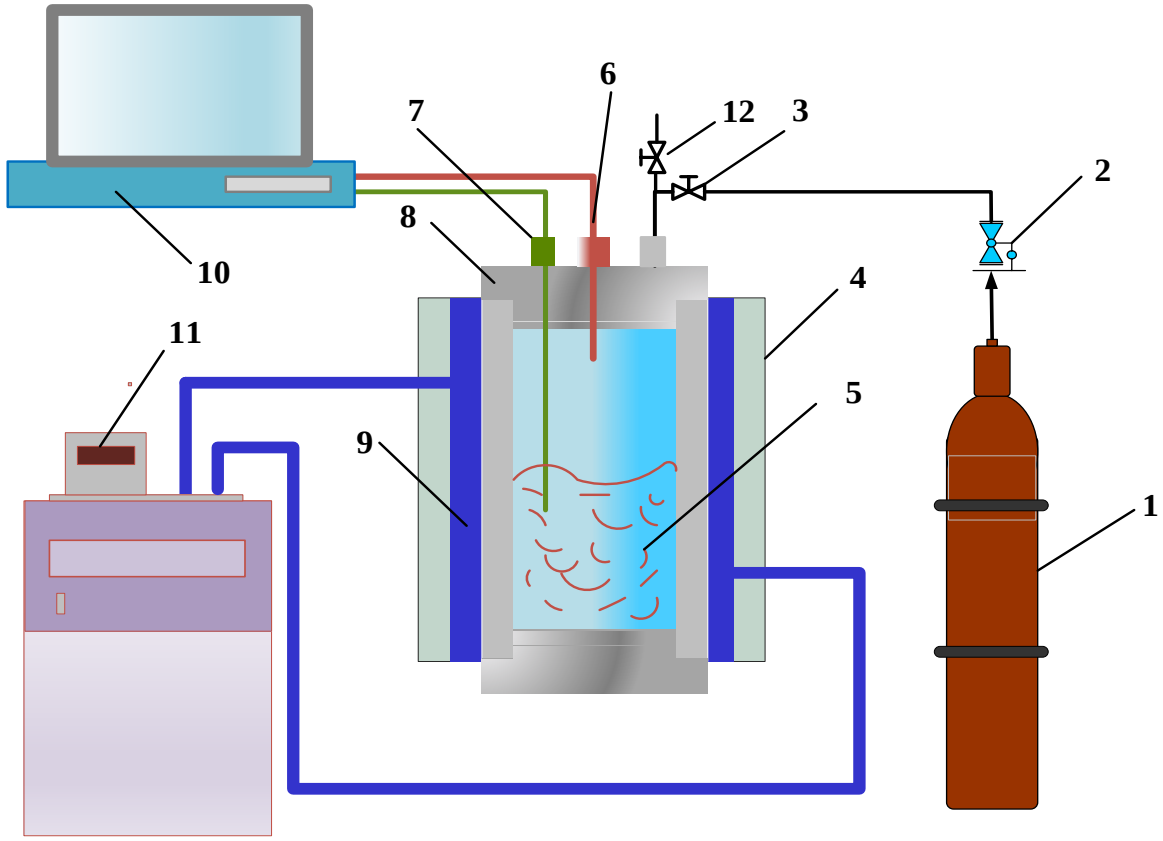

Figure 3.1 Experimental setup for hydrate sample preparation: (1)- gas supply; (2)- pressure regulator; (3)- valve; (4)- insulation material; (5)- hydrate formation vessel; (6)- pressure sensor; (7)- thermocouple; (8)- lid; (9)- cooling jacket; (10)- data acquisition computer; (11)- cryostat; (12)- exhaust valve

The setup shown in Figure 3.2 was employed for the macroscopic experimental study of hydrate depressurization. Each group of spherical samples was assembled in the main cell, shown as (4), with an inner volume of 100 mL, where depressurization took place. Depressurization operations for all experiments were controlled by a back pressure regulator. The gas released from hydrate decomposition flows into a gas collector, shown as (10) in Figure 3.2. To avoid the gas temperature drop caused by the Joule-Thomson effect, both the main cell and the gas collector were maintained at the same temperature by a cooling bath. Pressures of the depressurization vessel and gas collector were monitored by a data acquisition system, as well as the temperature of the vessel and collector.

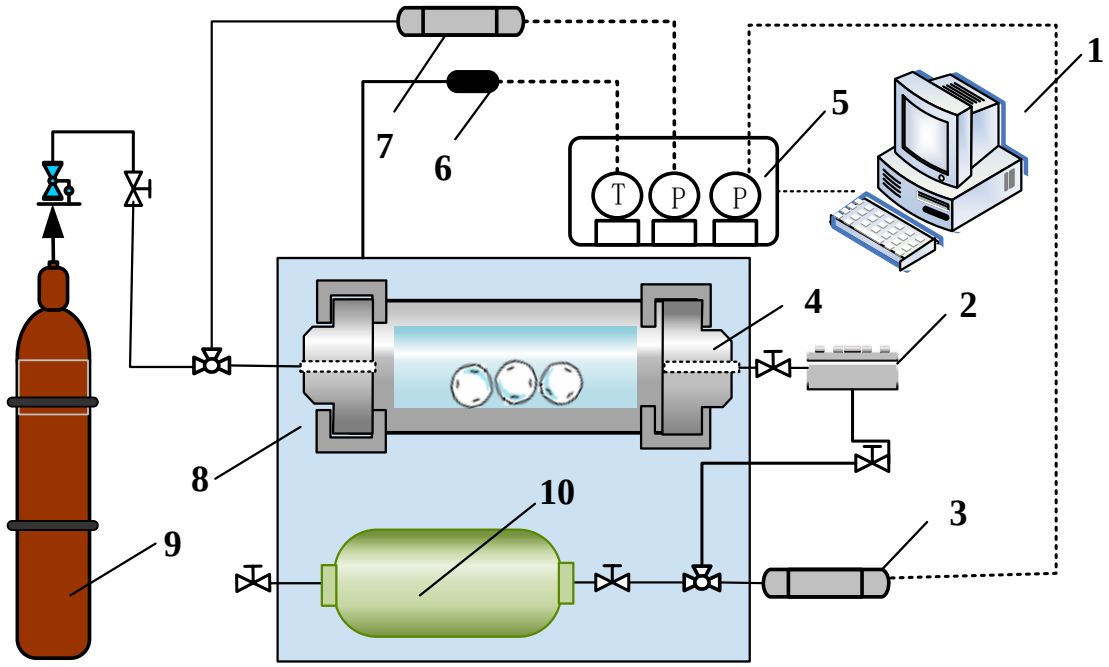

Figure 3.2 Experimental setup for hydrate depressurization: 1- data acquisition computer; 2- back pressure regulator; 3,7- pressure sensors; 4- hydrate depressurization vessel; 5- data acquisition; 6- thermocouple; 8- cooling bath; 9- methane gas supply; 10- gas collector.

3.2.2. Experimental Procedures

3.2.2.1. MH sample preparation

The spherical hydrate samples in this work were formed from a mixture of similarly sized ice powder and hydrate powder to ensure the even distribution of hydrate and the full conversion of water in the hydrate spheres, as in the following procedure:

1) Spray 0.5 kg distilled water into 1 liter of liquid nitrogen contained in mortar to form ice particles.
2) Collect the granular ice after the liquid nitrogen vaporizes.
3) Grind down the ice with a pestle.
4) Before packing into the vessel for hydrate conversion, sieve the ground ice into sizes ranging from 250 to 400 microns, as shown in Figure 3.3.

Figure 3.3 Methane hydrate powder, ranging from 250 to 400 microns.

5) Put the ice powder with known diameters into a pre-cooled vessel at 250 K, followed by injecting CH_4 to a pressure of 8.0 MPa. Temperature is then shifted to 273.15 K for 2 weeks in order to synthesize micro-sized hydrate particles, during which time the slow melting of the ice powder facilitates hydrate formation [30,31].
6) Remove the prepared hydrate powder and transfer them to spherical silicon molds (with diameters of 11 mm, 18 mm, and 22 mm) together with a small amount of ice powder in liquid nitrogen. Ice powder has the advantage of fast heat transfer and a specific surface area that results in a high conversion ratio.
7) Replace molds with the hydrate and ice powder into the crystallizer with pressurized CH_4 at 9 MPa and maintain at 263 K for two weeks before subsequently ramping 274 K to completely transform ice powder into hydrate for three weeks. In this period, ice in the sample is allowed to melt and merge with the hydrate powder as the temperature is raised above the ice point [31].
8) After preparing spherical hydrate samples of different specific sizes, take out the spherical hydrate samples by decreasing the system temperature to 250 K, followed by releasing extra CH_4 gas. The samples are stored in a liquid nitrogen Dewar before cryogenic electron microscopy analysis. The scanning is done under vacuum, and the temperature is set to 103 K, with a low-voltage mode of 5 kV and electron probe diameter (spot size) 3.0. Images are taken at 3000× magnification.

Samples with smooth surface morphology without distinct defects are chosen as candidates for the depressurization experiments. The equivalent order of weight of samples is gathered for the depressurization process. Typical hydrate samples of different sizes are

shown in Figure 3.4. Samples are shown with uniform surface morphology for the corresponding diameter. An overall summary of the hydrate sample properties is given in Table 3.1.

Figure 3.4 Spheritic hydrate samples were synthesized at diameters of 22 mm, 18 mm, and11 mm.

Table 3.1 Properties of prepared spherical hydrate samples.

Normal diameter (mm)	Quantity	Total mass (g)	GMD (mm)		MM (g)		Surface-area-mass ratio (mm^2/g)	
			Avg.	Std.	Avg.	Std.	Avg.	Std.
11	11	7.1250	11.3	0.8	0.6090	0.0282	660.4	14.69
18	3	8.6749	17.7	0.9	2.3947	0.3115	387.7	36.20
22	2	7.6885	21.8	0.6	3.8192	0.2982	349.5	48.20

Avg.: Average values measured by a digital caliper and a digital balance scale at an accuracy of 0.0001g.

Std.: Standard deviation.

3.2.2.2. MH decomposition by depressurization

The hydrate sample synthesized from section 3.1.1.1 is transferred into the hydrate depressurization vessel in Figure 3.2. Hydrate decomposition by depressurization was carried out as follows:

1） Cool the system to 250 K.

2） Remove the hydrate samples from the liquid nitrogen storage and quickly place them into the hydrate depressurization vessel as shown in Figure 3.2.

3） Direct precooled methane gas to the vessel from the gas cylinder. Set the vessel pressure at the desired value shown in Table 3.2 by adjusting the back pressure regulator.

4） Shut down the methane gas supply. Maintain the desired pressure and temperature for 24 h to compensate for slight decomposition during transfer.

5） First, the pressure setting for the back pressure regulator was set slightly higher than that in the vessel. The outlet valve was then opened, and the back pressure regulator turned down, decreasing the outlet pressure gradually to a predetermined value (decomposition pressure) in a controlled way. At this pressure, hydrate decomposition lasts until very little gas is left. During the entire decomposition process, data for the evolution of gas released from the hydrates were obtained. The volume of released gas was expressed under standard conditions.

After each run, the cell was allowed to warm up slowly to room temperature, thus causing the hydrate to release all of its absorbed methane gas. During depressurization decomposition, the real-time number of moles of methane gas flowing into the collector part was calculated. In these experiments, the influence of heat transfer was eliminated by immersing the high-pressure cell in a constant-temperature water bath.

3.2.2.3. Data processing

The following pseudo-chemical equation describes the methane hydrate decomposition process at the MH-gas interface:

$$CH_4 \cdot nH_2O(s) \rightleftarrows CH_4(g) + nH_2O \quad (3\text{-}1)$$

where *n* stands for the hydration number *n*=5.9 being considered [32], the solid or liquid state of any water produced depends on the operation conditions. In our study, the water produced is in the solid phase as the operation is below the water freezing point. During the decomposition process, pressures in the hydrate depressurization vessel and gas collector, temperature records every 20 s by the data logger system. The real-time number of moles of methane gas n_g in the hydrate depressurization vessel throughout depressurization is

calculated by the equation (3-2). The volume of hydrate (V_h) in the vessel before depressurization is defined by equation (3-3).

$$n_g = \frac{P_t V_c}{Z_t R T} \tag{3-2}$$

$$V_h = \frac{M_h n_h}{\rho_h} \tag{3-3}$$

where P_t is the real-time pressure inside the cell, T is the average temperature measured by the thermocouple, V_c is the volume of the vessel occupied by the gas, and Z_t is the real-time gas compressibility factor corresponding to the temperature at a specific pressure. This was determined using the Peng-Robinson Equation of State (PR EOS) [33], where R is the ideal gas constant. n_h is the amount of methane hydrate synthesized in vessel. M_h represents the molar volume of gas (0.0224 m^3/mol), which is determined according to the International Union of Pure and Applied Chemistry (IUPAC) definition of standard temperature and pressure conditions (STP, 100,000 Pa and 273.15 K). The theoretical density (ρ_h)of hydrate density was 925 kg/m^3 [32,34], which was treated as the average density in this study.

The gas production percentage is defined as the ratio between gas produced and total moles of methane gas, including gas in the vapor phase ($n_{CH_4,H}$) and hydrate phase ($n_{CH_4,v}$) calculated by equation (3-4).

$$\mathrm{CH_4\ production\ percentag} = \frac{(n_{CH_4,g})_t}{n_{CH_4,H} + n_{CH_4,v}} \times 100\% \tag{3-4}$$

in the above equation, $(n_{CH_4,g})_t$ methane is the gas released at any time t during the production period.

During hydrate decomposition via depressurization, the produced gas was collected and recorded via form of pressure via the pressure sensor. The evolution of cumulative gas production is equivalent to the sum of the free gas released and the dissociated methane gas from hydrates over time. The rate of hydrate production over time was calculated using the following equation:

$$(\frac{dn}{dt})_t = \frac{n_{t+\Delta t} - n_t}{\Delta t} \tag{3-5}$$

3.2 Results and discussion

3.2.1. Influence of pressure on MH decomposition

Depressurization experiments were conducted after preparing the hydrate samples, and each group of experiments was conducted quantitatively on these samples. Due to the complex behavior of hydrate production below the freezing point of water, namely producing ice and gas instead of water and gas, it is important to investigate factors influencing hydrate production in this case. Decomposition driving force refers to any kind of parameter that can be used to the dissociation of hydrate, such as the difference between system temperature and equilibrium value, or the difference between system pressure and equilibrium value. The gas hydrate decomposition rate is directly linked to the pressure driving force that we define as the tendency of a system from an unstable state to an equilibrium condition with the relation of excess fugacity, composition, or temperature of the hydrate. In our experimental runs, the operational conditions were isothermal, so for simplicity, we relate the driving force to production pressure on methane gas production. Negative driving force values indicate the lower chemical potential of methane in the gas phase than in clathrates, consequently leading to decomposition.

A series of isothermal experiments was conducted on three groups of samples at a final constant pressure between 1.6 MPa and 2.4 MPa. Previous studies were limited by relatively small hydrate particles in irregular shapes, resulting obscuring the mechanism of individual particle size's influence on the decomposition process. Three groups were investigated in this with CH_4 hydrate samples in diameter from 11 mm to 22 mm. The quantity of samples in each group corresponded to three sizes of spherical hydrate, between 11 and 2, along with a decreasing hydrate diameter. The depressurization operations on hydrate samples were conducted by holding the total volume of each group of hydrate samples identical. Table 3.2 summarizes the experimental conditions and results of the current work. The slight differences observed in initial conditions are likely due to both deviations in the thermal and pressure transducers as well as variations in the hydration number of the methane hydrate.

Table 3.2 Depressurization operations on hydrate samples 11 mm, 18 mm and 22 mm in diameter.

Run	1	2	3	4	5	6	7	8	9
Normal particle size (mm)	11	11	11	18	18	18	22	22	22
Initial pressure (MPa)	6.2	6.2	6.3	6.2	6.1	6.4	6.2	6.1	6.2
Temperature (K)	272.4	272.4	272.4	272.4	272.4	272.4	272.4	272.4	272.4
Depressurization pressure (MPa)	1.6	2.0	2.4	1.6	2.0	2.4	1.6	2.0	2.4
Gas production percentage (%)	73.88	64.80	55.03	70.40	62.95	55.69	74.96	65.75	54.64
Average production rate (SCC/min)	0.83	0.77	0.63	2.98	2.59	2.49	4.93	4.03	3.00

From run 1 to 3, different pressure reductions were employed on a spherical hydrate sample with a diameter of 11 mm Figure 3.5 shows the evolution of the production percentage of methane hydrate at different production pressures. The cumulative gas produced and corresponding production rates for the three runs are illustrated in Figure 3.6 and Figure 3.6, respectively. The rates of production are derived from the slopes of the cumulative gas production curve at production pressures of 1.6 MPa, 2.0 MPa, and 2.4 MPa, respectively. The corresponding average production rates of individual hydrate pellet are 0.83 SCC/min, 0.77 SCC/min, and 0.63 SCC/min, which negatively correlated with production pressure, which indicates that higher production pressure will extend the production time. As presented in Figure 3.7, gas is released from hydrate rapidly within first 1min, followed by a relatively stable production rate. Nevertheless, there were differences in the production percentage in the final period and that of production rates mainly in the second period. The production percentage and the cumulative produced gas were relatively higher in the presence of low production pressure than under higher pressures. It is evident that as production pressure increased, both the production percentage and the cumulative gas decreased. From 73.88 % of gas production percentage at the pressure of 1.6 MPa to

55.03 % at production pressure of 2.4 MPa. The effect of the pressure driving force might play a significant role when MH samples of the same size are used in this process.

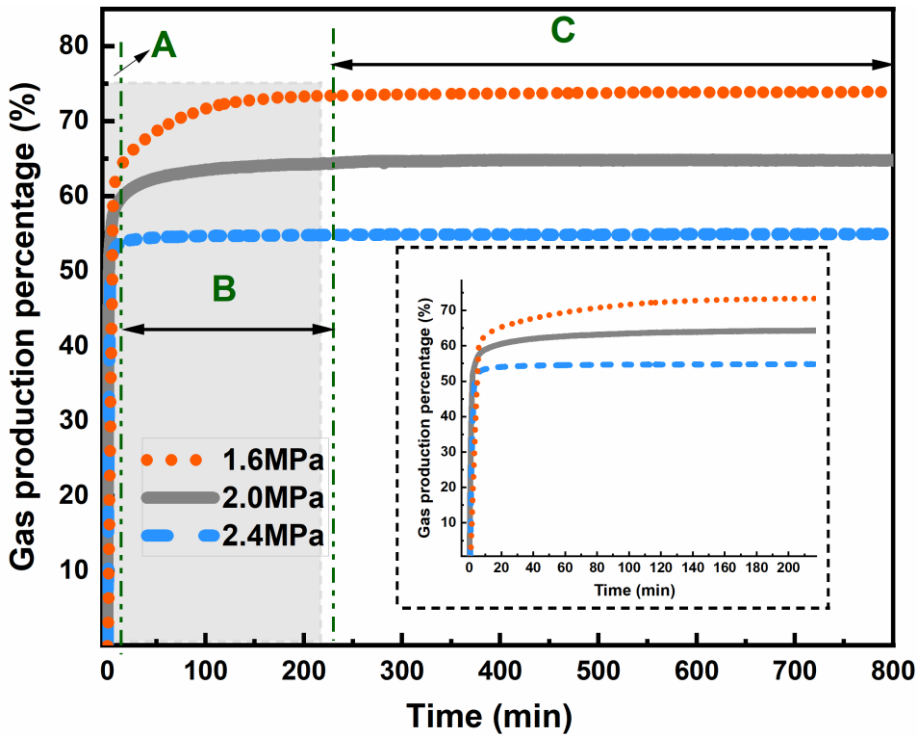

Figure 3.5 Gas production percentage from 11 mm-diameter hydrate samples at an initial pressure of 6.2 MPa and production pressures of 1.6 MPa (orange dotted line), 2.2 MPa (solid black line), and 2.4 MPa (blue dashed line) Temperature was maintained at 272.4 K during the whole process.

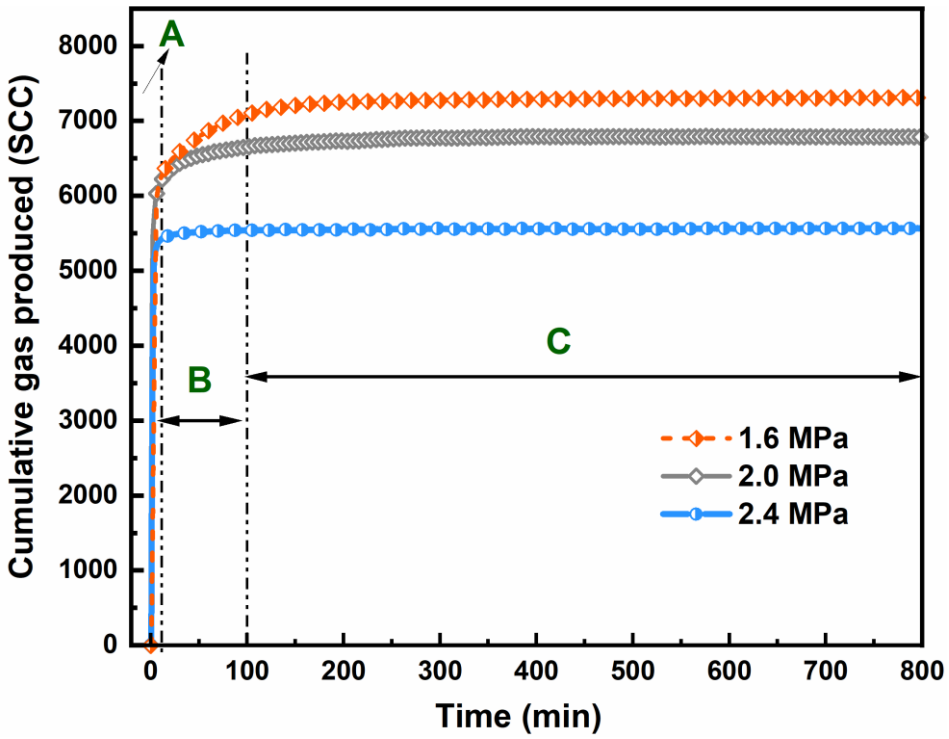

Figure 3.6 Cumulative gas produced from the hydrate sample and the gas production rate of an individual 11 mm-diameter sample at production pressures of 1.6 MPa, 2.0 MPa, and 2.4 MPa.

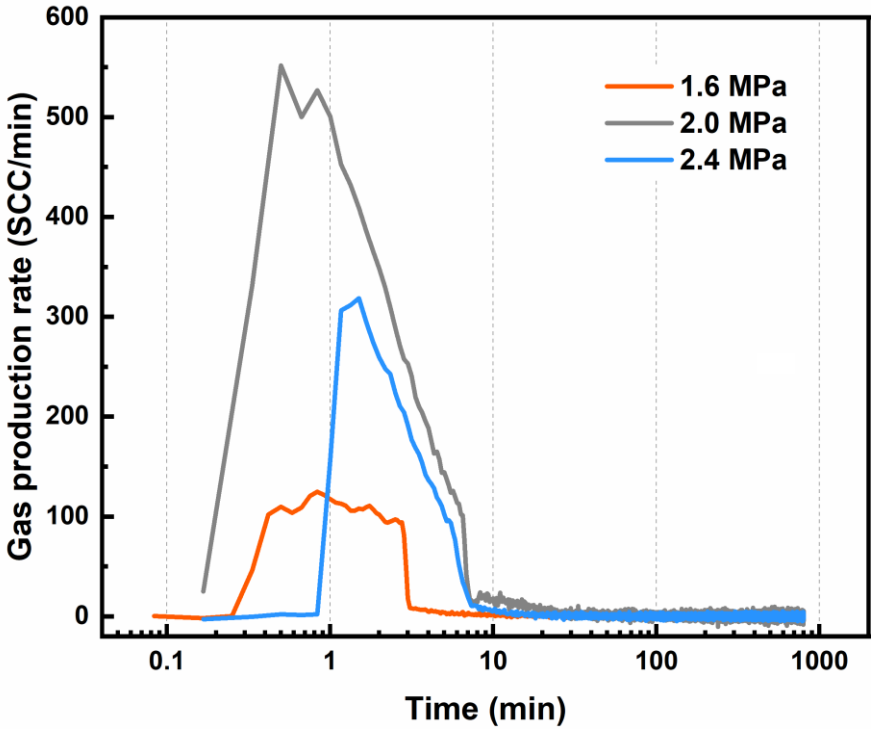

Figure 3.7 Gas production rate of an individual 11 mm-diameter sample at production pressures of 1.6 MPa, 2.0 MPa, and 2.4 MPa.

According to the production behavior of hydrate samples under the different depressurizations, the methane hydrate pellets follow a similar pattern whereby the overall production process was divided into three periods.

A) Rapid production period: At the beginning of production, the rapid monotonic increment was observed for both the production percentage and cumulative produced gas with decreasing pressure when methane gas was released quickly from excess free gas in the vapor phase.
B) Slow production period: The second period was the main stage of hydrate pellet decomposition. Once the system pressure dropped out of the hydrate stability zone, ice was formed immediately, and CH_4 leaked from the hydrate pellets following the slow incremental increase in the gas production percentage and produced gas. Production rates displayed slight variations before rapidly falling.
C) No production period: In the final period, the production percentage and cumulative gas gradually approached a constant, with the production rate infinitely close to zero.

3.2.2. Influence of surface-area-to-mass ratio on MH decomposition

Another factor that influences hydrate production kinetics is the dimension of the hydrate samples, which can be expressed as the surface area-to-mass ratio. The diameter range of laboratory-synthesized hydrate samples was 11 mm, 18 mm, 22 mm, corresponding to three groups of samples with an identical total volume of 8980 mm^3 but a surface area-to-mass ratio of 349 mm^2/g, 388 mm^2/g, and 653 mm^2/g. In order to compare gas production for different sizes of hydrate samples, an identical depressurization operation was carried out on spherical hydrate pellets with diameters of 18 mm and 22 mm. Figure 3.8 and Figure 3.9 show the time dependencies of the gas production percentage and the cumulative produced gas for different production pressures performed on hydrate pellets in a diameter of 18 mm. Figure 3.11 and Figure 3.12 are the time dependencies of the gas production percentage and the cumulative produced gas for different production pressures performed on hydrate pellets in a diameter of 22 mm. At the same production pressure of 1.6 MPa, hydrates samples in diameter of 11 mm to 22 mm show a production percentage of 73.88 %, 70.40 %, and 74.96 %. Regarding production rates, a larger hydrate pellet positively affects the maximum value immediately after free gas release. Figure 3.10 and Figure 3.13 are the

production rates of hydrate samples in diameter of 18 mm and 22 mm produced gas at the three experimental pressures. The production rates on hydrate samples in diameter of 18 mm to 22 mm increase from 0.83 SCC/min to 2.98 SCC/min, 4.93 SCC/min at production pressure of 1.6 MPa. This shows that the impact of production pressure on the production percentage might be significant in comparison to the size of the hydrate pellet.

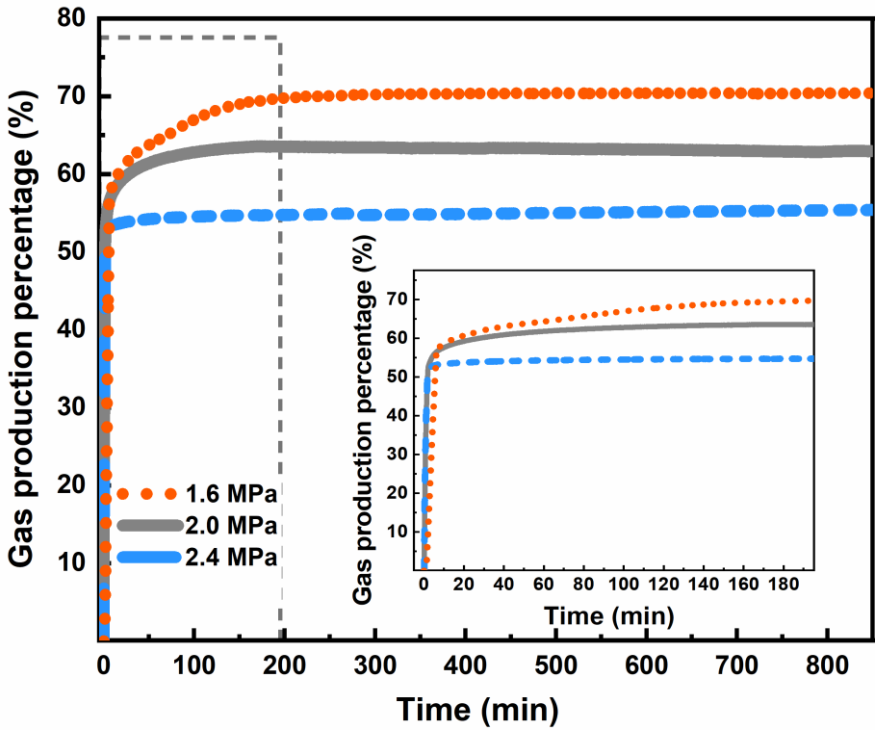

Figure 3.8 Percentage of gas production of hydrate samples 18 mm in diameter at production pressures of 1.6 MPa, 2.0 MPa, and 2.4 MPa.

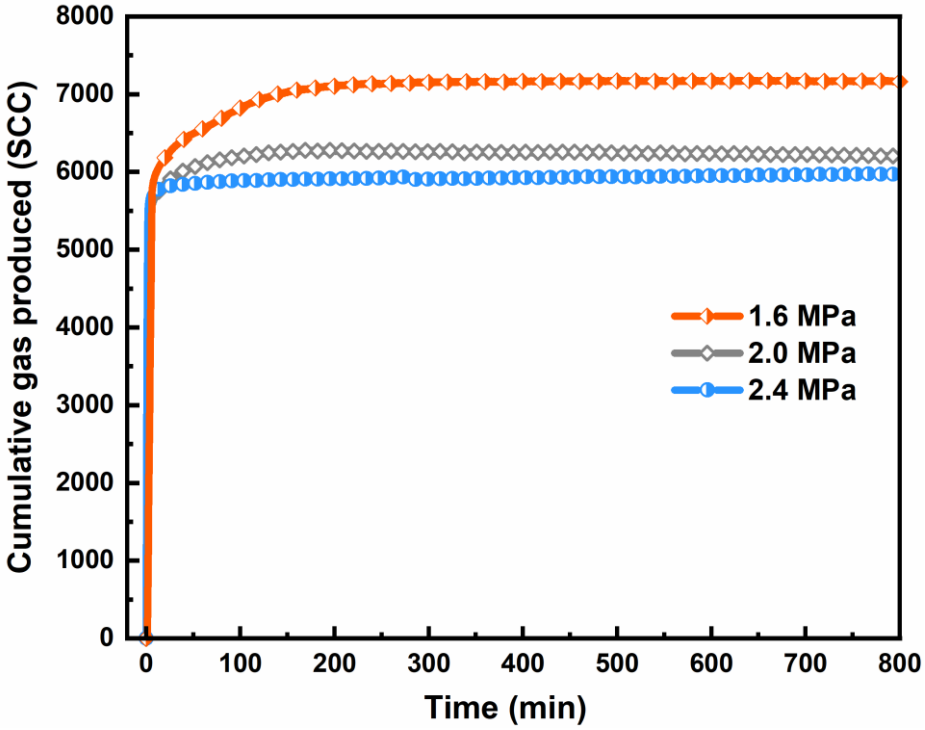

Figure 3.9 Cumulative produced gas of hydrate samples 18 mm in diameter at production pressures of 1.6 MPa, 2.0 MPa, and 2.4 MPa.

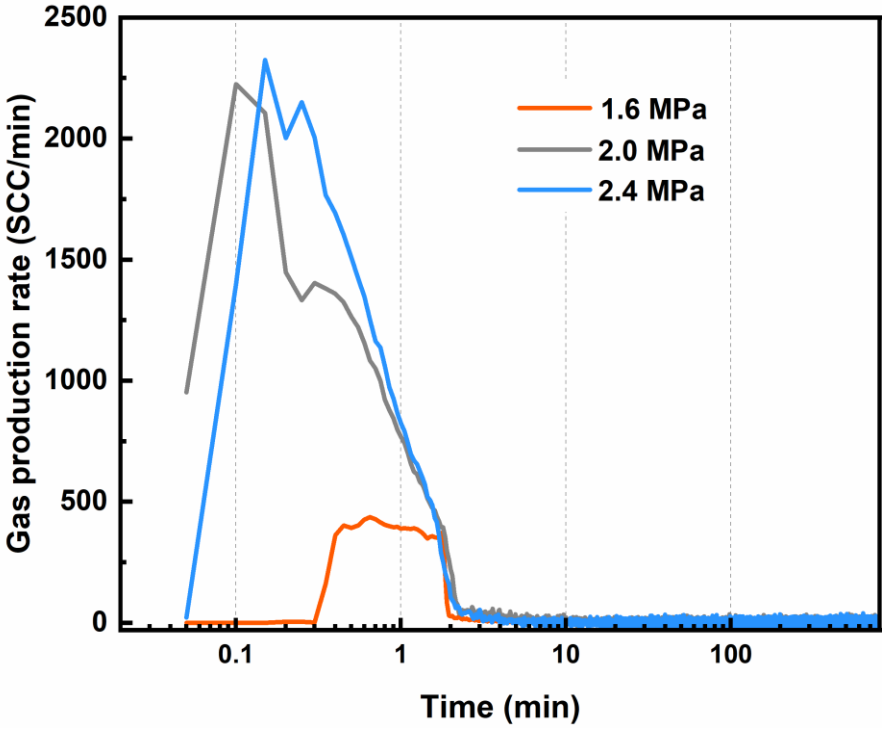

Figure 3.10 Gas production rates of hydrate samples 18 mm in diameter at production pressures of 1.6 MPa, 2.0 MPa, and 2.4 MPa.

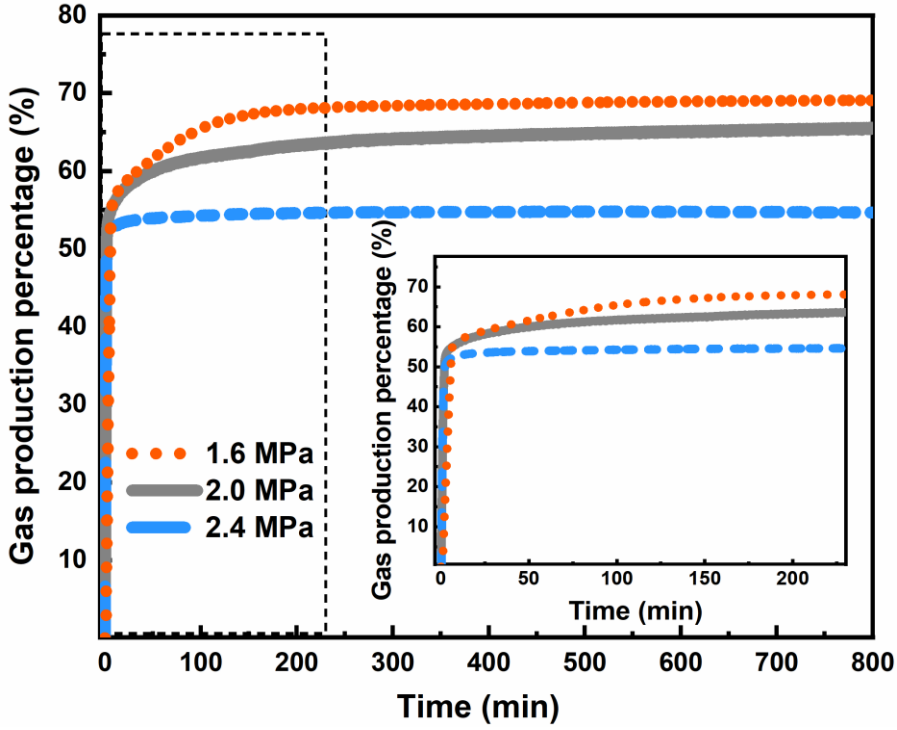

Figure 3.11 Percentage of gas production of hydrate samples 22 mm in diameter at production pressures of 1.6 MPa, 2.0 MPa, and 2.4 MPa.

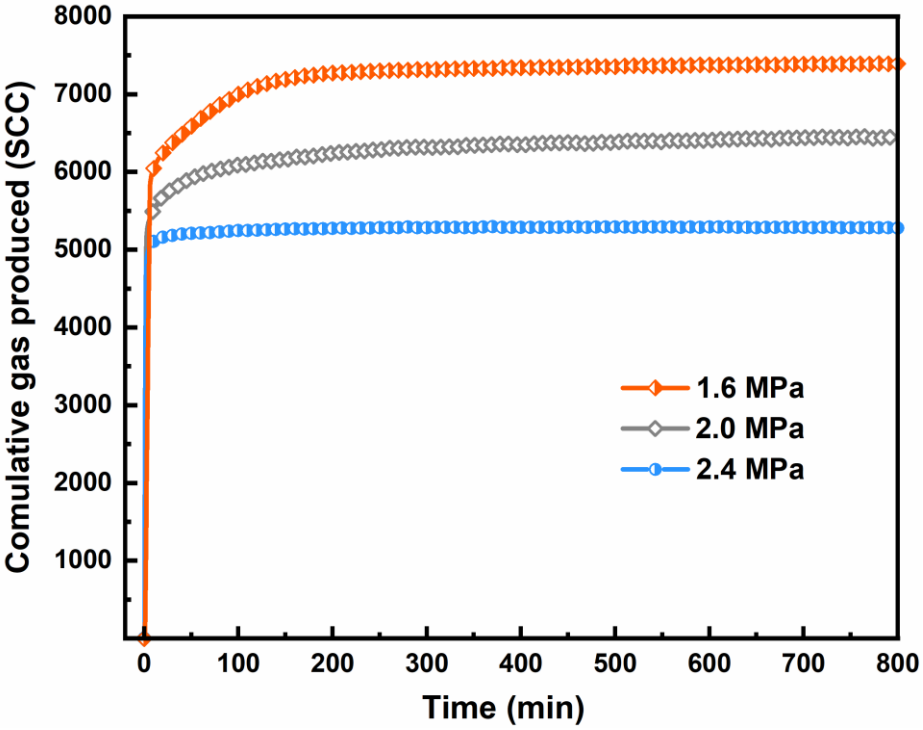

Figure 3.12 Cumulative produced gas of hydrate samples 22 mm in diameter at production pressures of 1.6 MPa, 2.0 MPa, and 2.4 MPa.

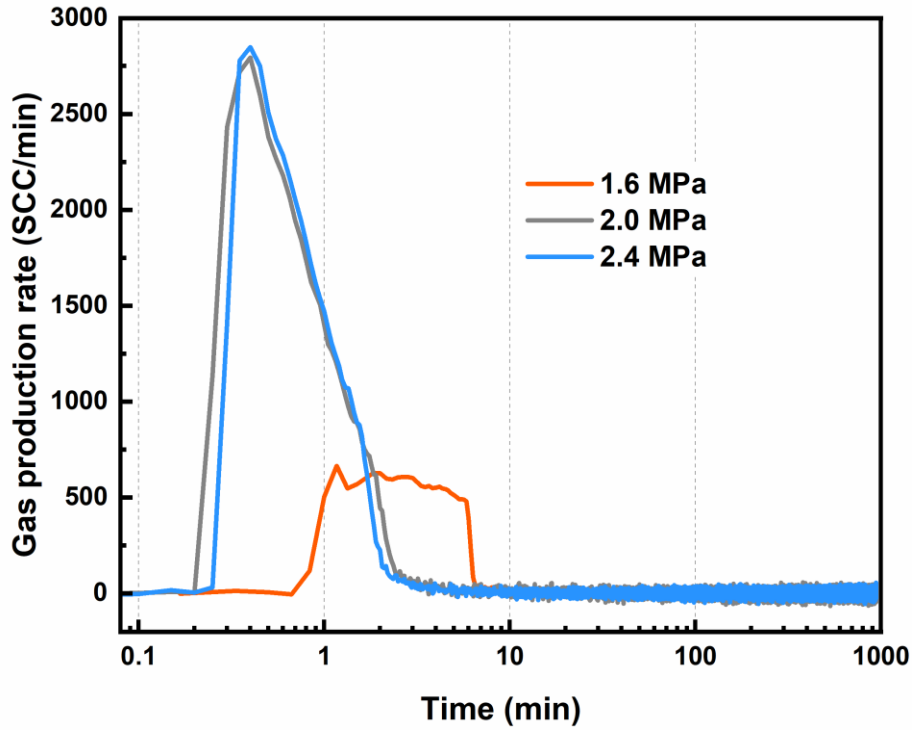

Figure 3.13 Percentage of gas production of hydrate samples 22 mm in diameter at production pressures of 1.6 MPa, 2.0 MPa, and 2.4 MPa.

The impact of surface area-to-mass ratio and production pressure on gas production percentage and average production rate related to surface area-to-mass ratio is shown in Figure 3.14. The gas production rates are affected by both production pressure and surface area-to-mass ratio. It was shown from the methane hydrate production behavior in the current study that the combined effect of the pressure and surface area-to-mass ratio of individual hydrate samples plays an important role in decomposition kinetics, as indicated in Figure 3.14.

The gas production profile achieved in these runs increased solely due to production pressure when using the same sized MH pellets (i.e. same surface area-to-mass ratio), leading us to conclude that production percentages and rates are dependent upon production pressure, corresponding to the pressure driving force. Pressure dependency acting as the pressure driving force was due to the difference in fugacity between the gas at equilibrium and at production pressures. Yet the production percentage for the linear relationship of the surface area-to-mass ratio was not prominent under the same pressure. This nonlinear tendency is clear under higher pressures (2.0 MPa, 2.4 MPa) compared to the one depressurized at 1.6 MPa. The effect of gas diffusion may play a more dominant role in this phenomenon. This argument is consistent with the finding of Minmachi et al. [82], who reported that the thickness of the ice layer grown on the surface of the hydrate was largely constant and did not depend on the particle size of the methane hydrate being over 1.0 mm.

The surface area-to-mass ratio is shown to have a negative impact on the production rate. Under a high driving force of pressure and consequently fast gas production, the influence of pellet size also becomes salient. When production is employed under a lower pressure driving force, the impact of the surface area-to-mass ratio on production rates weakens in comparison to a high-pressure driving force. Gas diffusion through the produced ice layer plays an important role by varying the surface area-to-mass ratio. In one instance, gas hydrate pellets with a high surface area-to-mass ratio dissociate slower due to faster ice layer over covering Based on these findings, it is evident that MH pellets with a higher surface area-to-mass ratio are subject to a lower production rate because the reduction in diffusion resistance becomes limited as the pellets increase in size. Both the pressure driving force and gas diffusion determine the average production rate, so a gas production

model that simultaneously accounts for these two factors should be applied in order to describe the experimental results correctly.

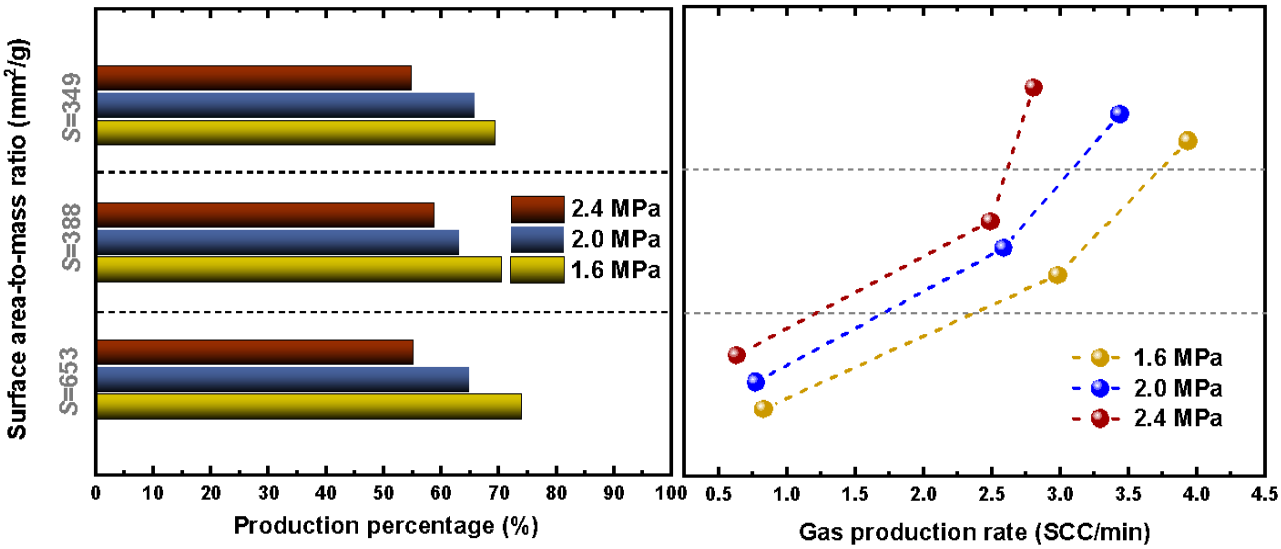

Figure 3.14 The effects of the surface area-to-mass ratio and production pressure on the production percentage and rate.

3.2.3. MH sample characterization

Laboratory-synthesized, sphere-shaped hydrate samples were characterized by cryo-SEM, as shown schematically in Figure 3.15. Samples were crushed into small parts, from which the one with the hydrate pellet surface was chosen for scanning. Our observation of the microstructures of all three MH sample sizes suggests that sub-micron porosity is a typical feature independent of the macroscopic shape, as confirmed by Sloan et al.[80]. However, the uniformity of porousness on the surface varies according to hydrate pellet sizes. The extent of porous surface uniformity decreases with an increase in the GMD of the hydrate pellet, which corresponds to the surface area-to-mass ratio. The surface morphology of all 11-mm samples displayed homogenous porosity, with the pores evenly distributed over the surface of the pellet. Unlike the uniformly distributed porous surfaces of the 11-mm and 17-mm samples, the 22-mm hydrate sample had a relatively smooth surface, and randomly distributed pores only existed in small regions.

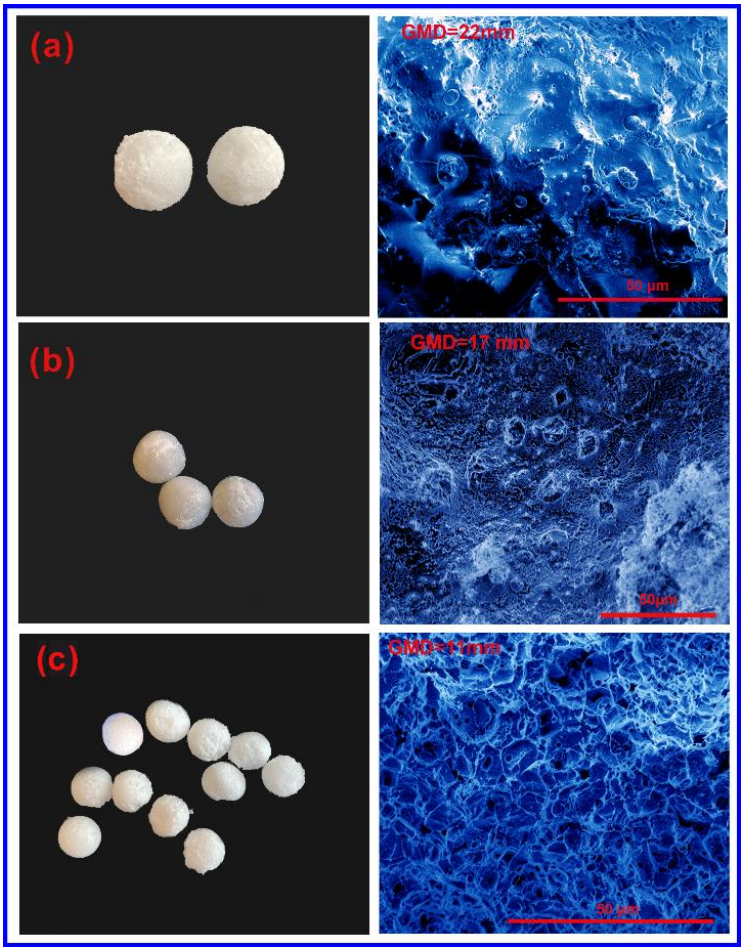

Figure 3.15 Macroscopic and electron micrographs of the CH_4 hydrate starting samples before depressurization. Top to bottom: (a) GMD=22 mm; (b) GMD=18 mm, (c) GMD=11

From the profiled of production percentage and rates, it is interesting to study the decomposition process microscopically, thus we made the following cryo-SEM observations to detect surface morphology changes during temperature increases. The temperature was raised from 103 K to 263 K during observation. Initial changes on the spherical hydrate surface were observed over time, as shown in Figure 3.16. The SEM images clearly indicate that an ice film developed, thus leading to a barrier coating on the hydrate pellet surface. As the temperature increased, it is clear that the ice did not create a continuous layer; instead, we saw the nucleation of small ice crystals on the surface of the hydrate sample, followed by the gradual formation of several bigger clusters (Figure 3.16 (a), ice is in blue). The dispersed ice crystal clusters floated over the hydrate surface and moved around occasionally rather than sticking to the surface of the initial region where they formed. The motion of the floating ice clusters may result from surface tension and surface energy, which

renders the alteration of ice crystals and clusters ineffective [83]. Further studies on ice cluster dynamics would help uncover the mechanism behind this phenomenon.

The ice crystals and clusters that form on the hydrate surface manifest in a loose, sponge-like shape with microstructural voids that create a feasible pathway for CH_4 gas molecule permeation. Ice crystals constantly grow during decomposition, and the interconnection of ice clusters strengthens effective thickness, thereby shortening the pathways for CH_4 molecule diffusion. A more accessible pathway that allows CH_4 molecules to permeate into the gas phase is offered by gaps between the ice clusters. The clusters gather into a single entity during the final stage of decomposition, covering the hydrate and therefore greatly hindering the diffusion of gas molecules inside the hydrate. Although the presence of ice crystals created are not uniformly distributed in the initial stage, in the final equilibrium stage, it is assumed they form a homogeneous coverage of methane hydrate with an ice thickness of 5-10 μm [84], which is significant for the establishment of a core-shrinking model. Additionally, we did not find any appreciable liquid water throughout the decomposition period. Compared with the larger hydrate samples, the production rates from small methane hydrates were slower in the initial ice nucleation phase, probably because of the inhomogeneous distribution nucleation of ice crystals in the initial methane release period. Full coverage of the pellet surface by ice clusters is much faster on small hydrate pellets due to their smaller surface area.

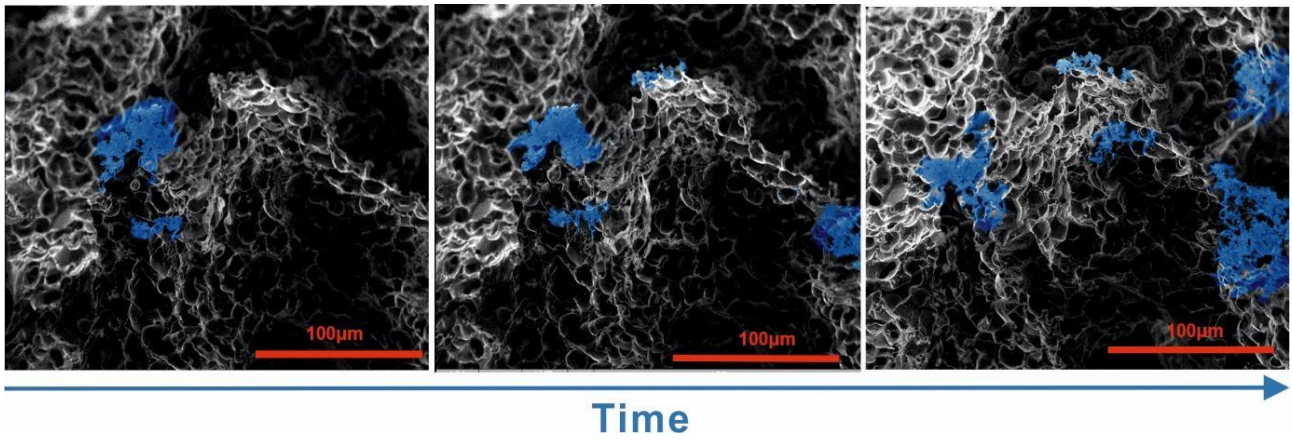

Figure 3.16 The microstructural appearance of the MH sample over time during decomposition.

3.2.4. MH decomposition modeling

3.2.4.1. MH decomposition mechanism

Researchers have proposed several mathematical models for hydrate decomposition. The notion that an ice-shielding mechanism can have some effect on hindering hydrate decomposition is accepted by most researchers, among them Takeya et al. [81] who were the first to propose a diffusion-limited model for decomposition with all particles having the same volume and the ice layer having a uniform thickness. Changyu Sun et al. [41] suggested that a moving boundary theory could be applied for decomposition below the freezing temperature, while Lijun Yan et al. [23] posited that the ice layer is tightly attached to hydrate surfaces through hydrogen bonds and built a porous ice layer model. The study by Takeya et al. [42] on the decomposition of NGH pellets illustrated that the outer surface was enveloped by an ice film initially, but the decomposition of NGH and the growth of an ice film, or the internal decomposition of the NGH pellet, did not occur after the initial decomposition of the outer surface. The mechanism is still a source of debate, but the generally accepted theory among different models is the following: the methane gas molecule is released first because of the destruction of the hydrate host lattice on the surface of the hydrate crystal, and then the diffusion process follows the formation of an ice-shielding layer.

Accordingly, we propose a depressurization production mechanism in which methane hydrate size is a significant factor. A schematic illustration of the mechanism proposed to explain this process is illustrated in Figure 3.17. This mechanism interpreted the increment of production rates by hydrate macroscopic size elevation. The production period can be divided into three periods. First is the initial fast CH_4 gas release phase due to chemical potential differences in methane between the vapor and the solid phase. After the initial production period where gas is released, the pressure driving force and hydrate size synergistically control the rates of hydrate production. For the driving force case of depressurization, the fugacity difference between the vapor and solid phases is taken into consideration. The ice layer increases in thickness by combining ice crystal clusters after the initial decomposition process. The rate-determining process for the entire hydrate production process in the second phase of production is also controlled by the diffusion of CH_4 molecules through the ice crystal layer, substantially owing to the size of the

macroscopic hydrate grain covered by the crystals. Residual CH_4 gas after the fast release phase compresses the ice-coated hydrate into a quasi-stationary equilibrium by maintaining the pressure, resulting in gas production during the third phase at a relatively slow rate.

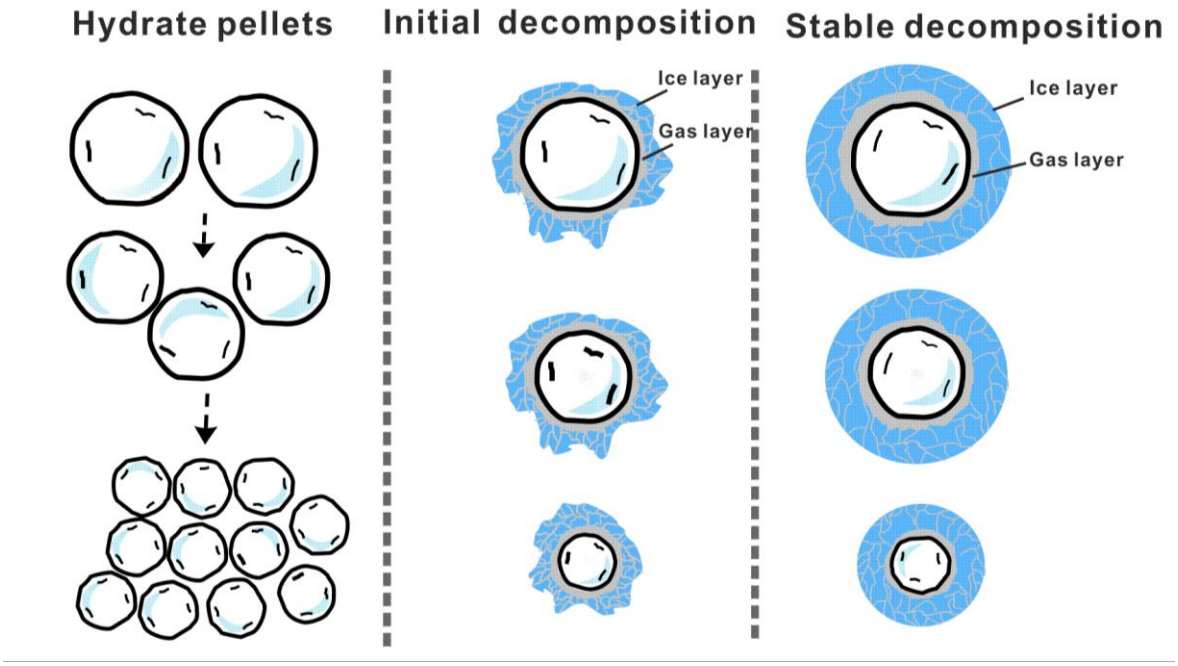

Figure 3.17 Illustration of the depressurization process on spherical hydrate pellets.

Gas hydrate kinetics decomposition is determined not only by the decomposition front motion but also by pore density and pore distribution over the entire collection of granules. When modeling isothermal decomposition for subzero temperatures, it is necessary to consider the properties of the ice layer around the gas hydrate particle. A more accurate simulation of the decomposition kinetics is required to improve the long-term storage and transportation of the gas hydrate.

Decomposition processes differ significantly in line with changes in the morphology of the ice layer on the hydrate surface, as well as with hydrate particle sizes. In this regard, the kinetics involved in the decomposition of the gas hydrate will differ significantly. A small pore diameter (10–100 nm) in the ice layer leads to a significant decrease in the rate of decomposition and the release rate of methane from the sample. Real natural and technical processes are nonstationary and non-uniform, and this should be considered when simulating gas hydrate decomposition. To improve simulation accuracy, additional experimental studies are required to determine the pore distribution of the ice layer and

derive the experimental dependence of pore density on the temperature at self-preservation, as well as when approaching the melting point. This modeling approach is important in solving the problems involved in storing and transporting gas hydrates and improving technological efficiency. It is also important for assessing the risk of explosion when transporting raw materials in tankers, as well as the sudden release of methane in coal mines and in the development of global warming models. It is conceivable that the macroscopic size of MH also has an influence on CH_4 recovery via gas injection and merits further study.

Another factor influencing the microstructure of ice is the pressure driving force, especially in the initial decomposition stage. As discussed, the modeling of gas hydrate decomposition is established as a function of pressure, temperature, guest gas, and time. Taking into consideration all factors will therefore be a formidable challenge. The diffusion-limited shrinking core model is generally used for hydrate formation and decomposition, assuming a homogeneous guest hydrate and an ice rind, respectively, coated onto the main subject. However, it is certainly fair to say that it will only be accurate over a limited time when decomposition enters the third phase, as elaborated in our study. Ice nucleation, growth, and conglomeration are time-dependent and difficult to solve in terms of our present knowledge when establishing a universal model. Further quantitative experimental work is needed before this goal can be achieved.

3.2.4.2. Model description of the MH sphere decomposition

A model based on decomposition kinetics and mass transfer was built to describe gas hydrate decomposition from a single MH sphere. The entire process can be regarded as a quasi-chemical decomposition reaction. Figure 3.18 illustrates how gas decomposes from a single MH sphere, with the gas concentration profile along the radial direction at the CH_4-ice and ice-MH interfaces.

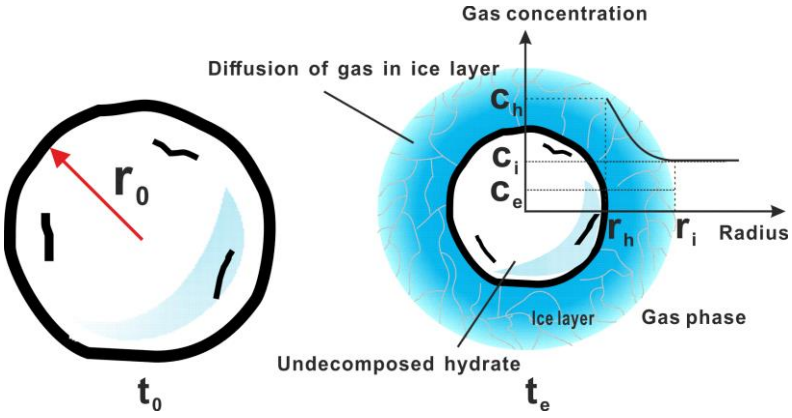

Figure 3.18 The schematic diagram for a spheric MH pellet decomposition. Decomposition reaction controlled and diffusion-controlled reaction with a variation of the concentration of gas in the radial direction (c_h: concentration of CH_4 in the MH phase; c_i: concentration of CH_4 at the gas-ice interface; c_e: equilibrium concentration of CH_4 under experimental temperatures and pressures).

It is assumed that interface movement occurs uniformly so that the radius of the MH sphere decreases as depressurization proceeds. As no liquid water is detected coming from the MH surface when decomposition proceeds, it is assumed that water from MH is transferred into ice immediately after decomposition. The schematic illustrates the final equilibrium stage when the ice layer entirely covers the MH spheric pellet. Furthermore, pellet size decreases from its original size but never increases due to density differences between ice and the hydrate. When $t = t_0$, $C = c_e$, where $r = r_0$; when $t = t_e$, $C = c_i$, where $r = r_i$, $C = c_{\hbar}$, where $r = r_{\hbar}$, $r_0$is the initial diameter of an MH pellet; c_e is the equilibrium concentration of CH_4 under experimental temperatures and pressures; c_i is the molar concentration of gas on the outer layer of a pellet ,and $c_{\hbar}$ is the concentration of CH_4 on the surface of the undecomposed hydrate sphere.

The governing equation for the initial rate of hydrate decomposition at the MH-CH_4 gas interface is expressed as:

$$(\frac{dn}{dt})_t = k_d A_{MH}(c_e - c_{\hbar}) \tag{3-6}$$

where $(\frac{dn}{dt})_t$ is the decomposition rate of the methane hydrate; A_{MH} is the surface area-to-mass ratio of the hydrate sample; k_d is the decomposition rate constant; c_e and $c_{\hbar}$ are the

concentrations of CH_4 in equilibrium and on the surface of state spherical MH. The thickness of the ice layer L increases in line with decomposition.

$$(\frac{dn}{dt})_t = \frac{D_{eff}}{L}(c_{\hbar} - c_g) \tag{3-7}$$

where D_{eff} is the diffusion coefficient c_g is the CH_4 concentration in the gas phase. Under quasi-steady state conditions, it is assumed that the rate of gas diffusion through the ice layer is equal to the rate of gas release on the surface of the undecomposed MH core. We obtain the following expression of the decomposition rate by combining equations (3-8) and (3-9)

$$(\frac{dn}{dt})_t = (c_e - c_g)\frac{1}{\frac{1}{k_d A_{MH}} + \frac{L}{D_{eff} A_{MH}}} \tag{3-8}$$

$$D_{eff} = \frac{L}{\frac{A_{MH}(c_e - c_g)}{(dn/dt)_t} - \frac{1}{k_d}} \tag{3-9}$$

When $t = t_0, n = 0,$ where $r = r_0,\ D_{eff} = \infty.\ L/D_{eff}A_{MH}$ is the diffusion resistance.

Applying the boundary condition $t = t_0, L = 0,$

$$k_d = \frac{dn/dt|_{t=t_0}}{(c_e - c_g)A_{MH}} \tag{3-10}$$

where the values of $c_e$and $c_g$can be obtained from the following equations:

$$c_e = \frac{P_e}{Z_e RT} \tag{3-11}$$

$$c_g = \frac{P_g}{Z_g RT} \tag{3-12}$$

where P_e and $P_g$are equilibrium pressure and system pressure, respectively, corresponding to the compressibility factors $Z_e$and Z_g. Data obtained for k_d are given in Table 3.3.

Table 3.3 Initial rate constants per sample on unit area to mass for decomposition in all runs.

GMD (mm)	P (MPa)	k_d (m/s)
11	1.6	0.26×10^{-3}
11	2.0	2.16×10^{-3}
11	2.4	5.12×10^{-3}
18	1.6	1.72×10^{-3}
18	2.0	15.78×10^{-3}
18	2.4	59.32×10^{-3}
22	1.6	2.86×10^{-3}
22	2.0	21.14×10^{-3}
22	2.4	75.41×10^{-3}

3.3 Summary

This study was designed to synthesize spherical methane hydrate in three different sizes, ranging from 11 to 22 mm. Specific attention was paid to macroscopically simulate hydrate particles and decomposing them via the depressurization method at subzero temperature. The decomposition characters were compared and characterized by combining scale work with a cryo-SEM investigation. The following conclusions were drawn based on the analysis of the experimental data:

1) The gas production process can be divided into three main periods.

Period 1: Excess gas release. As a result of depressurization, excess gas is released initially, while gas production increases sharply until it reaches a maximum, influenced by spherical hydrate size.

Period 2: Fast hydrate production. When the pressure falls to equilibrium, the hydrate started decomposition with the production rate fluctuating for a short time and then decreasing.

Period 3: Slow hydrate production. Gas production changes almost imperceptibly during this period. The curve of the cumulative gas production and production percentages tends to flatten.

2) The driving force of pressure difference and gas diffusion jointly govern the decomposition reaction. The extent of influence is consistent, depending on production pressure and pellet size. At low pressure, production is fast, and pressure driving force control prevails initially, whereas gas diffusion with ice coverage according to pellet size becomes more dominant.
3) Hydrate decomposition is time dominant, and initial ice nucleation and conglomeration play an important role in the initial hydrate decomposition rate. An inhomogeneous ice rind and a gas layer exist between the hydrate and the ice and should be taken into account when simulating the production of gas hydrate at the freezing temperature of water.

Although we are still far from combining the initial stage's decomposition into a universal model, the contribution offered by this study is of great importance in this regard.

b. Acknowledgments

Funding for the present work was provided by the Department of Chemical and Biochemical Engineering, Technical University of Denmark, and the State Scholarship Fund of China Scholarship Council. The authors also sincerely acknowledge Adam Fuller and Karen Tracy Hong Lin from Nanotech DTU for their support in carrying out the research of SEM characterization.

c. References

[1] E.D. Sloan, Fundamental principles and applications of natural gas hydrates, Nature. 426 (2003) 353–359.

[2] M.D. Max, Natural gas hydrate in oceanic and permafrost environments, Springer Science & Business Media, 2003.

[3] K. A. Udachin, C. I. Ratcliffe, J. A. Ripmeester, Structure, Composition, and Thermal Expansion of CO_2 Hydrate from Single Crystal X-ray Diffraction Measurements, J. Phys. Chem. B. 105 (2001) 4200–4204.

[4] K.A. Udachin, C.I. Ratcliffe, J.A. Ripmeester, Single Crystal Diffraction Studies of Structure I, II and H Hydrates: Structure, Cage Occupancy and Composition, J. Supramol. Chem. 2 (2002) 405–408.

[5] R. Martos-Villa, M. Francisco-Márquez, M.P. Mata, C.I. Sainz-Díaz, Crystal structure, stability and spectroscopic properties of methane and CO_2 hydrates, J. Mol. Graph. Model. 44 (2013) 253–265.

[6] Y. Lee, W. Choi, Y. Seo, J.Y. Lee, J. Lee, Y. Seo, Structural transition induced by cage-dependent guest exchange in CH4 + C3H8 hydrates with CO_2 injection for energy recovery and CO_2 sequestration, Appl. Energy. 228 (2018) 229–239.

[7] J.-R. Zhong, Y.-F. Sun, W.-Z. Li, Y. Xie, G.-J. Chen, C.-Y. Sun, L.-Y. Yang, H.-B. Qin, W.-X. Pang, Q.-P. Li, Structural transition range of methane-ethane gas hydrates during decomposition below ice point, Appl. Energy. 250 (2019) 873–881.

[8] M. Roostaie, Y. Leonenko, Analytical investigation of gas production from methane hydrates and the associated heat and mass transfer upon thermal stimulation employing a coaxial wellbore, Energy Convers. Manag. 209 (2020) 112616.

[9] M. Shi, J. Woodley, N. von Solms, An Experimental Study on Improved Production Performance by Depressurization Combined with CO_2-Enriched Air Injection, Energy & Fuels. 34 (n.d.) 7329–7339.

[10] B. Li, T. Xu, G. Zhang, W. Guo, H. Liu, Q. Wang, L. Qu, Y. Sun, An experimental study on gas production from fracture-filled hydrate by CO_2 and CO_2/N_2 replacement, Energy Convers. Manag. 165 (2018) 738–747.

[11] E. Villicaña-García, J.M. Ponce-Ortega, Sustainable strategic planning for a national natural gas energy system accounting for unconventional sources, Energy Convers. Manag. 181 (2019) 382–397.

[12] Y. Sun, G. Zhang, S. Li, S. Jiang, CO_2/N_2 injection into $CH_4 + C_3H_8$ hydrates for gas recovery and CO_2 sequestration, Chem. Eng. J. 375 (2019) 121973.

[13] A. Okwananke, J. Yang, B. Tohidi, E. Chuvilin, V. Istomin, B. Bukhanov, A. Cheremisin, Enhanced depressurization for methane recovery from gas hydrate reservoirs by injection of compressed air and nitrogen, J. Chem. Thermodyn. 117 (2018) 138–146.

[14] B. Chen, H. Sun, K. Li, D. Wang, M. Yang, Experimental investigation of natural gas hydrate production characteristics via novel combination modes of depressurization with water flow erosion, Fuel. 252 (2019) 295–303.

[15] S. Almenningen, P. Fotland, M.A. Fernø, G. Ersland, An Experimental Investigation of Gas-Production Rates During Depressurization of Sedimentary Methane Hydrates, SPE J. Preprint (2019) 9.

[16] M. Yang, Y. Gao, H. Zhou, B. Chen, Y. Li, Gas production from different classes of methane hydrate deposits by the depressurization method, Int. J. Energy Res. 43 (2019) 5493–5505.

[17] V.C. Nair, S.K. Prasad, R. Kumar, J.S. Sangwai, Energy recovery from simulated clayey gas hydrate reservoir using depressurization by constant rate gas release, thermal stimulation and their combinations, Appl. Energy. 225 (2018) 755–768.

[18] H.C. Kim, P.R. Bishnoi, R.A. Heidemann, S.S.H. Rizvi, Kinetics of methane hydrate decomposition, Chem. Eng. Sci. 42 (1987) 1645–1653.

[19] V.S. Yakushev, V.A. i Istomin, Physics and Chemistry of Ice, Hokkaido Univ. Press. Sapporo. (1992) 136.

[20] L. A. Stern, S. Circone, S. H. Kirby, W. B. Durham, Anomalous Preservation of Pure Methane Hydrate at 1 atm, J. Phys. Chem. B. 105 (2001) 1756–1762.

[21] B. Li, L.-L. Chen, Q.-C. Wan, X. Han, Y.-Q. Wu, Y.-J. Luo, Experimental study of frozen gas hydrate decomposition towards gas recovery from permafrost hydrate deposits below freezing point, Fuel. 280 (2020) 118557.

[22] V.A. Vlasov, Diffusion model of gas hydrate dissociation into ice and gas that takes into account the ice microstructure, Chem. Eng. Sci. 215 (2020) 115443.

[23] Y. Xie, T. Zheng, J.-R. Zhong, Y.-J. Zhu, Y.-F. Wang, Y. Zhang, R. Li, Q. Yuan, C.-Y. Sun, G.-J. Chen, Experimental research on self-preservation effect of methane hydrate in porous sediments, Appl. Energy. 268 (2020) 115008.

[24] M.A. Clarke, P.R. Bishnoi, Measuring and modelling the rate of decomposition of gas hydrates formed from mixtures of methane and ethane, Chem. Eng. Sci. 56 (2001) 4715–4724.

[25] T. Nakayama, K. Ogasawara, F. Kiyono, H. Torii, A. Yamasaki, T. Sato, Estimation of surface area of methane hydrate in the sand sediment using a dissociation-rate model, Mar. Syst. Ocean Technol. 13 (2018) 1–12.

[26] X. Yang, C.-Y. Sun, K.-H. Su, Q. Yuan, Q.-P. Li, G.-J. Chen, A three-dimensional study on the formation and dissociation of methane hydrate in porous sediment by depressurization, Energy Convers. Manag. 56 (2012) 1–7.

[27] L. Tomutsa, B. Freifeld, T.J. Kneafsey, L.A. Stern, X-ray Computed Tomography Observation of Methane Hydrate Dissociation, SPE Gas Technol. Symp. (2002).

[28] Y. Gao, Z. Ma, M. Yang, Y. Song, X. Lv, Dissociation Characteristic of Remolded Methane Hydrates Deposits from South China Sea using Depressurization, Energy Procedia. 158 (2019) 5355–5360.

[29] X. Sen Li, Y. Zhang, Study on dissociation behaviors of methane hydrate in porous media based on experiments and fractional dimension shrinking-core model, Ind. Eng. Chem. Res. 50 (2011) 8263–8271.

[30] L.A. Stern, S.H. Kirby, W.B. Durham, Peculiarities of Methane Clathrate Hydrate Formation and Solid-State Deformation, Including Possible Superheating of Water Ice, Science (80-.). 273 (1996) 1843 LP – 1848.

[31] L. A. Stern, S. H. Kirby, W. B. Durham, Polycrystalline Methane Hydrate: Synthesis from Superheated Ice, and Low-Temperature Mechanical Properties, Energy & Fuels. 12 (1998) 201–211.

[32] C. Liu, Q. Meng, X. He, C. Li, Y. Ye, G. Zhang, J. Liang, Characterization of natural gas hydrate recovered from Pearl River Mouth basin in South China Sea, Mar. Pet. Geol. 61 (2015) 14–21.

[33] D.-Y. Peng, D. B. Robinson, A New Two-Constant Equation of State, Ind. & Eng. Chem. Fundam. 15 (2002) 59–64.

[34] W.F. Waite, J.C. Santamarina, D.D. Cortes, B. Dugan, D.N. Espinoza, J. Germaine, J. Jang, J.W. Jung, T.J. Kneafsey, H. Shin, K. Soga, W.J. Winters, T.-S. Yun, Physical properties of hydrate-bearing sediments, Rev. Geophys. 47 (2009).

[35] M. Yang, J. Zheng, Y. Gao, Z. Ma, X. Lv, Y. Song, Dissociation characteristics of methane hydrates in South China Sea sediments by depressurization, Appl. Energy. 243 (2019) 266–273.

[36] E. Dendy Sloan, Clathrate hydrate measurements: microscopic, mesoscopic, and macroscopic, J. Chem. Thermodyn. 35 (2003) 41–53.

[37] S. Takeya, W. Shimada, Y. Kamata, T. Ebinuma, T. Uchida, J. Nagao, H. Narita, In Situ X-ray Diffraction Measurements of the Self-Preservation Effect of CH_4 Hydrate, J. Phys. Chem. A. 105 (2001) 9756–9759.

[38] H. Mimachi, M. Takahashi, S. Takeya, Y. Gotoh, A. Yoneyama, K. Hyodo, T. Takeda, T. Murayama, Effect of Long-Term Storage and Thermal History on the Gas Content of Natural Gas Hydrate Pellets under Ambient Pressure, Energy & Fuels. 29 (2015) 4827–4834.

[39] L. Lupi, A. Hudait, B. Peters, M. Grünwald, R. Gotchy Mullen, A.H. Nguyen, V. Molinero, Role of stacking disorder in ice nucleation, Nature. 551 (2017) 218–222.

[40] A. Falenty, W. F. Kuhs, “Self-Preservation” of CO_2 Gas Hydrates—Surface Microstructure and Ice Perfection, J. Phys. Chem. B. 113 (2009) 15975–15988.

[41] C.-Y. Sun, G.-J. Chen, Methane hydrate dissociation above 0°C and below 0°C, Fluid Phase Equilib. 242 (2006) 123–128.

[42] S. Takeya, T. Uchida, J. Nagao, R. Ohmura, W. Shimada, Y. Kamata, T. Ebinuma, H. Narita, Particle size effect of CH_4 hydrate for self-preservation, Chem. Eng. Sci. 60 (2005) 1383–1387.

4 An experimental study on improved production performance by depressurization combined with CO_2-enriched air injection

This chapter has been written in a manuscript format. A slightly modified version has been published in the peer-reviewed journal Energy&Fuels as,

Shi, Meng, John M. Woodley, and Nicolas von Solms. "An Experimental Study on Improved Production Performance by Depressurization Combined with CO_2-Enriched Air Injection." *Energy & Fuels* 34.6 (2020): 7329-7339.

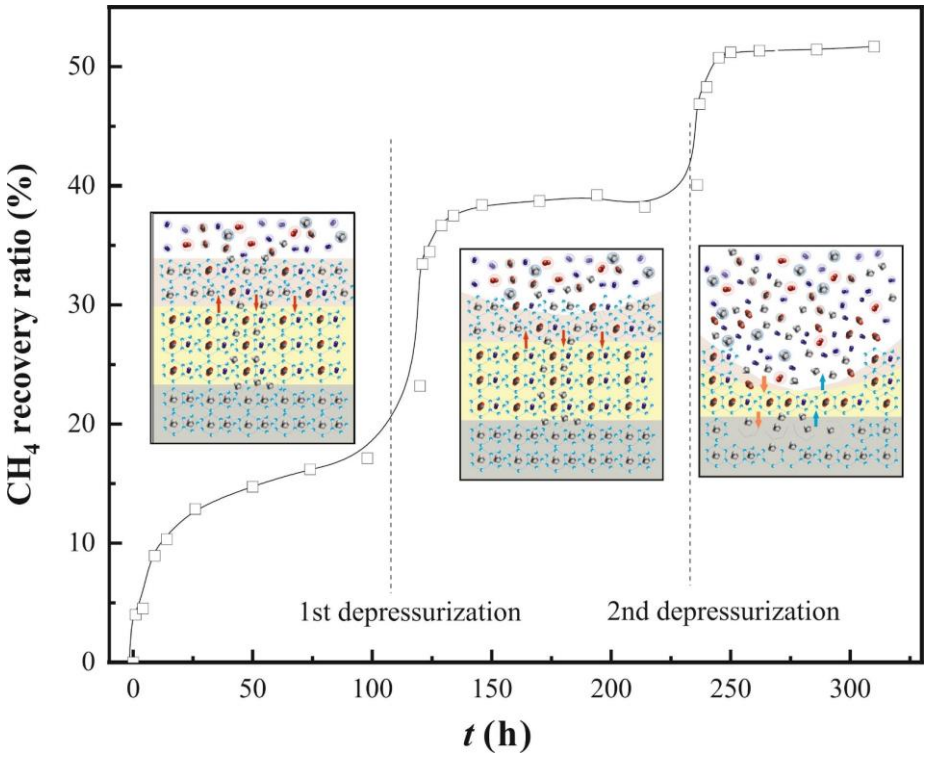

Highlights

1. Gas hydrate production behavior was experimentally investigated both through injecting air and CO_2-enriched air in multilayer sediments which simulating actual conditions in nature.
2. A combination of gas replacement and three stages of depressurization was conducted to improve methane gas production and carbon dioxide storage performance.
3. Gas hydrate production efficiency is primarily dependent on the injected gas and its injecting condition.
4. The novelty and originality of the work are a proposed new multilayer hydrate cap mechanism and an improved recovery method for gas from hydrate layers.

Abstract:

Efficiently and safely producing natural gas stored as gas hydrates remains an urgent and, as yet, unsolved challenge. The CO_2 replacement method is attractive for combining methane production and carbon dioxide storage but with low efficiency due to a barrier formed at the vapor and solid-phase interface. Although there has been previous work in this area, development is restricted by the unknown underlying mechanism of improving recovery efficiency for the long term. In this study, a series of experiments were conducted to obtain a new concept for improved recovery by the combination of depressurization and gas replacement methods. Air/CO_2-enriched air was injected into artificial multilayer hydrate sediment at pressures of 8.5 to 18.7 MPa. The recovery efficiency was investigated using a method that combines three-stage depressurization assisted with CO_2-enriched air injection. Initial production pressure was found to positively affect the recovery of methane via injecting of air, whilst an opposite influence by injecting CO_2-enriched air. Compared with injecting air, injecting CO_2-enriched air promotes the performance of gas hydrate production up to 74.4 % recovery ratio. Therefore, a novel multi-layer hydrate cap mechanism is proposed to describe the improved efficiency during the replacement-depressurization process for the first time. Multilayer hydrate cap and its composition are dependent mainly on the initial condition of injected gas, thereby causing limited recovery efficiency. The

results obtained from this study are beneficial for future optimizing operation conditions to maximize efficiency and develop planning for natural gas hydrate resources.

4.1 Introduction

The total global energy demand is on the rise at its fastest pace in the last decade, driven by robust human development and more substantial heating and cooling requisition in many regions. Natural gas demand is particularly pronounced for its green and efficiency, which grew at one of its fastest rates for over 30 years, accounting for over 40% of the growth in primary energy [1]. At the same time, global carbon dioxide (CO_2) emission in the atmosphere exceeded 415 parts per million (ppm) in May 2019 reported by the National Oceanic and Atmospheric Administration (NOAA) from 280 ppm at the start of the industrial revolution [2-4]. The rise in atmospheric CO_2 is the main contributor to global warming. At no previous time requires CO_2 capture technologies been greater. As a result, one of the biggest challenges of today is to fulfill the need to meet rising energy demand while at the same time reducing carbon emissions.

Gas hydrates can hold substantial amounts of methane (CH_4) as the dominant gas species in natural gas [5-6]. It has been estimated that the volume of gas ranges from 0.82×10^{13}~2.10×10^{15} m^3 thus making it a potentially abundant energy resource [7-8]. Despite the great abundance of resources around the world, a large portion of these resources is not generally considered producible with existing technology. Resultantly, gas hydrates production testing has not been actively exploited until recently with aiming also converted from an academic curiosity [9-12] into concerns of energy and environment [13-17]. Several exploitation methods have been proposed based on the thermodynamic and physical characteristics of natural gas hydrates. Among the several production methods, depressurization is particularly advantageous and has been studied extensively due to its energy efficiency [18-24]. Zhao et al. [25] analyzed hydrate dissociation behavior via depressurization, finding that all methane hydrate dissociates simultaneously at the beginning of depressurization followed by radial spread from outside of hydrates. The methane (CH_4) recovery rate decreased with higher initial saturation, and production time reduced under a higher pressure driving force, which Almenningen et al. [21] reported.

Based on successful lab-scale production experiences, the 2002 Research & Development (R&D) program was conducted to quantify and characterize in-situ gas hydrate occurrences at the Mallik gas hydrate field, Mackenzie Delta, Canada. This is the first full-scale thermal production but with limited gas flows at a maximum of 101940 m^3/day [26], reflecting that the test was a controlled production experiment rather than a long-duration test. The advantages of this method are simple, fast, and controllable, but the overall observed gas production rate was low throughout. Then in 2007, the BP-U.S. Department of Energy-U.S. Geological Survey (BP-DOE-USGS) collaborative project at Mount Elbert is initiated via drawing down pressure within the reservoir below gas hydrate equilibrium conditions, and the gas hydrate was dissociated to produce gas and water [27].

In 2008, much more extensive and more prolonged gas production was accomplished by Canada and Japan with a stepwise draw-down pressure testing to around 4.5 MPa at the Mallik gas hydrate field, achieving sustained gas flow for six days with 13000 m^3 gas totally, indicating the first sustainable gas production from hydrate reservoir to surface by depressurization method. The analysis of net energy spent for running depressurization reported that the total energy produced was about 30 times greater than that consumed [28-29]. Also, many issues concerning the depressurization process are yet to be resolved, not the least of which is the geological integrity of the sediment upon production of the vast amounts of gas and co-produced water [30]. Thus, a production project of high energy efficiency was expected for future production by depressurization. A more novel method that has been discussed for gas exploitation from gas hydrate reservoirs is a carbon dioxide (CO_2) replacement method via injection of CO_2 or mixtures containing CO_2. This technique has the advantage of methane production and carbon dioxide storage in the marine sediment as gas hydrates. The idea here is that the chemical potential of methane hydrate is higher than that of CO_2 hydrate, meaning that CO_2 hydrates are more stable [31-35]. As a result, the injection of CO_2 into a hydrate reservoir can replace methane with CO_2 and reduce the impact of hydrate dissociation on the geomechanical stability of the hydrate reservoir. Having the extensive investigations of CH_4-CO_2 exchange methodology on a laboratory scale, in 2011–2012, this technology was implemented through a project initiated by DOE and ConocoPhillips at a site on the Alaska North Slope and have been maintained for 25 days [36]. The program clarified the presence of free water within the gas hydrate

reservoir, and a finding gives significant inspiration for researchers to improve the complex process further [37].

The world's first marine gas hydrate production test attempt was executed at Nankai Trough, Japan, in March of 2013, with a production rate of around 20000 m^3/day during the six-day test [38]. A second depressurization production attempt was followed in 2017 at the nearby location; however, a higher water production rate confined the degree of reduction of pressure. This question was raised because of the heterogeneous hydrate reservoir that disturbed the efficiency of gas production. Therefore, the influence of heterogeneity is essential to be understood well to achieve a longer duration of gas production. Meanwhile, Chinese government successfully conducted a marine gas hydrate production in silty clay sediments at South China Sea for 60 days continuous test results in about 16000 m^3/day of average output. This testing provides essential data and assessment for us to understand the geological controls of gas hydrate occurrence. Therefore, more gas hydrate production testing has been proposed and is being planned for offshore of China, India, and Japan in the future. Also, a new gas hydrate testing project located on the Alaska North Slope was started in 2018 until 2020 to extend production testing operations. While each production test has shown the feasibility of depressurization or CH_4-CO_2 exchange method at an impressive amount of hydrate resource, each method has drawbacks and only remains a short term of the period, which raises questions about the commercial resource potential of gas hydrate. Therefore, an intense investigation in technical advancement would be necessary before full commercial production of methane could be achieved. The next milestone in the field would likely be understanding the mechanism of production tests to access extended-duration production.

CH_4 replacement efficiency was limited by mass transfer due to a newly formed hydrate layer on the surface of the methane hydrate after the initial hours of the rapid replacement stage [39]. Thus, attempts have been made to focus on decaying the layer to elevate recovery efficiency further and extend the production process. Some depressurizations were experimentally performed exceptionally by investigators, for instance, slow stepwise depressurization [40], multistage depressurization [41-42], and in combination with thermal stimulation [43-45], water injection [46-48], or gas injection [49-52]. Although hydrate production behavior in sandstone is relatively well known, hydrate production in multilayer

sediments has scarcely been investigated by researchers. The majority of natural gas hydrates are spatially distributed in subsurface marine reservoirs. The characteristics of these reservoirs are highly variable. Experiments done to date are limited to simulation of hydrate production in single media [53-55]. In reality, the reservoirs may occur in sandstone deposits, gravel, sand, clay, or silt sediments [56-59]. Davidson et al. [60] found that the properties of the deposits are of significance to their production. Several decades later, laboratory workers investigated hydrate production behavior in simulated sediments. In recent years, the effort has been expended researching deep-water gas hydrate exploration and production by gas and oil companies to determine the potential of natural gas hydrates as a source of hydrocarbons. However, research on the production of methane from multilayer hydrate reservoirs is scarce in the open literature. In addition, studies on the synergistic effect of the combination of injection of CO_2-enriched air and depressurization in hydrate reservoir are seldom reported.

For the above-mentioned reasons, improved technology should be developed to increase the hydrate recovery ratio for long-term production. The underlying understanding mechanism is a priority to this purpose. Since field tests are generally costly and time-consuming, laboratory works play an essential role in developing gas production technologies. It is to such a novel technology that the paper is presented. This study examined the factors that influence hydrate production from multilayer sediments by injection of air and CO_2 enriched air. Recovery of CH_4 with simultaneous CO_2 storage was investigated. A combined production method was introduced where gas injection and depressurization were used. Based on our experimental results, a novel hydrate mixture cap attenuation mechanism was proposed for gas production via depressurization with CO_2-enriched air for the first time. The results are of interest for the development of a comprehensive description of gas hydrate production technology.

4.2 Experimental methodology

4.2.1 Experimental apparatus

Figure 4.1 presents a schematic diagram of the apparatus for gas hydrate formation and recovery. The whole experimental apparatus consists of the main reactor and two buffer

cells. The main reactor with adjustable volume was designed to synthesize methane hydrate on the simulated multilayer seafloor and perform multi-step depressurization with CO_2-enriched air. The apparatus has an internal volume of 520 mL, with an inner diameter of 5 cm and length of 35 cm, and maximum working pressure of 25 MPa. A movable piston inside the reactor divides the cell into two separate sections. One is connected to a high-precision syringe pump (Teledyne® ISCO). The other section is used to perform hydrate formation and swapping. Internal pressure is adjusted for injection or expulsion of liquid water through appropriate operations with the syringe pump, removing the need to decrease the amount of gas. A circulating bath regulates the experimental temperature by circulating coolant through the jacket surrounding the reactor. To eliminate the influence of heat upon injection of air, gases were precooled for 6 hours before being transferred to the main reactor from the two buffer cells whose volumes are 315 mL and 365 mL, respectively. Gas injection rates were controlled by a mass flow controller (Bronkhorst® EL-FLOW®). During the experiments, the data acquisition unit recorded the following parameters as a function of time, temperature, pressure, volume changes of the syringe pump, gas injection rates, amount of gas fed in and out of the reactor. The pressure transducers and thermocouples were calibrated using a pressure test gauge with an error of 0.05% and a digital thermometer with a tolerance of 0.01 K, respectively.

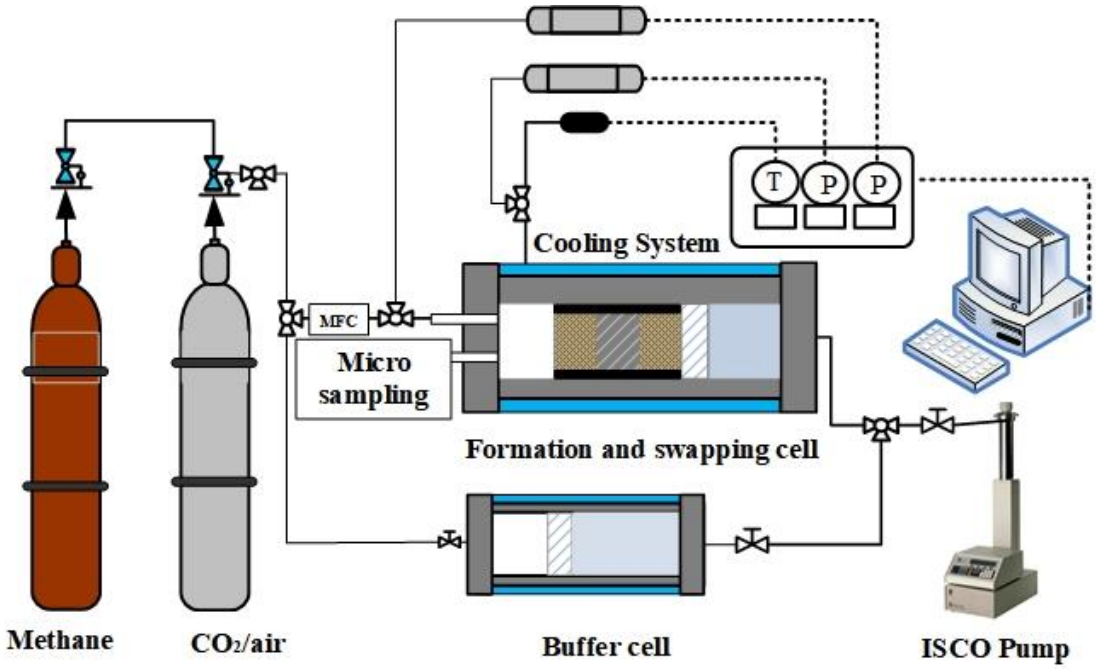

Figure 4.1 Schematic of the experimental setup for hydrate formation and recovery.

4.2.2 Materials

For all the experiments, methane, carbon dioxide, and synthetic air (20 mol % and N_2 80 mol %) were supplied by Air Liquid with a certified purity of 99.995 %. Quartz sand with 50–70 mesh particle size was purchased from Sigma Aldrich. Sandstone was obtained from Obernkirchener Sandstein. Appropriate sizes of sandstone samples were cut and polished before cleaning. The distilled water used in the study was made in the lab. The properties of sandstone and quartz sand are listed in Table 4.1.

Table 4.1 Physical properties of multilayer samples.

Properties	Sandstone A	Sandstone B	Quartz sand
Weight (g)	69.17	63.63	35.92
Diameter (mm)	37.21	36.92	-
Length (mm)	35.20	34.87	-
Pore volume (mL)	4.72	4.61	9.8

4.3 Experimental procedure

4.3.1 Sample preparation

An unconsolidated three-layer sample with a rubber surround was loaded in the main reactor. The sandstone was cleaned with methanol and toluene for the removal of organic and inorganic material. The cleaned sandstone and sand were subsequently dried at 373 K for over 24 hours. A simulated reservoir with three layers representing hydrate-bearing marine sediment is shown in Figure 4.2. The layers consist of sandstone A, quartz sand, and sandstone B (left to right).

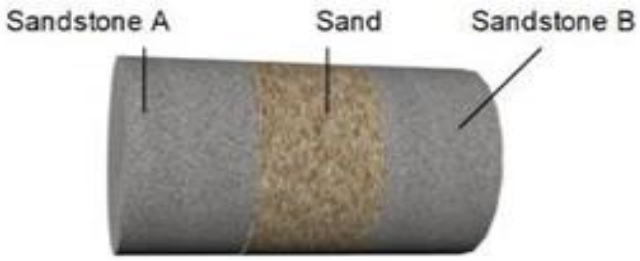

Figure 4.2 Multi-layer hydrate sediment. (Left to right: Sandstone A, Sand, Sandstone B)

The assembled multi-layer sediment was immersed in distilled water overnight before being placed in an ultrasonic bath for 4 h to achieve an even water distribution. X-ray computer tomography scans were conducted to confirm the distribution, which is shown in Figure 4.3 for both wet and dry sediments. CT values for sediment cross-section at each position were obtained. The CT value at each layer, equivalent to sample density, is nearly equal for dry and water-saturated sediment, indicating that water evenly distributes at each layer of the sediment.

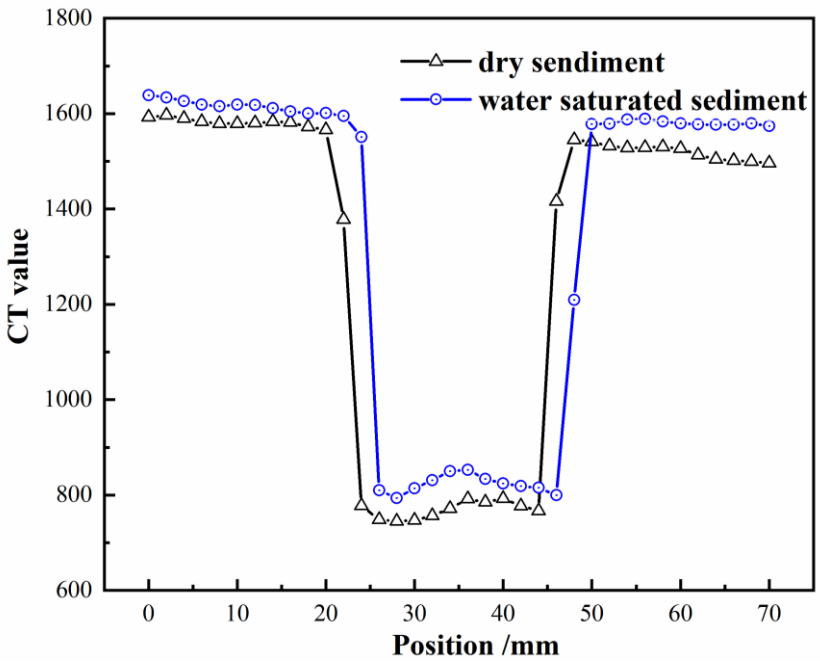

Figure 4.3 A typical CT value curve for dry and water-saturated sediment.

Experiments were carried out in two stages. In the first stage methane gas hydrate is formed, and the same procedure was followed for all runs. The second stage consisted of air/CO_2-enriched air injection and was associated with three stages of depressurization.

4.3.2 Hydrate formation process

The first step of the experimental procedure is the hydrate formation in the multi-layer sediment. The rubber sleeve containing the water-saturated multilayer sediment was placed inside the cell at room temperature. The volume of the hydrate formation cell was set at 100 mL by controlling the high-precision syringe pump. The cell was purged with methane several times to ensure the absence of air. Subsequently, methane was injected at a controlled rate into the cell until the desired pressure was achieved, sufficiently higher than the equilibrium pressure at the working temperature. The amount of gas injected was recorded from the high precise syringe pump. The inlet of the cylinder was then closed for 2 hours, where the pressure stabilized, and gases dissolved in the water. Subsequently, the temperature was decreased to its working value, and temperature and pressure data were logged. To obtain a high conversion of methane hydrate and homogenously distributed hydrates, a temperature ramping method was used. When the pressure of the cell was constant for more than 24 h, the hydrate formation period was considered complete. The amount of hydrate formed is determined from the difference between the initial and final pressure in the cell. The conversion to hydrates is then estimated by an equation-of-state assuming a hydration number of 5.67 [5].

After the hydrate formation was complete, the methane in the gas phase was removed by injecting air or CO_2-enriched air in the high-pressure cylinder. The production phase of the experiment could then proceed. The amount of gas consumed was calculated based on the pressure difference between the beginning and end of the experiments; thus, the amount of hydrate can be obtained as the decrease of methane in the vapor phase.

$$\Delta n_H = n_{g,0} - n_{g,t} = (\frac{PV}{ZRT})_0 - (\frac{PV}{ZRT})_t \quad (4\text{-}1)$$

where $n_{g,0}$ and $n_{g,t}$ is the amount of gas at time 0 and t, P represents the pressure in the system, T is the experimental temperature, V is the volume of the gas phase, and Z is the compressibility factor obtained from the Peng-Robinson equation of state [61]. R is the universal gas constant.

The following equation can calculate the initial hydrate saturation:

$$S_H = S_w \times \frac{\Delta n_H \times 5.67}{n_{H_2O}} \times 1.25 \times 100\% \quad (4\text{-}2)$$

where S_w is the initial water saturation in the sediment before hydrate formation. n_{H_2O} refers to the total number of moles of water in the system.

4.3.3 Methane production process

After CH_4 hydrate formation, air or CO_2-enriched air was injected into the pressure cell to sweep the residual CH_4 gas at a controlled rate, ensuring the absence of CH_4 in the gas phase. During the sweep, the pressure inside the cell was kept unchanged with the aid of a back-pressure controller. The gas from the outlet valve was analyzed by gas chromatography (Agilent 7890A). The sweep stage was terminated once no free CH_4 remained in the gas phase.

During hydrates soaking in the air or CO_2-enriched air for replacement, CH_4 produced from the hydrates was detected by GC at some time intervals. Later in this work, a three-stage depressurization method was introduced in the subsequent replacement process. During the reaction, the composition of gas collected from the cell is measured by GC. Approximately 100 μL of the gas phase was removed during each sampling process, too little to affect the process equilibrium due to a decrease in the amount of gas. At the end of each complete experiment, the temperature was increased to 298 K to dissociate all the remaining hydrate. This confirmed the total amount of methane in the hydrate. The recovery ratio was calculated as follows

$$\mathrm{CH_4\ recovery\ ratio} = \frac{(n_{CH_4,V})_t}{\Delta n_H} \times 100\% \quad (4\text{-}3)$$

In the above equation, $(n_{CH_4,y})_t$ methane is the gas phase at any time t during the recovery period, calculated by Equation (4-4).

$$(n_{CH_4,y})_t = y_{CH_4} n_{M,g} \quad (4\text{-}4)$$

$y_{CH_4}$and $n_{M,g}$are the mole fraction of methane and mole amount of gas mixture in the vapor phase of the reactor, respectively. The performance of CO_2 capture was investigated by calculation of the storage ratio of CO_2 during the replacement process, which is based on the composition of CO_2 in the vapor phase.

$$\mathrm{CO_2\ storage\ ratio}=\frac{(n_{CO_{2,V}})_0-(n_{CO_{2,V}})_t}{(n_{CO_{2,V}})_0}\times 100\% \quad (4\text{-}5)$$

where $(n_{CO_{2,V}})_0$ and $(n_{CO_{2,V}})_t$ are the number of moles of CO_2 at the beginning of replacement and sampling time *t* during the replacement process.

4.4 Results and discussion

4.4.1 Methane hydrate production behavior by injection of air

Air is abundant and easily obtained, making it a convenient and economical alternative to flue gases, which require transportation. In this work, two experiments were conducted by injection of air and CO_2-enriched air, respectively. Each series was carried out at an identical temperature to investigate the changes in reservoir pressure, gas production rates, and gas recovery ratios during methane hydrate production. Air injection experiments were conducted in multilayer sediments at injection pressures of 8.5 MPa, 10.2 MPa, 18.7 MPa, and a production temperature of 274.7 K.

Figure 4.4 shows the recovery ratio of methane over time under these different pressures when synthetic air was injected into a simulated hydrate reservoir. The evolution of methane recovery ratio reveals how methane is released. A longer lasting slow methane release stage follows a fast methane release stage associated with rapid methane hydrate decomposition as the system approaches a new equilibrium. It can be seen that the recovery of methane increased fast during the first 25 hours as the chemical potential difference between methane in the gas phase and methane in the solid hydrate phase dominates the driving force for methane production. The graph also shows that the production behavior can be divided into two stages: At the beginning of production, methane gas is rapidly liberated from the solid hydrate reservoir, and afterward, nearly stable recovery is shown concerning time, which is the second stage. During this stage, hydrate decomposition was constrained due to the gradually decreasing difference of methane chemical potential between the two phases and a reduced contact area between air and hydrate. The equilibrium boundary also slowly moves toward the CH_4-rich hydrate region due to the continuous liberation of CH_4 until a new thermodynamic equilibrium is achieved. The importance of the influence of initial pressure on methane recovery was explored in the

pressure range 8.5 to 18.7 MPa. Figure 4.4 compares the recovery of methane at three different pressures in the same sediment. Recovery ratios rapidly increase in the initial production period, followed by a stage where the ratio increases more slowly. The same behavior was observed at all experimental pressures. This shows that the recovery ratio of methane from simulated hydrate increases as the initial production pressure increases.

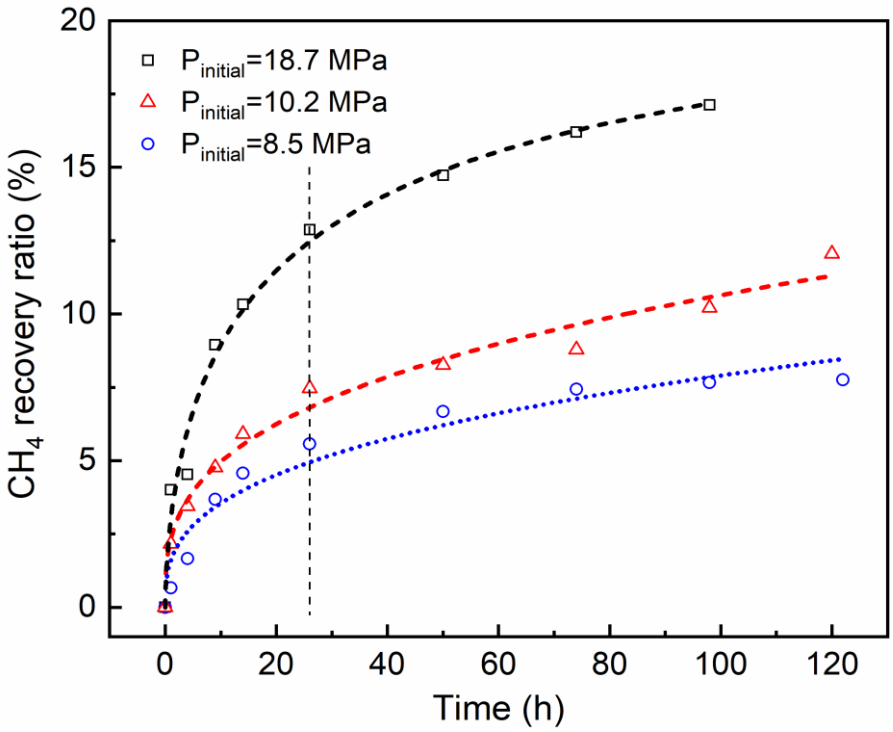

Figure 4.4 The recovery ratio of CH_4 by injection of air under different initial pressures as a function of time.

Figure 4.5 shows a typical profile of the recovery ratio of methane over time by introducing three stages of depressurization. Once the pressure of the system was reduced, an apparent sudden rise of the recovery ratio is obtained. The gas production behavior of each pressure reduction period exhibits a similar pattern, showing two stages of gas release.

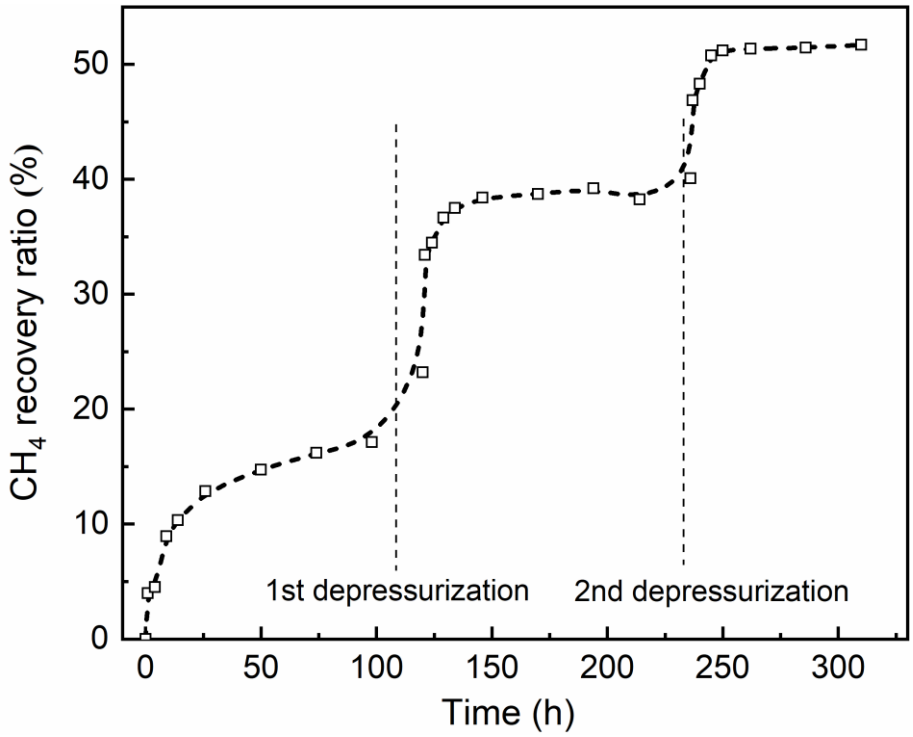

Figure 4.5 A typical experiment for CH_4 recovery ratio with time during three stages of depressurization at 274.7 K and 18.7-5.1 MPa.

Pressure and temperature profile during depressurization operation as shown in Figure 4.6. The conditions of each experiment and results are summarized in Table 4.2.

Table 4.2 Gas hydrate production conditions and recovery ratios.

	1st stage of production			2nd stage of production			3rd stage of production		
Initial water saturation (%)	16.4	20.2	31.6	-	-	-	-	-	-
Initial hydrate saturation (%)	57.5	53.3	42.7	-	-	-	-	-	-
Initial pressure (MPa)	18.7	10.2	8.5	9.5	7.1	6.8	5.6	4.8	5.1
Production temperature (K)	274.7	274.7	274.7	274.7	274.7	274.7	274.7	274.7	274.7
CH_4 Recovery ratio (%)	23.2	12.1	10.8	40.1	27.3	25.8	51.7	36.6	34.6

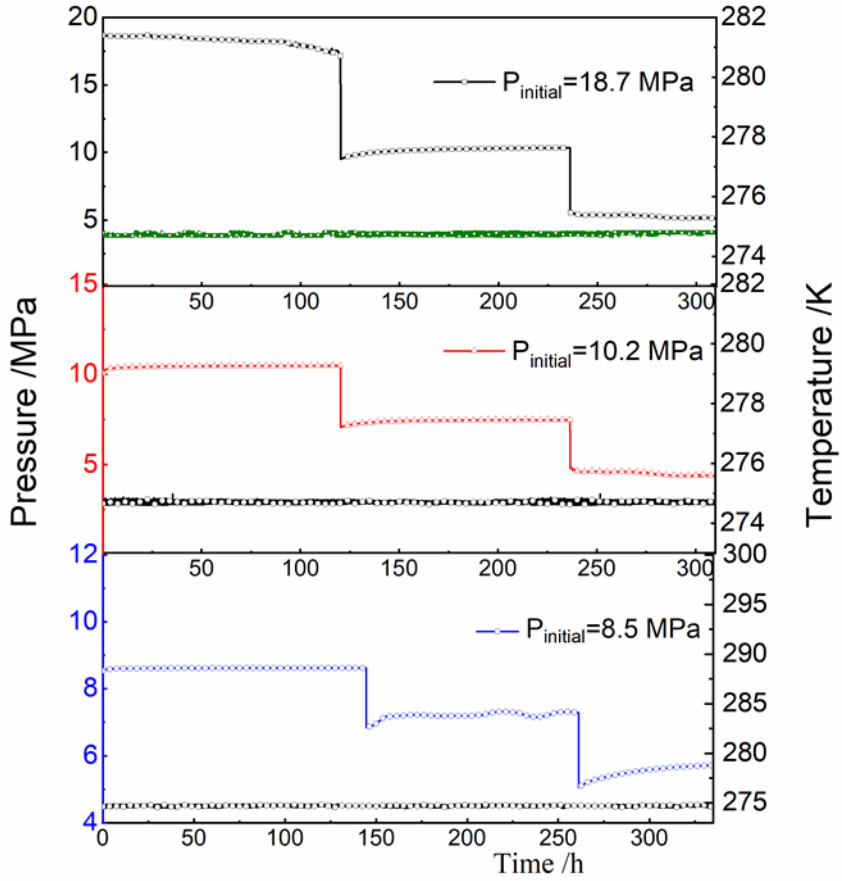

Figure 4.6 Temperature and pressure profile during gas production via air injection.

Figure 4.7 presents the recovery changes with elapsed time throughout the procedure, indicating that the introduction of depressurization can improve the performance of methane recovery efficiency and the final recovery ratio positively based on the initial recovery pressures. If only the effect of gas injection is considered, 23.2 % methane recovery was achieved at 18.7 MPa. This increases to 51.7 % when the pressure in the system is reduced. The H-L_w-V phase equilibrium pressure for air is 18.3 MPa at 274.7 K [63], which excludes the possibility of recovery ratio increment due to the inclusion of air hydrate.

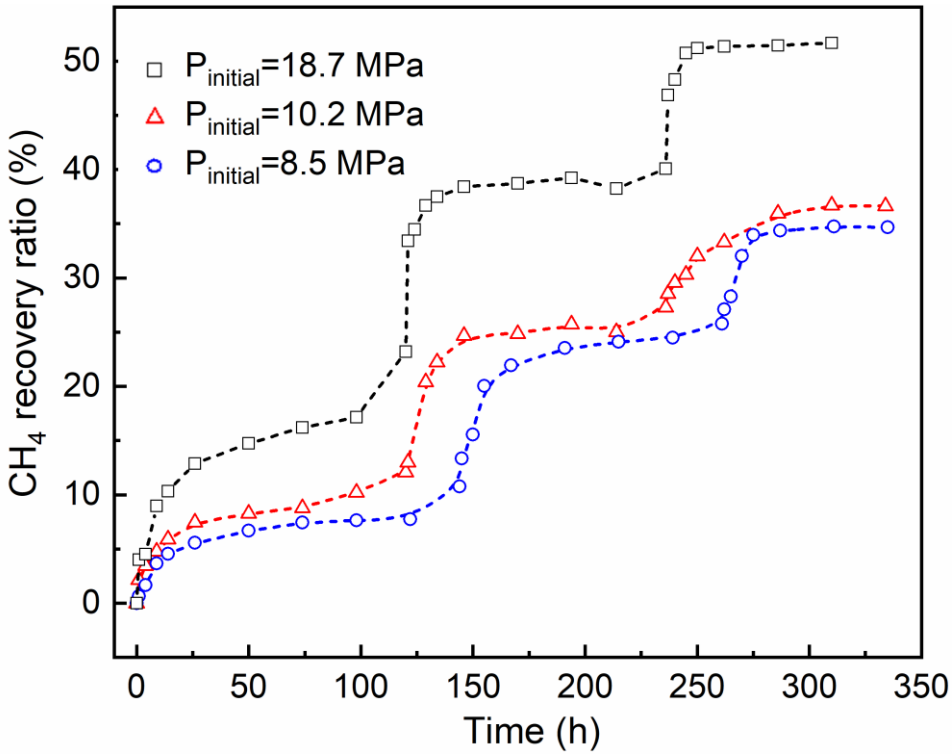

Figure 4.7 CH_4 recovery ratio with time during three stages of depressurization at 274.7 K.

4.4.2 Production behavior by injection of CO_2-enriched air

Replacement experiments were conducted at the identical temperature of 275.3 K under three different initial pressures ranging from 8.5 to 14.5 MPa. Methane recovery and CO_2 storage ratio were measured to explore methane production behavior and CO_2 storage performance with production time. Kang et al. [63] concluded that high-CO_2 in air leads to replacement-dominant hydrate recovery during production. This study introduced CO_2-enriched air (20 mol% CO_2 + 80 mol% air) into a simulated hydrate reservoir using the procedure described in section 4.3.

The recovery ratio of methane reveals the absolute recovery ability, which is in the light of the composition of increment of methane in the vapor phase. CO_2 in the vapor phase was captured simultaneously. Figure 4.7 (a) shows that the CH_4 recovery ratio increased dramatically within 20 hours at the beginning of the replacement stage. Gradually, a slower release of methane was detected from 15 to 30 hours, followed by a stable period. Compared with the recovery ratio obtained by air injection, the addition of CO_2 into air significantly increases the yield, in this case, up to 41.5 % at 8.5 MPa. Additionally, initial

production pressure negatively influences methane recovery, but a positive effect on the CO_2 storage ratio is illustrated in Figure 4.9. Research on gas hydrate production is mostly focused on methane recovery [32,33], while little attention has been paid to the potential for CO_2 storage.

Figure 4.8 (b) presents the profile of CO_2 storage percentage as the production proceeds. At the early methane rapid release stage, CO_2 in the vapor phase also shows a sudden decrease corresponding to the fast capture of CO_2. This indicates a fast conversion of CO_2 gas into hydrate. Yang et al. [64] showed a similar fashion of methane hydrate decomposition and CO_2 storage process for flue gas-induced methane hydrate dissociation on a single layer of sediment. Based on the results shown in Figure 4.8, it is concluded that methane was rapidly liberated from the solid hydrate phase at the start of injection due to the chemical potential difference of methane between vapor and solid phase, resulting in a rapid change in gas composition. Simultaneously, a mixed hydrate layer from injected gas covers the methane hydrate, which blocks the subsequent transfer of methane into the vapor phase. The effects of pressure on methane recovery exhibit very different behaviors between injecting air and CO_2 is added. The two opposite patterns of methane recovery and CO_2 storage evolution demonstrate that there is a new hydrate formed by injected gas on the surface of the methane hydrate.

A higher production pressure corresponds to a larger driving force (the difference between the actual and the pressure at the equilibrium boundary). This driving force increases with pressure. Thus a strengthened hydrate formed from injected gas slows methane hydrate decomposition. A proposed explanation for this process is shown in the next section. A larger driving force is imposed for forming hydrate from injected gas with high injection pressure, resulting in an elevated storage ratio. Over the course of the production, both methane recovery and CO_2 storage gradually reach a constant value. This indicates that decreasing production pressure can significantly increase the recovery ratio of methane from the hydrate reservoir.

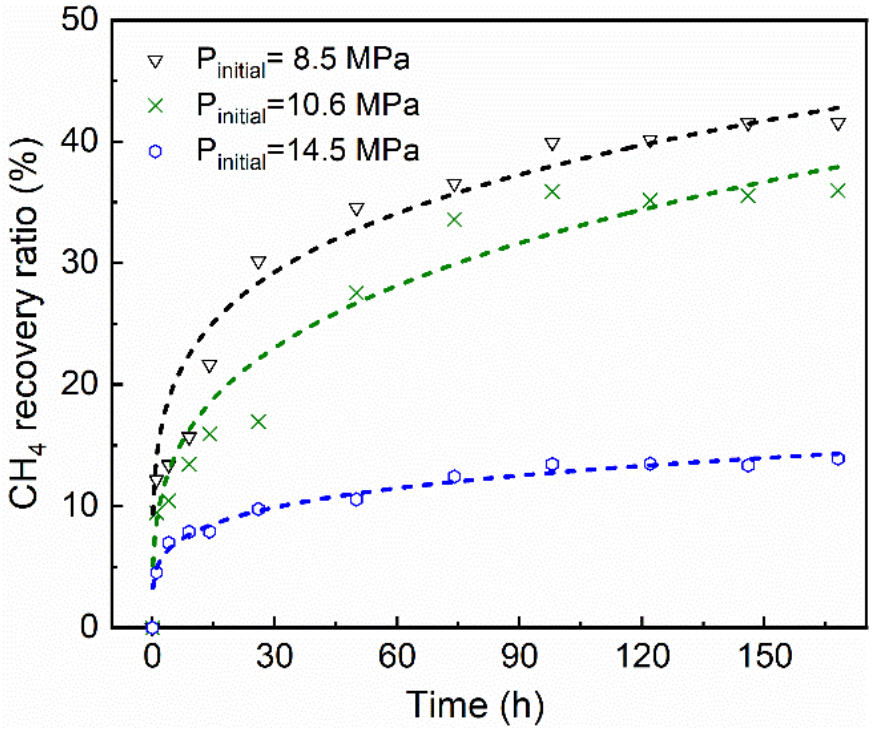

Figure 4.8 CH_4 recovery ratio at different pressures at 275.3K as the function of time.

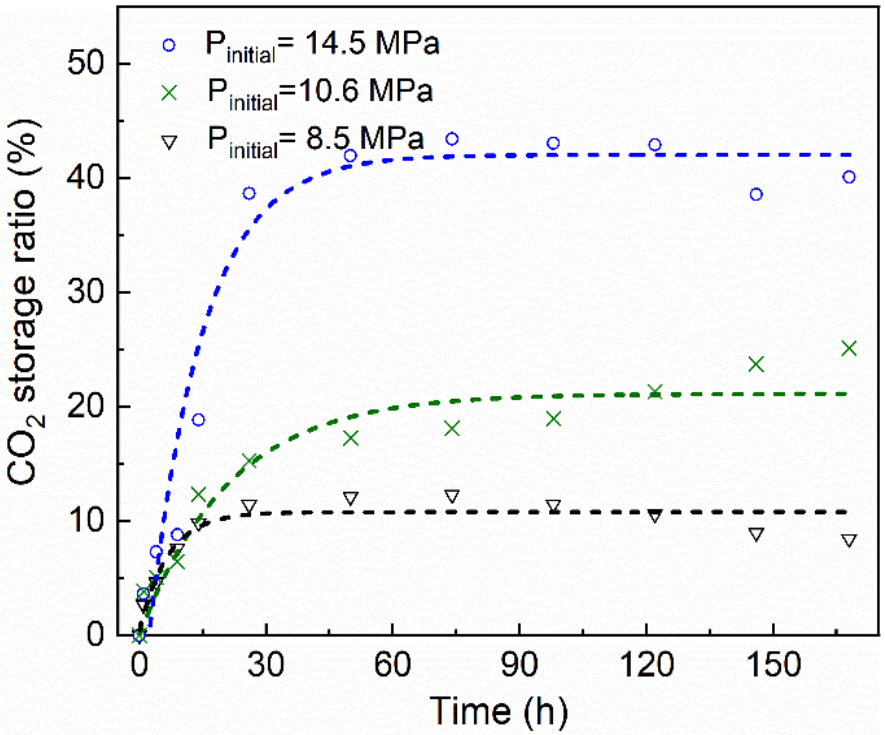

Figure 4.9 CO_2 storage ratio at different pressures (14.5 MPa 10.6 MPa, 8.5 MPa) at 275.3K as the function of time.

After the system reached a steady composition in the vapor phase, a staged decreasing pressure experiment was conducted to investigate the production behavior. The operation was performed again after the second stage of stability was reached. Figure 4.10 shows the CH_4 recovery ratio changes during the decreasing pressure experiments. As shown in the figure, after recovery of CH_4 is stable in each stage, the ratio has consistently increased to a higher value stage in a short time and then gradually reaches a new steady level, lasting for a longer time. The enhanced recovery is evident, especially under lower pressure (8.5 MPa).

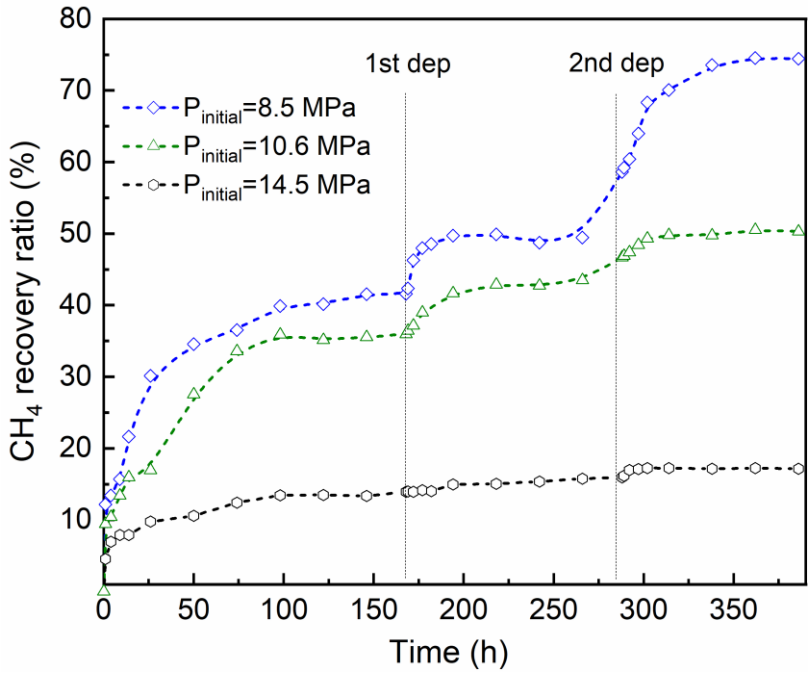

Figure 4.10 Variation of methane recovery with time during the replacement process at different initial pressures and at 275.3 K.

Meanwhile, the storage percentage of CO_2 over the same course is presented in Figure 4.11. The pressure of the system is decreased at 168 h and 266 h, where a change in the ratio is seen. It should be noted that the operating conditions at 14.5 MPa and 275.3 K are well above the hydrate equilibrium boundary for the injected gas [63], indicating a methane lean mixed hydrate is formed as a barrier for further recovery. This boundary is shifted towards the CH_4-rich region as the replacement process proceeds. These results show that the first pressure reduction in the system led to a slight decrease in CO_2 storage ratio and increase in CH_4 storage percentage, implying this pressure reduction can decompose the

methane lean mixed hydrate layer at the surface formed during the previous stage whereby the storage of CO_2 decreases from 42.9 % to 39.5 %. Thus, the gas hydrate layer is exposed to a higher contact area with the injected gas. As the layer decomposes, this stage proceeds with the phase boundary moving towards the CO_2-rich region and simultaneously contributes to a CO_2 rich hydrate barrier. An increase of CH_4 recovery and CO_2 storage ratio is observed at 266 h, where the second depressurization is performed, indicating methane in the unexploited hydrate much easier penetrate through those mixed hydrate barriers attributed to the attenuated hydrate layers due to depressurization. Similarly, the attenuated hydrate layer by further depressurization could leave some water molecules which are easier incorporated with CO_2 molecules under this condition, leading to an increased tendency in CO_2 storage ratio.

A significant enhancement CH_4 recovery ratio is observed after each depressurization is conducted at a pressure of 8.5 MPa though a slight decrease in CO_2 storage ratio. This condition is not enough to induce a barrier from injected gas at the initial stage of the injecting compared with 14.5 MPa. A sharp rise in the CH_4 recovery ratio is obtained after depressurization is applied to attenuate the weak mixed hydrate cap, increasing the opportunity for methane gas to get out of unexploited hydrate reservoirs.

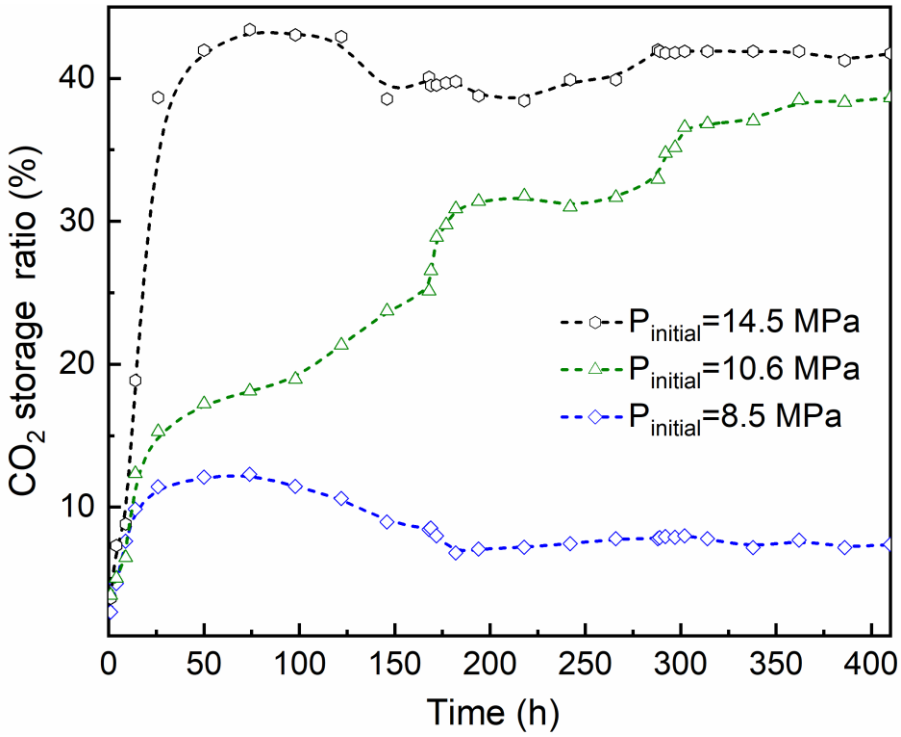

Figure 4.11 CO_2 storage ratio evolution during the replacement process under different initial pressures at 275.3 K.

CH_4 recovery and CO_2 storage ratio at each end of the stage are summarized in Table 4.3. It is shown that initial injection pressure influences the overall ratio even inconsistent of that on every stage. The figure shows that the initial exploitation condition well above the phase equilibrium boundary of injected gas facilitates CO_2 storage while a decrease in performance on CH_4 recovery compared to pressures carried out in this study. The introduction of depressurization is efficient for CH_4 recovery under lower initial production pressure. It is indicated by Yang et al. that the permeability of porous media was important for the mass transfer process, which is the main constrain for methane recovery before the introduction of depressurization.

Table 4.3 Experimental conditions conducted and resultant recovery ratio in this work.

	1st stage of production			2nd stage of production			3rd stage of production		
Initial water saturation (%)	19.2	25.1	28.5	-	-	-	-	-	-
Initial hydrate saturation (%)	55.9	49.4	46.2	-	-	-	-	-	-
Initial pressure (MPa)	14.5	10.6	8.5	10.2	8.1	5.3	6.4	6.7	3.3
CH_4 recovery ratio (%)	13.9	35.9	41.5	16.1	46.7	58.6	17.1	50.3	74.4
CO_2 storage ratio (%)	40.1	35.1	8.4	39.9	31.7	7.8	41.7	38.6	7.4

4.4.3 Novel proposed mechanism of production behavior

Based on the results obtained above, we proposed a multi-layer hydrate cap attenuation mechanism for explaining the production behavior via injected gas combined with depressurization. When injecting air in this study, the initial condition of injected gas can not form hydrate on the interface between vapor and hydrate solid, and methane gas is released mainly driven by the difference between methane vapor and hydrate phase, which is predicted as Figure 4.12 (a). While the system is in equilibrium, methane hydrate decomposition equals its reverse, resulting in a stable recovery ratio of methane. The first depressurization is employed, as illustrated in Figure 4.12 (b). The decrease of pressure affects the fugacity of methane in the vapor phase, decomposition can thus continue, which is in similar manner as the second depressurization is conducted in Figure 4.12 (c).

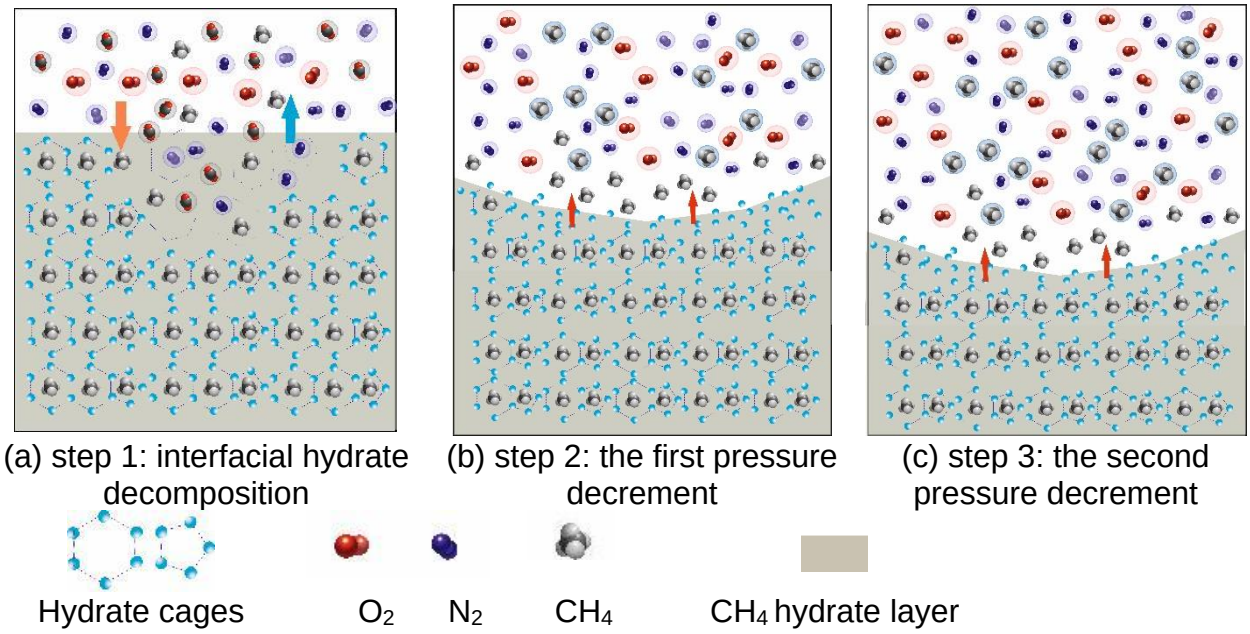

Figure 4.12 Proposed mechanism for production by non-replacement combined with depressurization.

Combined with the above mechanism for the non-replacement process, a cap attenuation mechanism was thus speculated. Figure 4.13 shows a proposed mechanism for explaining methane hydrate production behavior by CO_2-air injection combined with depressurization, which consists of five steps. Step 1 is an interfacial decomposition process similar to step 1 in Figure 4.12. After CO_2-enriched air was injected into the hydrate reservoir, injection gas spreads out and fills up the space above the solid methane hydrate as shown in Figure 4.13 (a). Once injection gas occupies the vapor space, the cages of CH_4 hydrate probably become unstable, and some methane molecules leave the hydrate cages driven by the chemical potential difference between the gaseous and solid-phase described in step 1. This assumption is consistent with Ota et al. [65] and Xun [66]. Results from the first stage of Figure 4.4 also macroscopically support this process, a fast increase in recovery ratio of methane followed by a slight tendency that is in agreement with the literature of Seo [67].

On the contrary, the molecules of injected gas that have transferred to decomposition sites can penetrate, leading to a new hydrate from the injected gas at intervals of vapor phase and solid methane hydrate. The formation of the new hydrate acting as a cap rapidly forms a mass transport barrier that slows down any further transfer of methane shown in Figure 4.13 (b), which has previously been demonstrated using a theoretical approach, concluding that methane gases transport through these hydrates, in order to sustain further

growth, is extremely slow, and even to grow 1 millimeter may take several hours [68]. The main diffusion of gas, in this step, occurs on the interface between the newly formed hydrate cap and solid hydrate, the second stage in Figure 4.4. The thickness of cap hydrate is mainly controlled by the system's initial injection pressure, which subsequently influences following recovery performance. The composition of the vapor phase changes as methane gas is released. The phase equilibrium boundary gradually moves towards the CH_4-rich region. Compared to results from the non-replacement process, the CH_4 recovery ratio relatively increases slowly due to the existence of the barrier. As mentioned from the above results, there is a transition period between the fast and slow-down stage, leading to the continuous occurrence of CH_4 recovery and CO_2 storage. This could be attributed to that there exists another barrier that hindered the replacement process goes further. We speculated that the refreshing molecules in vapor keep engaging with residue water molecules. Thus, another hypothetical hydrate layer is formed based on the vapor composition in the presence of CH_4 mixed hydrate, as shown in Figure 4.13 (c). Figure 4.13 (d) illustrates depressurization applied to the system once equilibrium is reached. The introduction of depressurization moves the equilibrium state of the system, thus the hydrate cap formed by the CH_4-rich injected gas becomes unstable, resulting in a new unstable hydrate cap. As a result, more methane hydrate in the unexploited hydrate reservoir decomposes, and more methane penetrates the two possible hydrate caps into the vapor phase. This explains the faster recovery shown in Figure 4.9, where pressure was reduced. Step 5 shows the second pressure decrement period where the cap is further attenuated in a manner similar to step 4, the injected gas hydrate layer in the absence of CH_4 is also being influenced by the depressurization. This attenuated second layer contributes to increased methane recovery. It can be concluded that the introduction of depressurization attenuates two of the hydrate caps on the hydrate reservoir, improving the production efficiency of methane from the hydrate. This mechanism is of importance for the development of a complete description of the technology of gas hydrate production.

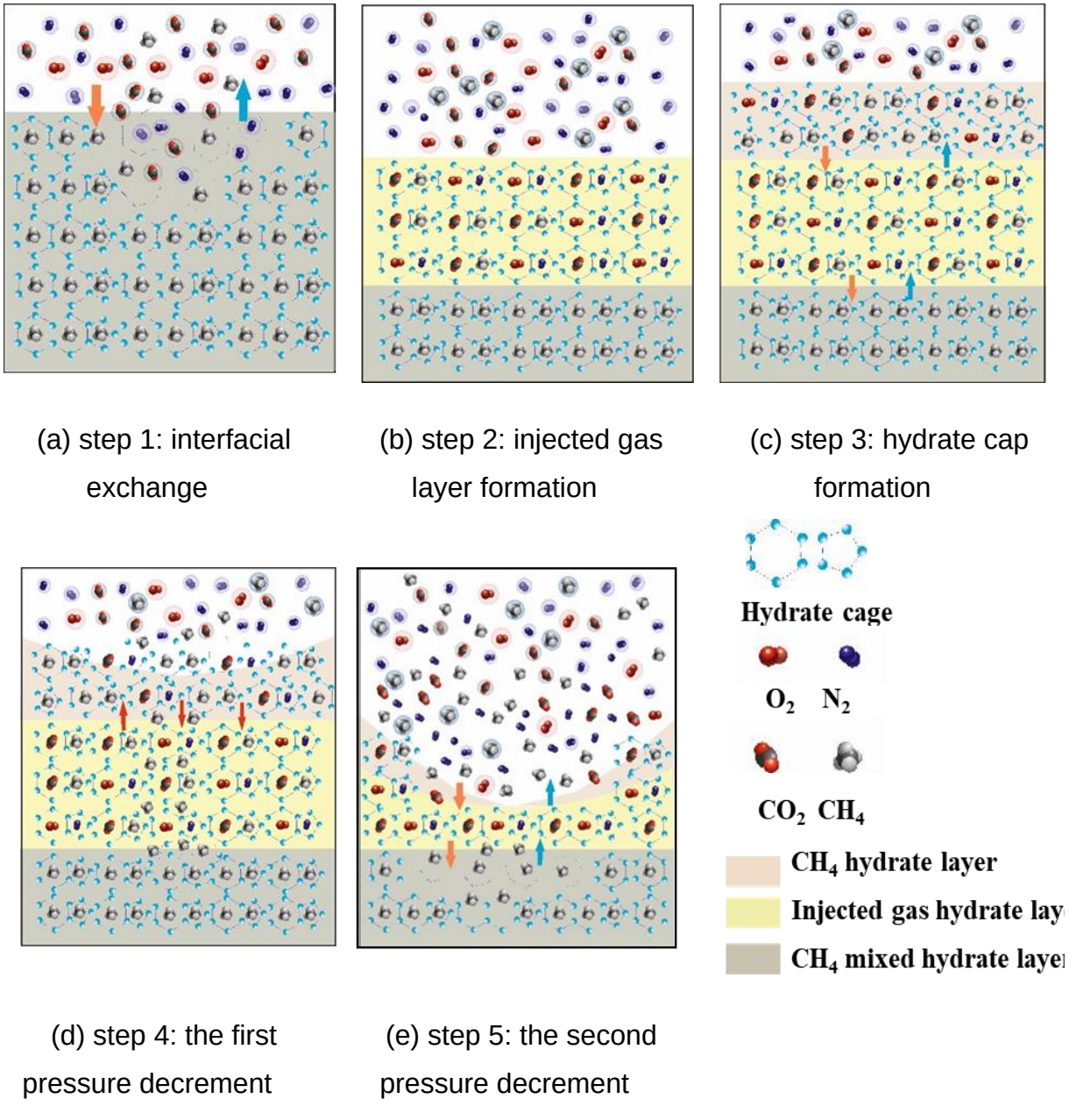

Figure 4.13 Proposed mechanism for production by replacement combined with depressurization.

4.5 Summary

This work presents an experimental study of the gas recovery and CO_2 storage behavior from multilayer methane hydrate sediment using an air or CO_2-enriched air replacement method combined with depressurization. Results from experiments show that injecting air into methane hydrate reservoir is a feasible and potentially economical method for methane production but with low recovery. Injecting CO_2-enriched air demonstrated significantly

increased methane production efficiency while also storing CO_2 concerning initial production pressures. The introduction of depressurization can increase methane recovery in both scenarios. Recovery ratios are shown to increase when a three-stage depressurization method was introduced in the process at three different initial injection pressures at the same gas hydrate reservoir temperature.

Pressure reduction with gas injection significantly increased methane production efficiency, while its improvement on CO_2 storage performance is not very markable for CH_4 recovery. Based on the hydrate production behavior, a novel multilayer hydrate cap attenuation mechanism was proposed for gas production behavior via depressurization with CO_2-enriched air behavior for the first time, which well explained the behavior during the production process multilayer hydrate cap and its composition are largely dependent on the initial condition of injected gas, thereby causing limited recovery efficiency. The introduction of 3 stages of depressurization can prolong this production process and, most importantly, enhance the recovery ratio via attenuating such multilayer cap. The results obtained from this study provide important insights into optimizing operation conditions to maximize efficiency and prolong the production period for field hydrate production. The novelty and originality of the work are a proposed new multilayer hydrate cap mechanism and an improved recovery method for gas from hydrate layers.

d. Acknowledgment

This work is supported by the Department of Chemical and Biochemical Engineering, Technical University of Denmark, and the State Scholarship Fund of China Scholarship Council.

e. References

[1] B.P.E. Outlook Energy Outlook 2030; BP Publishers: London, 2012.

[2] Rotty, R. M. Distribution of and changes in industrial carbon dioxide production. J. Geophys. Res. 1983, 88, 1301−1308.

[3] Keeling, C.D., The concentration and isotopic abundances of atmospheric carbon dioxide in rural areas. Geochim. Cosmochim. Acta. 13, (1958) 322–334.

[4] R. Nydal, Further investigation on the transfer of radiocarbon in nature, J. Geophys. Res. 73 (1968) 3617–3635.

[5] E.D. Sloan Jr, C.A. Koh, Clathrate hydrates of natural gases, CRC press, 2007.

[6] E.D. Sloan, Fundamental principles and applications of natural gas hydrates, Nature. 426 (2003) 353–359.

[7] G.J. Moridis, L. Berkeley, T.S. Collett, U.S.G. Survey, E.D. Sloan, Toward Production From Gas Hydrates : Current Status , Assessment of Resources , and Simulation-Based Evaluation of Technology and Potential, (2009) 745–771.

[8] Y.F. Makogon, Natural gas hydrates – A promising source of energy, J. Nat. Gas Sci. Eng. 2 (2010) 49–59.

[9] M. Faraday, H. Davy, XIV. On fluid chlorine, Philos. Trans. R. Soc. London. 113 (1823) 160–165.

[10] W.I. Wilcox, D.B. Carson, D.L. Katz, Natural gas hydrates, Ind. Eng. Chem. 33 (1941) 662–665.

[11] D.W. Davidson, Y.P. Handa, C.I. Ratcliffe, J.S. Tse, B.M. Powell, The ability of small molecules to form clathrate hydrates of structure II, Nature. 311 (1984) 142–143.

[12] J.C. Platteeuw, J.H. van der Waals, Thermodynamic properties of gas hydrates, Mol. Phys. 1 (1958) 91–96.

[13] S.L. Patil, A.Y. Dandekar, S. Khataniar, Alaska Gas Hydrate Research and Field Studies, in: R. Malhotra (Ed.), Foss. Energy, Springer New York, New York, NY, 2020: pp. 185–202.

[14] Y.F. Makogon, Perspectives for the development of gas hydrate deposits, in: Gas Hydrates Permafr. Proc. 4th Can. Permafr. Conf., 1982: pp. 299–304.

[15] L. Kroenke, R. Moberly Jr, G.R. Heath, 26. LITHOLOGIC INTERPRETATION OF CONTINUOUS REFLECTION PROFILING, DEEP SEA DRILLING PROJECT, LEG V, Proc. Ocean Drill. Progr. Initial Report. Part A. (1971) 1161.

[16] J. Li, J. Ye, X. Qin, H. Qiu, N. Wu, H. Lu, W. Xie, J. Lu, F. Peng, Z. Xu, C. Lu, Z. Kuang, J. Wei, Q. Liang, H. Lu, B. Kou, The first offshore natural gas hydrate production test in South China Sea, China Geol. 1 (2018) 5–16.

[17] Overview and introduction: Pressure core-sampling and analyses in the 2012–2013 MH21 offshore test of gas production from methane hydrates in the eastern Nankai Trough, Mar. Pet. Geol. 66 (2015) 296–309.

[18] X. Jiang, S. Li, L. Zhang, Sensitivity analysis of gas production from Class I hydrate reservoir by depressurization, Energy. 39 (2012) 281–285.

[19] J. Zhao, Z. Zhu, Y. Song, W. Liu, Y. Zhang, D. Wang, Analyzing the process of gas production for natural gas hydrate using depressurization, Appl. Energy. 142 (2015)

[20] V.N. Khlebnikov, S.V. Antonov, A.S. Mishin, M. Liang, I.V. Khamidullina, P.M. Zobov, N.V. Likhacheva, P.A. Gushchin, Major factors influencing the generation of natural gas hydrate in porous media, Nat. Gas Ind. B. 4 (2017) 442–448.

[21] S. Almenningen, P. Fotland, M.A. Fernø, G. Ersland, An Experimental Investigation of Gas-Production Rates During Depressurization of Sedimentary Methane Hydrates, SPE J. Preprint (2019) 9.

[22] A. Hassanpouryouzband, J. Yang, B. Tohidi, E. Chuvilin, V. Istomin, B. Bukhanov, A. Cheremisin, Insights into CO2 Capture by Flue Gas Hydrate Formation: Gas Composition Evolution in Systems Containing Gas Hydrates and Gas Mixtures at Stable Pressures, ACS Sustain. Chem. Eng. 6 (2018) 5732–5736.

[23] Y. Chen, Y. Gao, Y. Zhao, L. Chen, C. Dong, B. Sun, Experimental investigation of different factors influencing the replacement efficiency of CO2 for methane hydrate, Appl. Energy. 228 (2018) 309–316.

[24] Y. Lee, W. Choi, K. Shin, Y. Seo, CH_4-CO_2 replacement occurring in sII natural gas hydrates for CH4 recovery and CO_2 sequestration, Energy Convers. Manag. 150 (2017) 356–364.

[25] J. Zhao, Z. Zhu, Y. Song, W. Liu, Y. Zhang, D. Wang, Analyzing the process of gas production for natural gas hydrate using depressurization, Appl. Energy. 142 (2015) 125–134.

[26] S.R. Dallimore, T.S. Collett, Scientific results from the Mallik 2002 gas hydrate production research well program, Mackenzie Delta, Northwest Territories, Canada, Geological Survey of Canada Ottawa, Ontario, Canada, 2005.

[27] R.B. Hunter, S.A. Digert, R. Boswell, T.S. Collett, Alaska gas hydrate research and stratigraphic test preliminary results, Proc. Arct. Energy Summit, Anchorage, Alaska, Inst. North, Oct. 2007. (2007).

[28] S.R. Dallimore, J.F. Wright, K. Yamamoto, G. Bellefleur, Proof of concept for gas hydrate production using the depressurization technique, as established by the JOGMEC/NRCan/Aurora Mallik 2007-2008 Gas Hydrate Production Research Well Program, Bull. Geol. Surv. Canada. 601 (2012) 1–15.

[29] M. Kurihara, A. Sato, K. Funatsu, H. Ouchi, K. Yamamoto, M. Numasawa, T. Ebinuma, H. Narita, Y. Masuda, S.R. Dallimore, F. Wright, D.I. Ashford, Analysis of Production Data for 2007/2008 Mallik Gas Hydrate Production Tests in Canada, Int. Oil Gas Conf. Exhib. China. (2010) 24.

[30] D.R. McConnell, Z. Zhang, Review of progress in evaluating gas hydrate drilling hazards, Mar. Pet. Geol. 34 (2012) 209–223.

[31] P. Linga, R. Kumar, P. Englezos, Gas hydrate formation from hydrogen/carbon dioxide and nitrogen/carbon dioxide gas mixtures, Chem. Eng. Sci. 62 (2007) 4268–4276.

[32] Y.-F. Sun, J.-R. Zhong, R. Li, T. Zhu, X.-Y. Cao, G.-J. Chen, X.-H. Wang, L.-Y. Yang, C.-Y. Sun, Natural gas hydrate exploitation by CO_2/H_2 continuous Injection-Production mode, Appl. Energy. 226 (2018) 10–21.

[33] A. Hassanpouryouzband, J. Yang, B. Tohidi, E. Chuvilin, V. Istomin, B. Bukhanov, A. Cheremisin, CO_2 Capture by Injection of Flue Gas or CO_2–N_2 Mixtures into Hydrate Reservoirs: Dependence of CO_2 Capture Efficiency on Gas Hydrate Reservoir Conditions, Environ. Sci. Technol. 52 (2018) 4324–4330.

[34] C.-G. Xu, X.-S. Li, Research progress on methane production from natural gas hydrates, RSC Adv. 5 (2015) 54672–54699.

[35] B. Kvamme, A. Graue, T. Buanes, T. Kuznetsova, G. Ersland, Storage of CO_2 in natural gas hydrate reservoirs and the effect of hydrate as an extra sealing in cold aquifers, Int. J. Greenh. Gas Control. 1 (2007) 236–246.

[36] D. Schoderbek, H. Farrell, J. Howard, K. Raterman, S. Silpngarmlert, K. Martin, B. Smith, P. Klein, ConocoPhillips gas hydrate production test, ConocoPhillips Co., Houston, TX (United States), 2013.

[37] D. Schoderbek, K.L. Martin, J. Howard, S. Silpngarmlert, K. Hester, North Slope Hydrate Fieldtrial: CO2/CH4 Exchange, OTC Arct. Technol. Conf. (2012) 17.

[38] K. Yamamoto, Y. Terao, T. Fujii, T. Ikawa, M. Seki, M. Matsuzawa, T. Kanno, Operational overview of the first offshore production test of methane hydrates in the Eastern Nankai Trough, Offshore Technol. Conf. (2014) 11.

[39] B.R. Lee, C.A. Koh, A.K. Sum, Quantitative measurement and mechanisms for CH_4 production from hydrates with the injection of liquid CO_2, Phys. Chem. Chem. Phys. 16 (2014) 14922–14927.

[40] S.C. Phillips, P.B. Flemings, K. You, D.W. Meyer, T. Dong, Investigation of in situ salinity and methane hydrate dissociation in coarse-grained sediments by slow, stepwise depressurization, Mar. Pet. Geol. 109 (2019) 128–144.

[41] K.U. Heeschen, S. Abendroth, M. Priegnitz, E. Spangenberg, J. Thaler, J.M. Schicks, Gas Production from Methane Hydrate: A Laboratory Simulation of the Multistage Depressurization Test in Mallik, Northwest Territories, Canada, Energy & Fuels. 30 (2016) 6210–6219.

[42] Y. Konno, Y. Masuda, K. Akamine, M. Naiki, J. Nagao, Sustainable gas production from methane hydrate reservoirs by the cyclic depressurization method, Energy Convers. Manag. 108 (2016) 439–445.

[43] V.C. Nair, S.K. Prasad, R. Kumar, J.S. Sangwai, Energy recovery from simulated clayey gas hydrate reservoir using depressurization by constant rate gas release, thermal stimulation and their combinations, Appl. Energy. 225 (2018) 755–768.

[44] Y. Song, C. Cheng, J. Zhao, Z. Zhu, W. Liu, M. Yang, K. Xue, Evaluation of gas production from methane hydrates using depressurization, thermal stimulation and combined methods, Appl. Energy. 145 (2015) 265–277.

[45] S. Falser, S. Uchida, A. C. Palmer, K. Soga, T. S. Tan, Increased Gas Production from Hydrates by Combining Depressurization with Heating of the Wellbore, Energy & Fuels. 26 (2012) 6259–6267.

[46] X. Yang, C.-Y. Sun, Q. Yuan, P.-C. Ma, G.-J. Chen, Experimental Study on Gas Production from Methane Hydrate-Bearing Sand by Hot-Water Cyclic Injection, Energy & Fuels. 24 (2010) 5912–5920.

[47] J. Phirani, K.K. Mohanty, Warm water flooding of confined gas hydrate reservoirs, Chem. Eng. Sci. 64 (2009) 2361–2369.

[48] G. Li, X.-S. Li, B. Li, Y. Wang, Methane hydrate dissociation using inverted five-spot water flooding method in cubic hydrate simulator, Energy. 64 (2014) 298–306.

[49] A. Okwananke, J. Yang, B. Tohidi, E. Chuvilin, V. Istomin, B. Bukhanov, A. Cheremisin, Enhanced depressurisation for methane recovery from gas hydrate reservoirs by injection of compressed air and nitrogen, J. Chem. Thermodyn. 117 (2018) 138–146.

[50] Q. Yuan, C.-Y. Sun, B. Liu, X. Wang, Z.-W. Ma, Q.-L. Ma, L.-Y. Yang, G.-J. Chen, Q.-P. Li, S. Li, K. Zhang, Methane recovery from natural gas hydrate in porous sediment using pressurized liquid CO_2, Energy Convers. Manag. 67 (2013) 257–264.

[51] Y. Chen, Y. Gao, L. Chen, X. Wang, K. Liu, B. Sun, Experimental investigation of the behavior of methane gas hydrates during depressurization-assisted CO_2 replacement, J. Nat. Gas Sci. Eng. 61 (2019) 284–292.

[52] L. Mu, N. von Solms, Methane Production and Carbon Capture by Hydrate Swapping, Energy & Fuels. 31 (2017) 3338–3347.

[53] Y. Zhu, H. Wang, C. Chen, T. Luo, Effects of sand contents on mechanical characteristics of methane hydrate-bearing sediments in the permafrost, J. Nat. Gas Sci. Eng. 75 (2020) 103129.

[54] Z.-F. Sun, S. Jia, Q. Yuan, C.-Y. Sun, G.-J. Chen, One-dimensional study on gas production characteristics of methane hydrate in clayey sediments using depressurization method, Fuel. 262 (2020) 116561.

[55] T. Luo, Y. Li, B.N. Madhusudhan, J. Zhao, Y. Song, Comparative analysis of the consolidation and shear behaviors of CH_4 and CO_2 hydrate-bearing silty sediments, J. Nat. Gas Sci. Eng. 75 (2020) 103157.

[56] W.F. Waite, J.C. Santamarina, D.D. Cortes, B. Dugan, D.N. Espinoza, J. Germaine, J. Jang, J.W. Jung, T.J. Kneafsey, H. Shin, K. Soga, W.J. Winters, T.-S. Yun, Physical properties of hydrate-bearing sediments, Rev. Geophys. 47 (2009).

[57] K.U. Heeschen, J.M. Schicks, G. Oeltzschner, The promoting effect of natural sand on methane hydrate formation: Grain sizes and mineral composition, Fuel. (2016).

[58] W. Liu, F. Yu, Y. Song, J. Zhao, Y. Li, Experimental study on mechanical properties of gas hydrate-bearing sediments using kaolin clay, China Ocean Eng. 25 (2011) 113–122.

[59] Z. Jin, A. Firoozabadi, Effect of water on methane and carbon dioxide sorption in clay minerals by Monte Carlo simulations, Fluid Phase Equilib. 382 (2014) 10–20.

[60] DAVIDSON, D. W., Natural gas hydrates in northern Canada, Proc. 3rd Int. Conf. Permafr. 1 (1978) 938–943. http://ci.nii.ac.jp/naid/10008802737/en/ (accessed May 10, 2019).

[61] D.-Y. Peng, D. B. Robinson, A New Two-Constant Equation of State, Ind. & Eng. Chem. Fundam. 15 (2002) 59–64.

[62] A. H. Mohammadi, B. Tohidi, R. W. Burgass, Equilibrium Data and Thermodynamic Modeling of Nitrogen, Oxygen, and Air Clathrate Hydrates, J. Chem. Eng. Data. 48 (2003) 612–616.

[63] H. Kang, D.Y. Koh, H. Lee, Nondestructive natural gas hydrate recovery driven by air and carbon dioxide, Sci. Rep. (2014).

[64] J. Yang, A. Okwananke, B. Tohidi, E. Chuvilin, K. Maerle, V. Istomin, B. Bukhanov, A. Cheremisin, Flue gas injection into gas hydrate reservoirs for methane recovery and carbon dioxide sequestration, Energy Convers. Manag. 136 (2017) 431–438.

[65] M. Ota, K. Morohashi, Y. Abe, M. Watanabe, R.L. Smith, Jr., H. Inomata, Replacement of CH4 in the hydrate by use of liquid CO2, Energy Convers. Manag. 46 (2005) 1680–1691.

[66] C.-G. Xu, J. Cai, F. Lin, Z.-Y. Chen, X.-S. Li, Raman analysis on methane production from natural gas hydrate by carbon dioxide–methane replacement, Energy. 79 (2015) 111–116.

[67] Y. Lee, W. Choi, K. Shin, Y. Seo, CH_4-CO_2 replacement occurring in sII natural gas hydrates for CH4 recovery and CO2 sequestration, Energy Convers. Manag. 150 (2017) 356–364.

[68] B. Kvamme, Environmentally Friendly Production of Methane from Natural Gas Hydrate Using Carbon Dioxide, Sustain. 11 (2019).

5 A molecular-scale approach to the multi-step depressurization of methane hydrate

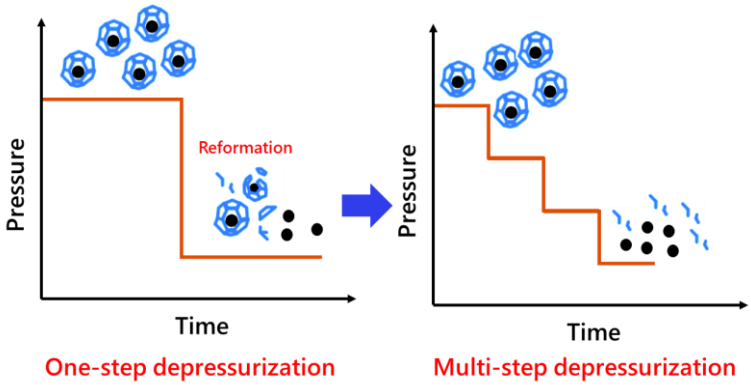

Abstract:

Hydrate reservoirs are regarded as promising contributors to energy storage. In order to understand gas hydrate behavior during exploitation, it is important to study the challenges related to hydrate decomposition. The multi-step depressurization method applied in our previous study displayed enhanced performance for gas production. While the mechanism behind this process is still not understood, here, by using a molecular dynamics (MD) simulation, we successfully introduce a multi-step depressurization method and compare it with a model of the hydrate decomposition process induced by a single-step reduction in pressure.

In this work, we focus on theoretical modeling and molecular simulations applied to gas hydrate dissociation in one- and multi-step depressurization in order to understand the role of stepwise decreasing pressure during this process. We also discuss the order parameters of water used to characterize the state of water in different systems, which reveal the important role of temperature during hydrate dissociation. We also examine the potential

energy landscapes during hydrate decomposition. These molecular insights provide a new understanding of the hydrate decomposition process via stepwise depressurization.

5.1 Introduction

Natural gas hydrate (NGH) is an inclusion compound in which hydrogen-bonded water molecules engage with guest molecules such as methane (CH_4), nitrogen (N_2), hydrogen (H_2), and carbon dioxide (CO_2) [1,2]. Depending on the properties of the guest molecule, there are several possible structures, but the most common structure found in nature is structure I, with six $5^{12}6^2$ cages and two 5^{12} cages. In addition, structure II, with eight $5^{12}6^4$ cages and 16 cages of 5^{12}, also exists [3]. Since NGH contains tremendous energy reserves, its exploitation has been extensively explored [4]. However, the challenges of high-efficiency exploitation have yet to be fully overcome [5-7].

There are three basic techniques are employed to extract methane gas from a gas hydrate reservoir, including depressurization, thermal stimulation, and chemical/gas injection. The most well-known and economically sound method is depressurization, which reduces the reservoir pressure below the range at which the natural gas hydrate is stable [8–10]. During the depressurization process, ice formation, hydrate reformation and insufficient decomposition driving forces during the later stages of depressurization are the main issues [11–13]. Depressurization is currently classed as the most promising method, but only if economic and efficiency issues can be thoroughly resolved. As a result, modifying depressurization, or combining it with another exploitation method, is an emerging research area [14–21].

Researchers have proposed a few modifications to experimental depressurization techniques. Wang et al. [22], for instance, have proposed a novel cycling pressure-deduction technique, which resulted in a much higher effective production rate. Sangwai et al. [23] have investigated the effect of the gas release rate on hydrate dissociation via depressurization, and the results showed that rapid gas release could assist hydrate dissociation. Stephen et al. [24] have discussed a long-term and stepwise degassing process and found that production performance is improved. By conducting depressurization in a multi-step manner, Zhao et al. [25] have determined that moderate heat plays an important role in hydrate dissociation. Ice generation and hydrate reformation are the two major challenges for methane hydrate recovery related to the memory effect during hydrate decomposition. Hydrate reformation mainly caused by an insufficient heat supply and is a common occurrence at the interface between the hydrate and the gas [6,26-

28]. One of the most important parameters influencing production is the initial temperature of the reservoir. In terms of production, the higher the temperature is, the better the production [29].

Despite these findings, most depressurization investigations have been carried out in the laboratory, and very few microscopic-scale studies of gas production behaviors during depressurization have been conducted. Over the past two or three decades, molecular dynamics (MD) simulation has been demonstrated to be a powerful tool in providing an understanding of microscopic mechanisms at a molecular level [28,30,31]. Compared with experimental methods, MD models can correctly initialize cage occupancies and the starting configuration. These models contain instructions for how the structural and dynamical properties of the hydrate change at a molecular level [31-35]. Formation and dissociation processes in hydrates, based on molecular simulations, have been studied during the past several years, and hydrate decomposition is commonly regarded as a two-step process. The first step relates primarily to the behavior of the water molecules. During decomposition, the hydrate lattice consists of water molecules distorted into broken cages, leaving incomplete 4-, 5-, 6-, and 7-membered rings [36]. The second stage involves the escape mechanism of the methane molecules from these broken cages and their subsequent aggregation. The dissociation process for methane hydrate has been modeled by Yan et al., who proposed a “vacuum removal method” to simulate depressurization. The results showed that hydrate decomposition is promoted by depressurization.

In our previous experimental study [38], we examined whether a multi-step depressurization would improve performance in terms of hydrate production; however, the mechanism was not well explained due to the complexity and difficulty involved in performing the experiments. This MD approach allows for a more detailed analysis of some aspects of the data. NVT ensemble simulations have the merit of combined temperature and volume control during hydrate dissociation, which neglects the effect of heat transfer. This constraint is a more realistic approach to simulating hydrate production in a deep marine environment, where the temperature is constant. Two different depressurization MD simulation strategies using NVT ensembles were utilized in this study in order to analyze the effects of multiple factors on methane hydrate (MH) dissociation in an aqueous environment. The influence of

temperature on hydrate decomposition was also studied in order to further understand the mechanism underlying hydrate dissociation at the microscopic level.

5.2 Simulation details and procedures

5.2.1 Water and methane interaction potentials

In this simulation, methane and water molecules were represented by the TraPPE UA (means Transferable Potentials for Phase Equilibria United Atom) model and the TIP4P/2005 model, respectively. The TIP4P/2005 (Transferable Intermolecular Potential 4−sit water models model) was selected for water, as it can reliably describe the dynamics and structure of water and ice during hydrate dissociation.

5.2.2 Simulation procedure

For the simulations using hydrates as the host molecules and methane as the guest molecules, the TraPPE-UA model was used for methane gas without hydrogen atoms. The positions of the atoms in the hydrate lattice were obtained from X-ray diffraction data [39]. A structure I hydrate unit with 2×2×2 replication of unit cell was constructed with dimensions of 2.4007×2.4007×2.4007 nm. The structure I (sI) hydrate unit cell belongs to the *Pm3n* cubic space group with a lattice constant of 12.03 Å. Figure 5.1 shows the methane sI hydrate structure, comprising small (5^{12}) and large ($5^{12}6^2$) cages. The resulting hydrate supercell contained 368 water and 64 methane molecules.

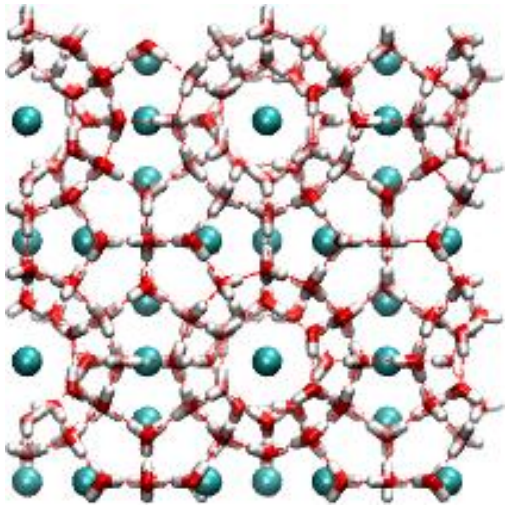

Figure 5.1 Supercell of methane (sI) hydrate structures (2×2×2) consisting of 5^{12} and $6^2 5^{12}$ cages.

To investigate the impact of multi-step depressurization on hydrate decomposition, we modeled the coexistence of sI hydrate and methane in a vacuum. The region of vacuum was positioned in the x-direction, beyond the hydrate layer. The initial configuration can be seen in Figure 5.2. Energy minimization via steepest descent and a short NVT simulation were applied to the methane hydrate model before the NVT-MD simulation was allowed to proceed.

The MD simulation was performed with the NVT ensemble, using GROMACS 2020.0 MD simulations software [38]. The Verlet–leapfrog method was used for Newton's equation of motion with a time step of 2 fs. Periodic boundary conditions were applied in the x-, y- and z-directions. The short-range non-bonded interactions were modeled with the Lennard–Jones (LJ) potential, while long-range electrostatic interactions were calculated by the particle–mesh Ewald (PME) method with a mesh size of 0.12 nm. The system temperature was maintained with a Berendsen thermostat with a coupling time of 1 ps. All simulations were carried out at 265 K with a 3.5 K offset, making the simulation temperature 268.5 K. Three scenarios were selected for study: temperature differences (265–285 K), one-step depressurization, and multi-step depressurization. Production runs at different temperatures were carried out for 50 ns in the NVT-MD simulation.

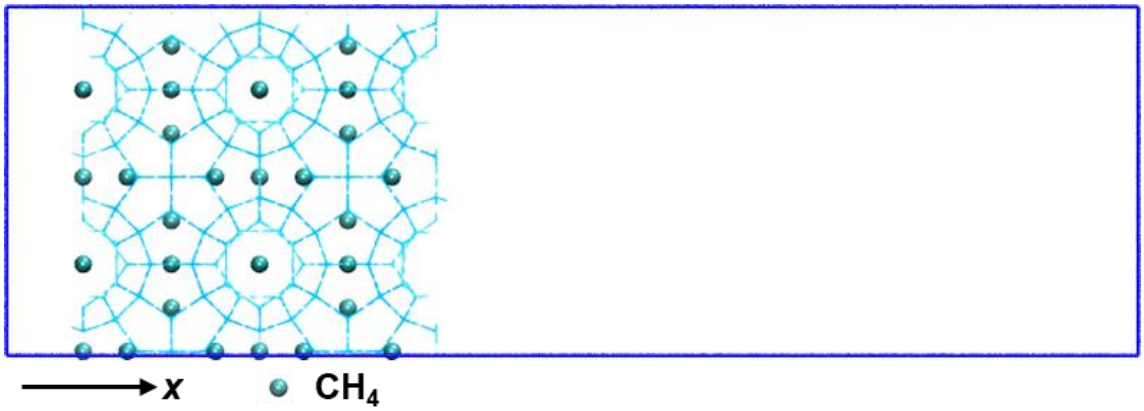

Figure 5.2 Initial configuration of the MH-vacuum simulation. The water molecules of the hydrate are presented in a consistent color with hydrogen bonds in blue; methane hydrate is shown as a cyan sphere.

The vacuum removal methodology, which has been developed by Yan et al. [39], was explained by the decomposition of hydrated via depressurization. We utilized this method and the normal method in our system to perform multi-step depressurization. The system is simulated by multi-step depressurization, which can be summarized as follows. We first simulated 1 ns, and while retaining the vacuum region, the methane molecules entering this vacuum region were removed to reduce the pressure in the system at 1 ns. This 1 ns configuration, with partial removal of methane molecules, was regarded as the initial configuration for the next 1 ns of simulation. The initial configuration of every depressurization step is illustrated in Figure 5.2. The same operation was performed every 1 ns.

To investigate the temperature effect on hydrate decomposition, the simulations were performed continuously for 50 ns. Temperatures above and below the freezing point were set at 265 K and 275 K, respectively.

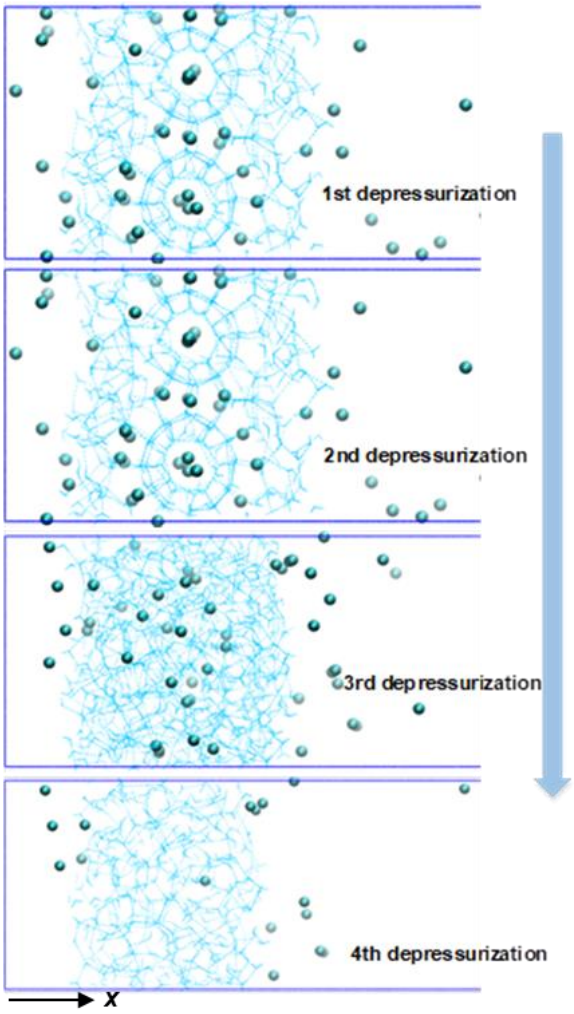

Figure 5.3 Initial configuration of each step in the depressurization process during the MD-NVT simulation. The water molecules of the hydrate are shown in the same color as hydrogen bonds in blue; methane hydrate is shown as a cyan sphere.

5.3 Results and discussion

5.3.1 One-step depressurization process

This section outlines the influence of temperature on the one-step depressurization process. The decomposition of methane hydrate was simulated under constant volume and temperature conditions.

5.3.1.1 Energy and simulation configuration analysis

System configurations after 5 ns of simulation at three initial temperatures are shown in Figure 5.4. The system temperature was constant at the assigned value, and three different temperatures were considered for hydrate decomposition (265 K, 275 K, 285 K). As seen from the configuration, the hydrate decomposed layer by layer, with the layer closest to the low-pressure region dissociating first, followed by the release of methane molecules from the surface with a water layer left behind. Methane molecules from the interior are transferred through the residual water and decomposed from the hydrate into the region of vacuum. Decomposition occurred to a greater extent in simulations at higher system temperatures. However, the released methane gas did not dissolve in the surrounding water due to the pressure gradient from the hydrate to the vacuum region. Methane molecules tended to gather in the low-pressure region.

The hydrate decomposition process proceeds with increasing potential energy, and in the NVT-MD simulations, we observed that the system potential energy elevated when hydrate decomposition occurred. The potential energy profile for the system at temperatures of 265 K, 275 K, and 285 K are plotted in Figure 5.5. The overall trends for the three scenarios are similar: the methane hydrates are not stable, and the potential energy is increased due to hydrate decomposition. When the system temperature increases, clathrate decomposition rates are significantly enhanced.

The potential energy in Figure 5.5 shows that only the simulation at 285 K presents a consecutive decomposition process. The potential energy simulations for 275 K and 265 K display plateaus at 2 ns and 6 ns, respectively.

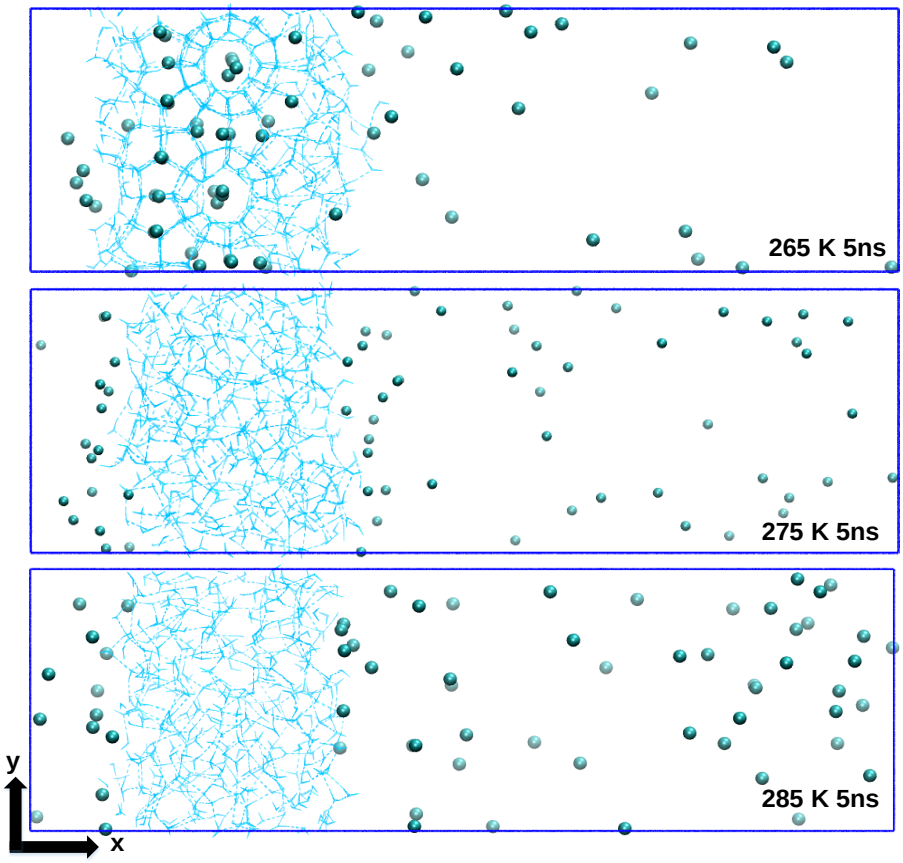

Figure 5.4 Snapshot (following 5 ns of simulation) of the system configuration for different temperatures. The water molecules of the hydrate are shown as the same color as the hydrogen bonds in blue; methane hydrate is shown as a cyan sphere.

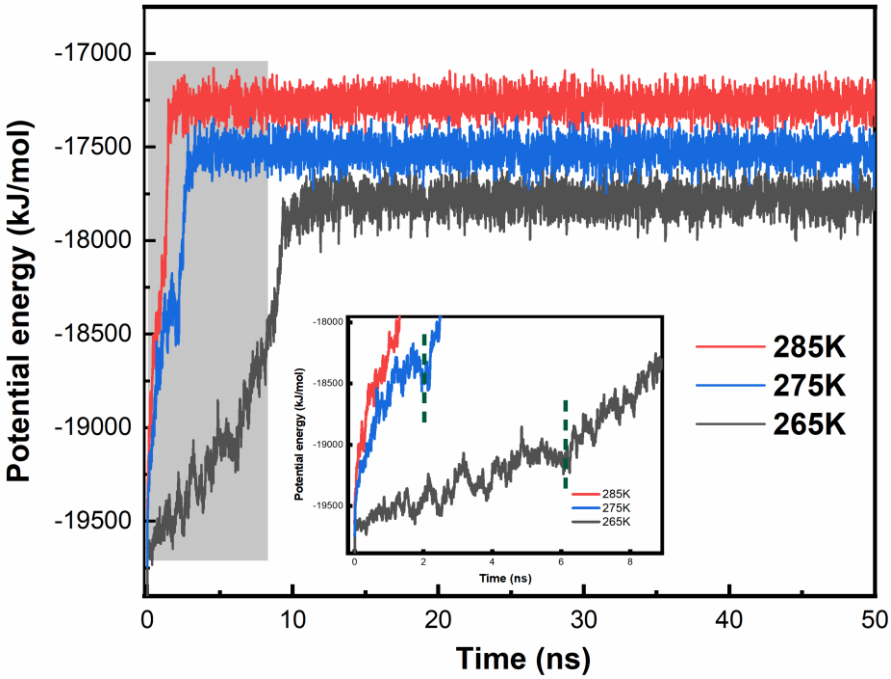

Figure 5.5 Variations in potential energies of the systems with elapsed NVT-MD simulation time.

5.3.1.2 Radial distribution function

In order to focus on interfacial behavior along the vacuum region, a 1.2-nm layer of hydrate along the x-axis was isolated at the interface of the simulation, as shown in Figure 5.6. The quantitative analysis of decomposition below is based on this layer.

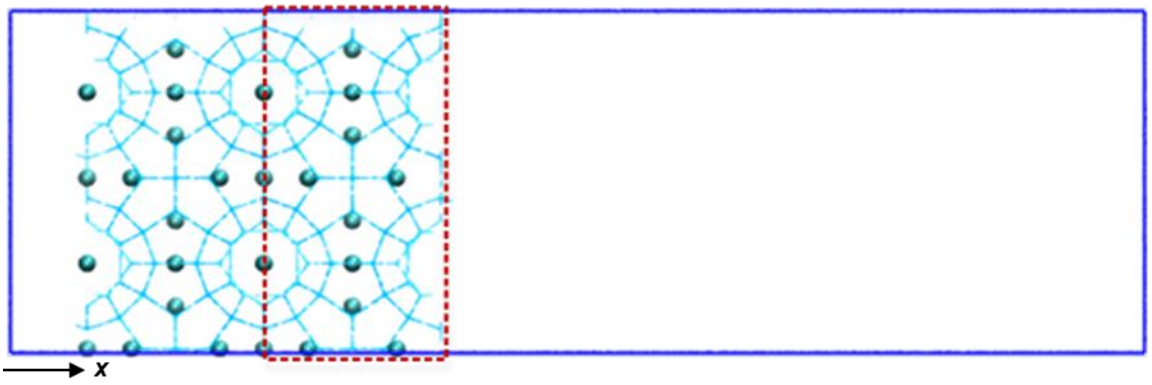

Figure 5.6 The interfacial layer selected for quantitative analysis.

The radial distribution function (RDF) $g(r)$ [40] is a parameter used to characterize the degree order of solid or liquid structures and to describe any variation in density as a function of the distance from a reference particle.

$$g_{\alpha\beta}(r) = \frac{V_s}{N_\alpha N_\beta}\left\{\sum_{i=1}^{N_\alpha}\frac{n_{i\beta(r)}}{4\pi r^2 \Delta r}\right\} \quad (5\text{-}1)$$

where N_α, N_β are the numbers of α and β atoms; r is the distance between them; is the simulation volume; and represents the number of atoms within a radius $r \rightarrow r+$ away from the atom.

In Figure 5.7, we observe the changes in the RDF, $g_{CO}(r)$, of methane hydrate at different time windows in systems with temperatures ranging from 265 K to 285 K. The plots of $g_{CO}(r)$ show that the amplitude of the peaks decreases in line with increasing temperature. Three peaks at r=0.65, 0.8, and 1.0 nm are the characteristic peaks of solid methane hydrate.

Figure 5.8 depicts the RDFs for $g_{OO}(r)$. This is the O-O distance between two hydrogen-bonding water molecules. Within the 1 ns simulation window, the maximal RDF peaks of the O atoms in water molecules appear at r_{oo}=0.278 nm, indicating that the nearest oxygen atoms are separated from each other by a distance of 0.278 nm. The r_{oo}=0.278 nm peaks are in nearly the same location at a simulation time of 50 ns, but this distance decreases with simulation time. Therefore, after hydrate decomposition, the tetrahedral hydrogen-bonding structure of the water molecules does not allow for transformations over time; however, the arrangement of the water molecules is irregular. Within the final 1 ns of the simulation, the other peaks become lower and broader, which indicates that the water molecules entered the liquid phase. The g_{OO} and g_{CO} peaks become lower and broader with increased temperature, which implies that the hydrate becomes less stable.

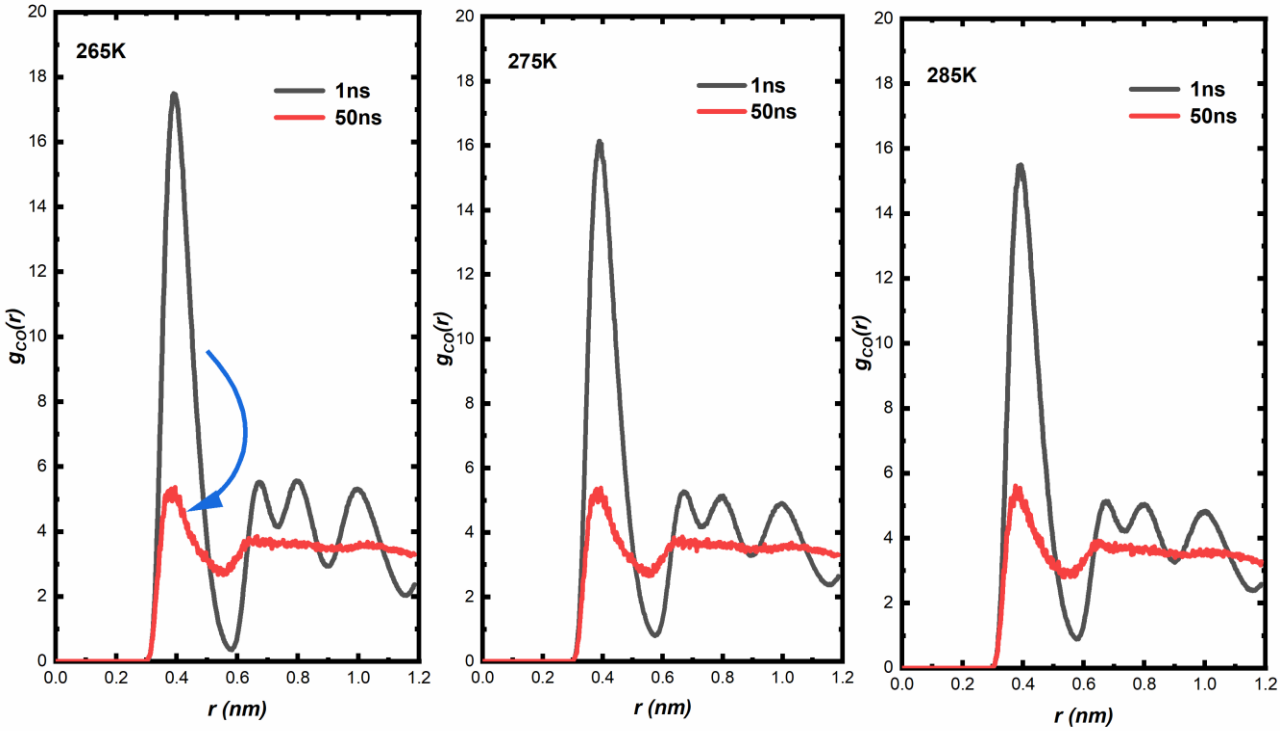

Figure 5.7 Comparison of the radial distribution functions of methane carbon and water oxygen ($g_{CO}(r)$) at different temperatures (265 K, 275 K and 285 K).

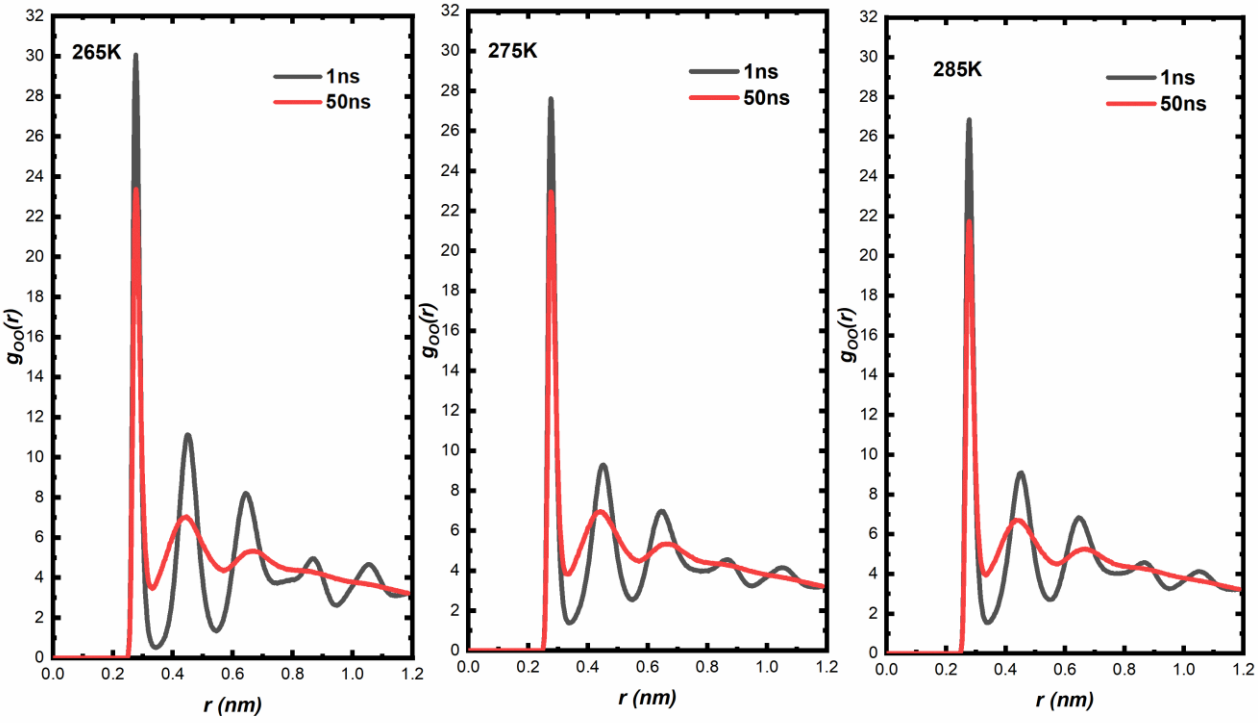

Figure 5.8 Comparison of radial distribution functions of water oxygens ($g_{OO}(r)$) at different temperatures (265 K, 275 K, and 285 K).

5.3.1.3 F_4 order parameter

The behavior of water molecules is important in the first decomposition step, as the local F_4 order can measure the deviation from perfect tetrahedral coordination [41]. During the simulations, F_4 was monitored as a function of time for different temperatures and is plotted in Figure 5.9. For the hydrate phase, the value of F_4 was approximately 0.7, and for amorphous liquid water, it was −0.04; ice could also be detected with values of −0.5 to −0.3 for different structures. The F_4 value for three temperatures was near 0.6 during the initial decomposition stage. A drop in F_4 occurred upon hydrate dissociation. In Figure 5.9, at 275 K and 285 K, the system shows larger decreases in the F_4 order parameter.

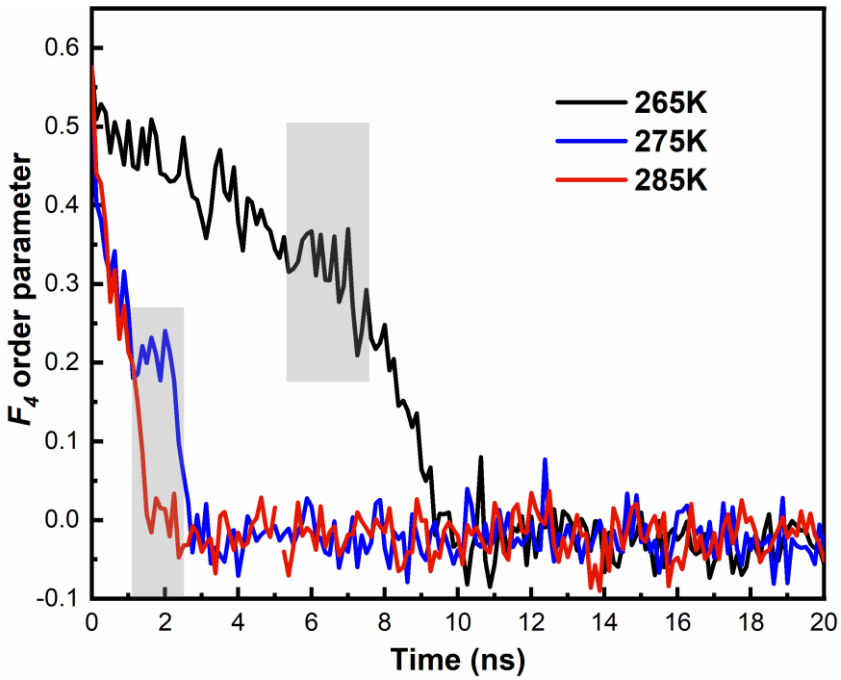

Figure 5.9 F_4 order parameter for the hydrate as a function of time at different temperatures (265K, 275 K and 285 K).

5.3.1.4 Mean square displacement

Mean square displacement (MSD) is employed not only to evaluate the average distance a molecule travels, but also to indicate whether a lattice is stable. Molecular vibrations around a crystal lattice will not result in a stable crystal. The definition of MSD is as follows [42]:

$$MSD = (|\overline{r_i} - \overline{r_{i0}}|^2 = \frac{1}{N}\sum_{i=1}^{N}(|\overline{R_i}(t) - \overline{R_i}(t_0)|^2) \quad (5\text{-}2)$$

where $\overline{R_i}(t)$ is the position of atoms at t, $\overline{R_i}(t_0)$ is the initial position of the particle, and N is the total number of particles.

In this study, we obtained the MSDs within the interface layer at temperatures ranging from 265 K to 285 K. MSDs thus reflect the movement and behavior of water molecules under different temperature conditions.

Figure 5.10 shows the MSDs of H_2O molecules at different temperatures after a 50-ns NVT-MD simulation. The vibration and rotation of water molecules were initiated upon dissociation. The MSD correspondingly rose from zero, indicating that the hydrate at the interface was still a crystalline solid before decomposition. Water cages broke into several rings as the value of MSD gradually increased. Similarly, the MSDs of H_2O molecules in all temperature scenarios were analyzed, and diffusion was greater when the temperature increased, indicating that an increase in temperature can prompt significant diffusion of water molecules.

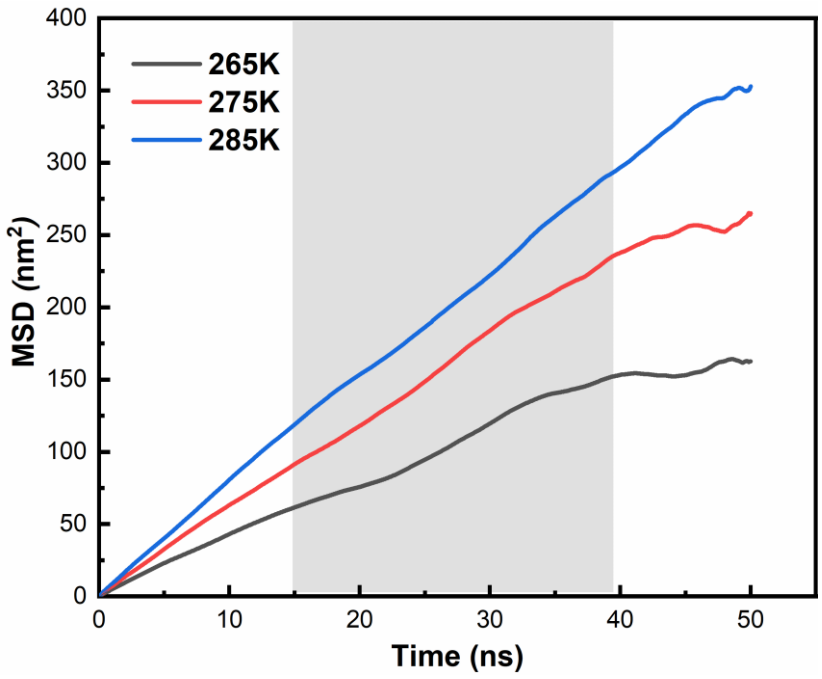

Figure 5.10 MSDs of H_2O molecules in hydrates on the interface layer at temperatures of 265 K, 275 K and 285 K.

From the MSDs of the H_2O molecules, the diffusive capability of H_2O in hydrate was evaluated by obtaining the diffusion coefficients for all temperature scenarios, as shown in Figure 5.10. The increase in the diffusion coefficient for H_2O molecules provides valuable information on hydrate structure behaviors at elevated temperatures. Diffusivity is calculated with the aid of MSDs, which the following equation expresses:

$$MSD = 6Dt \tag{5-3}$$

where D is the coefficient of diffusion within simulation time t. Figure 5.11 shows that the diffusion coefficient of water molecules increased gradually, in line with temperature, due to the vibration of water molecules in the hydrate cages. The diffusion coefficient increased from 0.603 × 10^{-5} cm^2/s to 1.205 × 10^{-5} cm^2/s when the temperature increased from 265 K to 285 K. The higher diffusion coefficient after decomposition was due to the enhanced freedom of movement and rotation of water molecules. This finding agrees with the trends in the RDFs with respect to increased temperature.

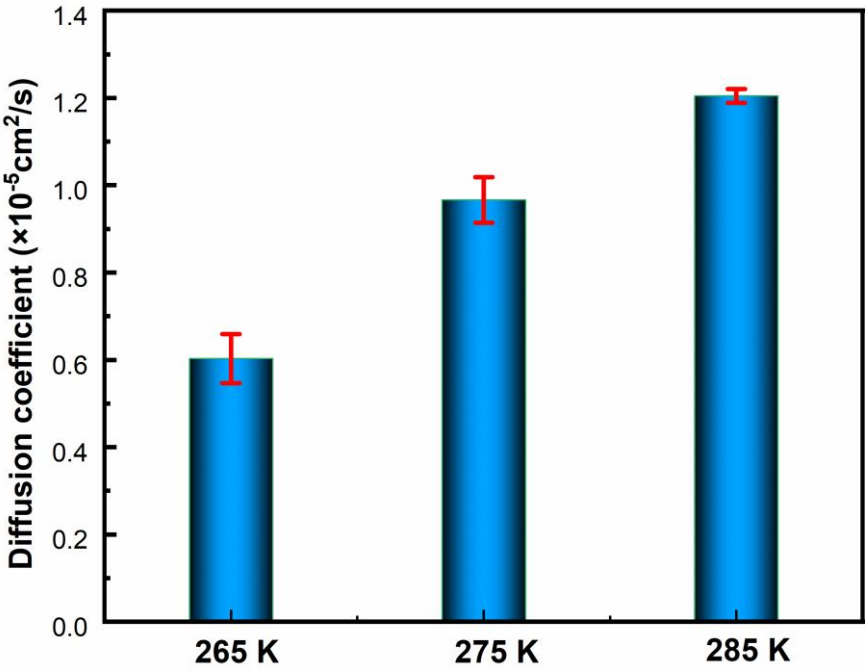

Figure 5.11 Diffusion coefficient of H_2O molecules in hydrates on the interface layer at temperatures of 265 K, 275 K and 285 K.

5.3.2 Multi-step depressurization

The system behavior during hydrate decomposition at 2 ns at a temperature of 275 K and 6 ns at 265 K merits further study. We performed a multi-step depressurization method on the same system at 275 K. The overall process was divided into five periods, and the depressurization operation was conducted four times consecutively. We aimed to understand the enhanced performance of the multi-step depressurization operation [38] from our previous study, albeit from a microscopic perspective.

5.3.2.1 Simulation configuration and energy analysis

The entire multi-step depressurization process was simulated for 5 ns, with each period lasting 1 ns. We performed the first depressurization after 1 ns elapsed. The updated configuration was then regarded as the initial configuration for the start of the second depressurization. All subsequent depressurizations were done in the same manner. In this example, the potential energy of the system, as well as snapshots corresponding to 3 ns, provided a graphical depiction of hydrate decomposition as simulation time progressed.

An obvious alteration in the hydrate decomposition configuration was detected at 3 ns, shown in Figure 5.12. Figure 5.12 (a) shows the final snapshot of the 3 ns one-step simulation, while Figure 5.12 (b) depicts the corresponding multi-step depressurization. Methane molecules that escaped from the hydrate cage under multi-step depressurization exhibited a different behavior than one-step depressurization. Specifically, the methane molecules have a stronger tendency to form clusters in the water phase after hydrate decomposition. As a consequence, the system is more unstable due to the aggregation of the methane molecules.

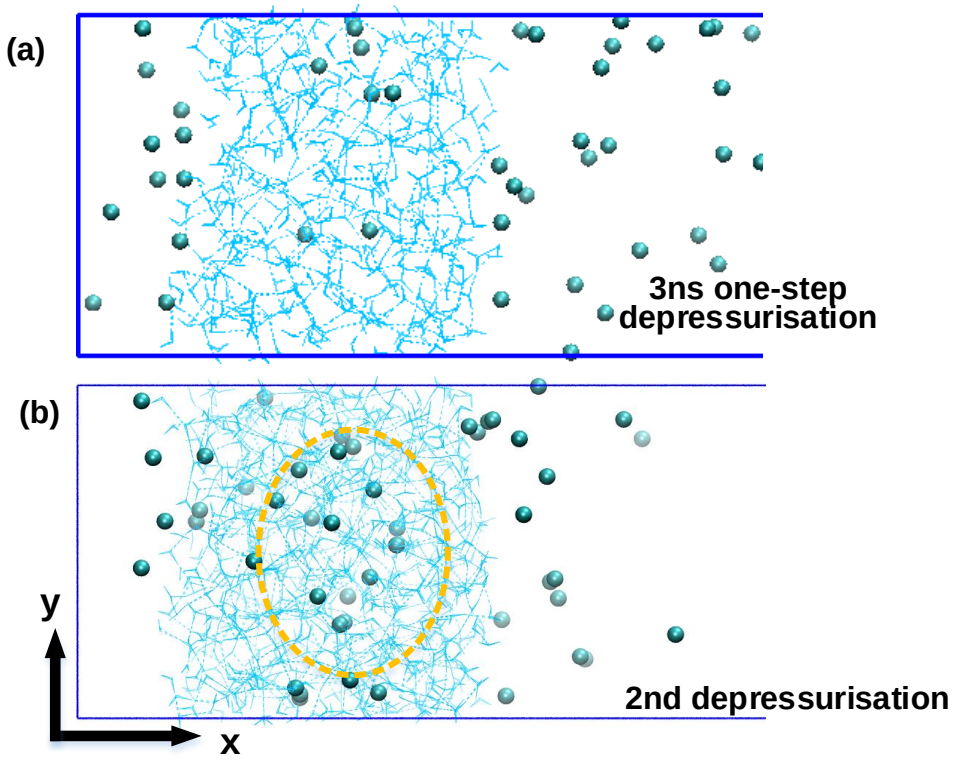

Figure 5.12 Snapshot of (a) the final 3 ns configuration for one-step depressurization and (b) the final configuration for the second depressurization.

The potential energy of the system confirms the unstable state caused by multi-step depressurization, as illustrated in Figure 5.13. A discrepancy in the potential energy exists between 2000 ps and 3000 ps. When a multi-step depressurization is performed, additional energy compensates for the slight plateau in the simulation, which can destabilize the instantaneous stable state. The high dissolution of methane molecules in the water phase can increase the potential energy of the system.

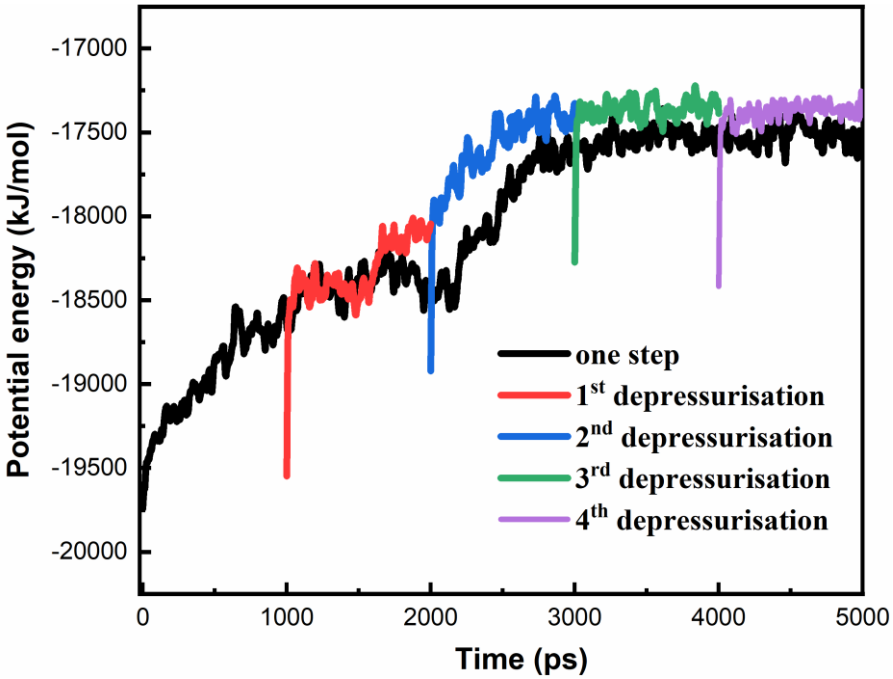

Figure 5.13 Variations in the potential energy of the bulk system of the one-step and multi-step depressurization methods as a function of NVT-MD simulation time.

5.3.2.2 Radial distribution function

To further investigate the decomposition of the hydrate, RDF profiles of the oxygen atoms of the water molecules were calculated. The $g_{oo}(r)$ function shown in Figure 5.14 is defined with respect to the oxygen-oxygen distance between two water molecules. The $g_{oo}(r)$ is the most informative since it allows a comparison with known pair occurrences, which determine the RDF of oxygen in the water and the clathrate hydrate. Figure 5.14 compares these RDFs for one- and multi-step depressurization. This function represents the effect of the multi-step method on water molecules. As expected, a lower peak height is observed from the multi-step simulation within the final nanosecond. According to the MD simulation for hydrate structure I, the O-O distances are around 0.28 nm, the O-H lengths are around 1.82 nm, and the H-H distances are around 0.23 nm [42].

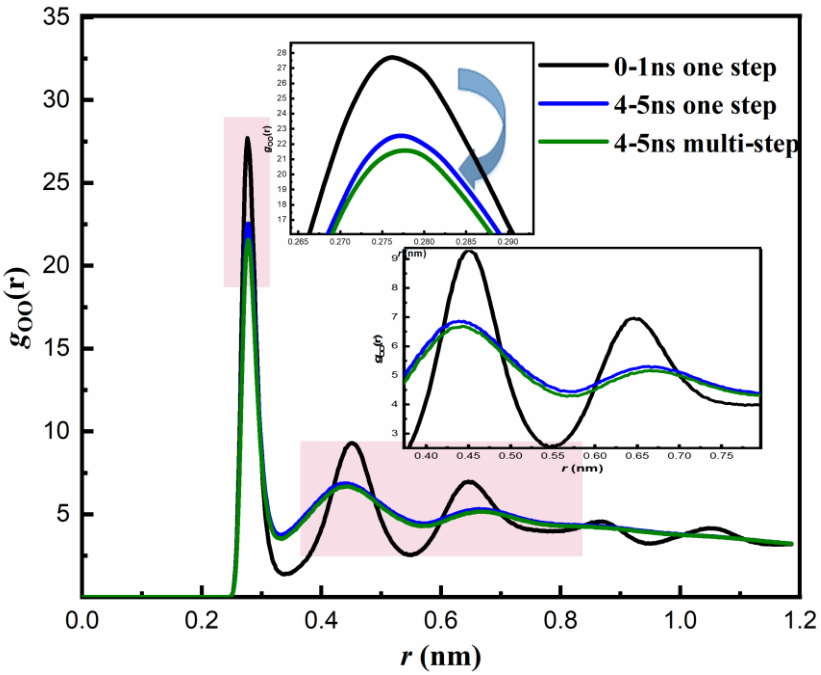

Figure 5.14 Comparisons of O-O RDF of water molecules at different time windows.

5.3.2.3 F_4 order parameter

In Figure 5.15, we compare the F_4 order parameters of the one-step depressurization and the multi-step approach. On examining variations in the F_4 order parameter of water, the system tended to form hydrate under one-step depressurization, indicated by a sudden increase in the order parameter between 2000 and 3000 ns. This increase indicated that hydrate reformation from residual water occurred during this period. However, consecutive decreases in the F_4 order parameter were observed in the multi-step depressurization simulation, illustrating that hydrate decomposition in multi-step depressurization can overcome the reformation of hydrate caused by a sudden drop in pressure. However, no ice was generated during the production period. Taking the results from the system at different temperatures into account, a higher production temperature can avoid the reformation of hydrate crystals.

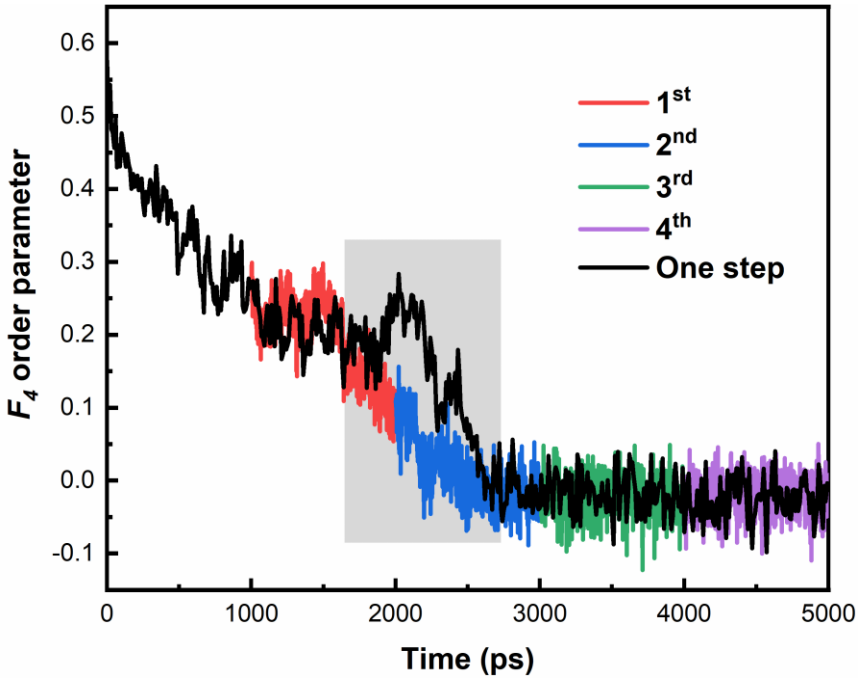

Figure 5.15 F_4 order parameter of the water in one and multi-step depressurization MD simulations.

5.3.2.4 Mean square displacement

In Figure 5.16, the MSDs of the two depressurization methods increased linearly over time due to the altered positions of water molecules in all scenarios. By conducting multi-step depressurization, the stepwise-increasing changes in the MSD of the water molecules are attributed to the vibration of water molecules in the clathrate hydrate structure. The hydrate decomposition induced by step-by-step decreases in pressure can accelerate the molecular rotation and vibration of the water in the hydrate structure, and eventually, these molecules will abandon the clathrate structure altogether.

The coefficient of diffusion is calculated based on MSDs of the different scenarios. The decomposition of gas hydrate can be investigated by calculating the coefficient of diffusion of the water molecules using (3). Figure 5.17 plots the diffusion coefficients of the water in the simulation box for each depressurization period. This diffusion coefficient increases after hydrate decomposition until it equals the diffusion coefficient of gas and liquid water systems, with an order of magnitude of 10^{-9} m^2/s [30].

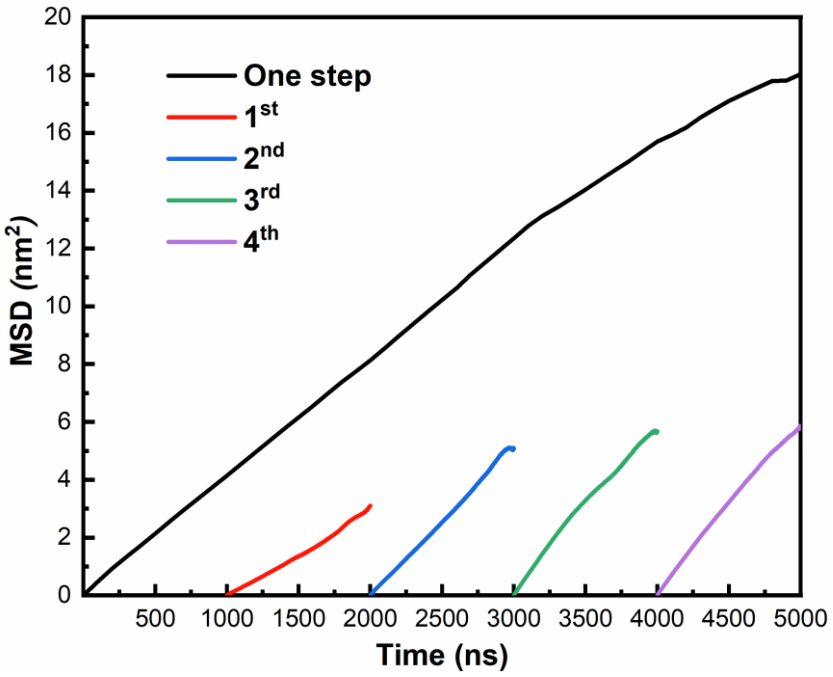

Figure 5.16 Comparison of the mean square displacements (MSDs) of two depressurization methods.

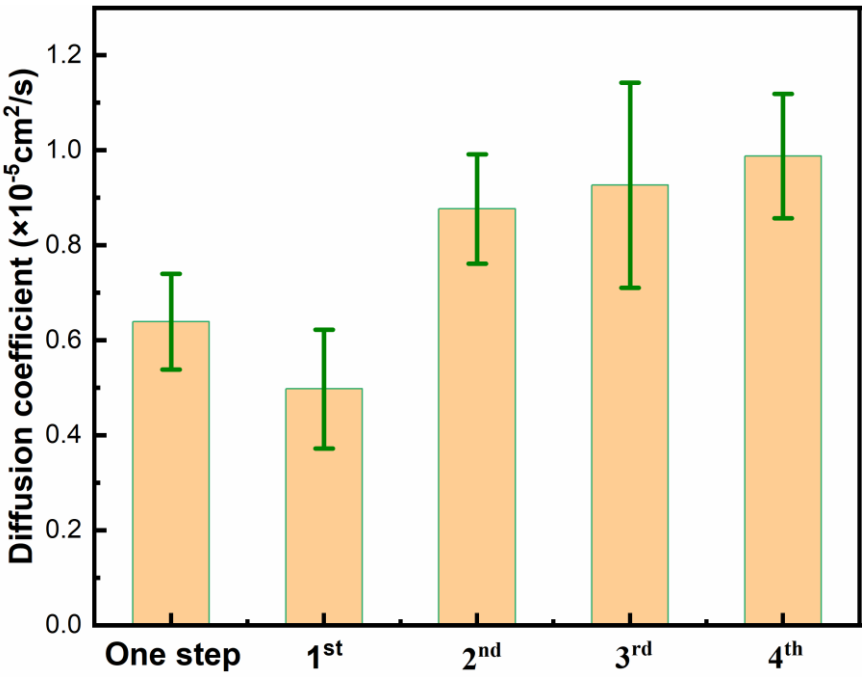

Figure 5.17 Diffusion coefficient of H_2O molecules over different periods.

5.4 Summary

In this simulation work, the structural and dynamic properties of methane hydrate decomposed in vacuum conditions were investigated by conducting MD simulations. All simulations were run under an NVT ensemble. Simulation runs at different temperatures were performed. A multi-step depressurization simulation was introduced by removing released methane molecules at each step to compare it with the single depressurization method. Structural properties, including configuration, potential energy, the RDF, the F_4 order parameter, MSD, and the diffusion coefficient, were utilized to analyze the hydrate decomposition. MSDs and RDFs showed similar behaviors in line with increasing temperature, which can reduce hydrate stability. The diffusion coefficient can also be improved by an increase in temperature.

We studied the decomposition of methane hydrate using two depressurization strategies: one-step depressurization and multi-step depressurization via the stepwise removal of released methane molecules. A sudden decrease in potential energy was observed for the one-step depressurization during simulation times ranging from 1.5 to 3 ns. The F_4 order parameter confirmed that the hydrate tended to regenerate during this period. Multi-step depressurization compensates for energy loss by including the released methane molecules dissolved in the liquid water phase, thus breaking the trend for hydrate reformation during decomposition. We have successfully introduced the concept of multi-step depressurization in an MD simulation, and we investigated the mechanisms behind hydrate production performance improvements on a molecular scale, thereby providing significant implications for hydrate resource exploitation in the field.

f. Acknowledgments

This work is supported by the Department of Chemical and Biochemical Engineering, Technical University of Denmark and the State Scholarship Fund of China Scholarship Council.

g. References

[1] Sloan ED. Fundamental principles and applications of natural gas hydrates. Nature 2003;426:353–9.

[2] SLOAN, D. Clathrate Hydrates of Natural Gases. Bull Geol Soc 1991;41:80–5.

[3] Dendy Sloan E. Clathrate hydrate measurements: microscopic, mesoscopic, and macroscopic. J Chem Thermodyn 2003;35:41–53.

[4] Makogon YF. Natural gas hydrates – A promising source of energy. J Nat Gas Sci Eng 2010;2:49–59.

[5] Zheng J, Wang X, Ma Z, Yang M. Production Behaviors of Water-Saturated Methane Hydrate Deposits during the Depressurization with/without Thermal Water Compensation Process. Energy & Fuels 2020;35:1638–47.

[6] Ripmeester JA, Alavi S. Some current challenges in clathrate hydrate science: Nucleation, decomposition and the memory effect. Curr Opin Solid State Mater Sci 2016;20:344–51.

[7] Max MD. Natural gas hydrate in oceanic and permafrost environments. vol. 5. Springer Science & Business Media; 2003.

[8] Chong ZR, Yin Z, Tan JHC, Linga P. Experimental investigations on energy recovery from water-saturated hydrate bearing sediments via depressurization approach. Appl Energy 2017;204:1513–25.

[9] Rutqvist J, Moridis GJ, Grover T, Collett T. Geomechanical response of permafrost-associated hydrate deposits to depressurization-induced gas production. J Pet Sci Eng 2009;67:1–12.

[10] Zhao J, Zhu Z, Song Y, Liu W, Zhang Y, Wang D. Analyzing the process of gas production for natural gas hydrate using depressurization. Appl Energy 2015;142:125–34.

[11] Jiang X, Li S, Zhang L. Sensitivity analysis of gas production from Class I hydrate reservoir by depressurization. Energy 2012;39:281–5.

[12] Moridis GJ, Kowalsky MB, Pruess K. Depressurization-Induced Gas Production From Class-1 Hydrate Deposits. SPE Reserv Eval Eng 2007.

[13] Bhade P, Phirani J. Gas production from layered methane hydrate reservoirs. Energy 2015;82:686–96.

[14] Li X-S, Yang B, Zhang Y, Li G, Duan L-P, Wang Y, et al. Experimental investigation into gas production from methane hydrate in sediment by depressurization in a novel pilot-scale hydrate simulator. Appl Energy 2012;93:722–32.

[15] Song Y, Cheng C, Zhao J, Zhu Z, Liu W, Yang M, et al. Evaluation of gas production from methane hydrates using depressurization, thermal stimulation and combined methods. Appl Energy 2015;145:265–77.

[16] Zhao J, Zhang L, Chen X, Zhang Y, Liu Y, Song Y. Combined replacement and depressurization methane hydrate recovery method. Energy Explor Exploit 2016;34:129–39.

[17] Falser S, Uchida S, C. Palmer A, Soga K, S. Tan T. Increased Gas Production from Hydrates by Combining Depressurization with Heating of the Wellbore. Energy & Fuels 2012;26:6259–67.

[18] Feng Y, Chen L, Suzuki A, Kogawa T, Okajima J, Komiya A, et al. Enhancement of gas production from methane hydrate reservoirs by the combination of hydraulic fracturing and depressurization method. Energy Convers Manag 2019;184:194–204.

[19] Chen B, Sun H, Li K, Wang D, Yang M. Experimental investigation of natural gas hydrate production characteristics via novel combination modes of depressurization with water flow erosion. Fuel 2019;252:295–303.

[20] Jin Y, Li S, Yang D, Jiang X. Determination of dissociation front and operational optimization for hydrate development by combining depressurization and hot brine stimulation. J Nat Gas Sci Eng 2018;50:215–30.

[21] Minagawa H, Ito T, Kimura S, Kaneko H, Noda S, Tenma N. Depressurization and electrical heating of methane hydrate sediment for gas production: Laboratory-scale experiments. J Nat Gas Sci Eng 2018;50:147–56.

[22] Wang Y, Feng J-C, Li X-S, Zhan L, Li X-Y. Pilot-scale experimental evaluation of gas recovery from methane hydrate using cycling-depressurization scheme. Energy 2018;160:835–44.

[23] Lv T, Li X, Chen Z, Sun D, Zhang Y, Yan K, et al. Experimental Investigation on the Production Behaviors of Methane Hydrate in Sandy Sediments by Different Depressurization Strategies. Energy Technol 2018;6:2501–11.

[24] Phillips SC, Flemings PB, You K, Meyer DW, Dong T. Investigation of in situ salinity and methane hydrate dissociation in coarse-grained sediments by slow, stepwise depressurization. Mar Pet Geol 2019;109:128–44.

[25] Zhao J, Zhu Z, Song Y, Liu W, Zhang Y, Wang D. Analyzing the process of gas production for natural gas hydrate using depressurization. Appl Energy 2015;142:125–34.

[26] Seol Y, Myshakin E. Experimental and Numerical Observations of Hydrate Reformation during Depressurization in a Core-Scale Reactor. Energy & Fuels 2011;25:1099–110.

[27] Kou X, Li X-S, Wang Y, Zhang Y, Chen Z-Y. Distribution and reformation characteristics of gas hydrate during hydrate dissociation by thermal stimulation and depressurization methods. Appl Energy 2020;277:115575.

[28] Myshakin EM, Jiang H, Warzinski RP, Jordan KD. Molecular dynamics simulations of methane hydrate decomposition. J Phys Chem A 2009;113:1913–21.

[29] Song Y, Kuang Y, Fan Z, Zhao Y, Zhao J. Influence of core scale permeability on gas production from methane hydrate by thermal stimulation. Int J Heat Mass Transf 2018;121:207–14.

[30] Kondori J, Zendehboudi S, James L. New insights into methane hydrate dissociation : Utilization of molecular dynamics strategy. Fuel 2019;249:264–76.

[31] Wang L, Jiang G, Zhang X. Modeling and molecular simulation of natural gas hydrate stabilizers. Eur J Remote Sens 2020:1–12.

[32] Liang S, Kusalik PG. Explorations of gas hydrate crystal growth by molecular simulations. Chem Phys Lett 2010;494:123–33.

[33] Kvenvolden KA. Gas hydrate and humans. Ann N Y Acad Sci 2000;912:17–22.

[34] Bi Y, Porras A, Li T. Free energy landscape and molecular pathways of gas hydrate nucleation. J Chem Phys 2016;145:211909.

[35] Kondori J, Zendehboudi S, James L. New insights into methane hydrate dissociation: Utilization of molecular dynamics strategy. Fuel 2019;249:264–76.

[36] Li L, Zhong J, Yan Y, Zhang J, Xu J, Francisco JS, et al. Unraveling nucleation pathway in methane clathrate formation. Proc Natl Acad Sci 2020;117:24701–8.

[37] Yan K, Li X, Chen Z, Li B, Xu C. Molecular dynamics simulation of methane hydrate dissociation by depressurisation. Mol Simul 2013;39:251–60.

[38] Shi M, Woodley J, von Solms N. An Experimental Study on Improved Production Performance by Depressurization Combined with CO2-Enriched Air Injection. Energy & Fuels n.d.;34:7329–39. h

[39] T. Kirchner M, Boese R, Edward Billups W, R. Norman L. Gas Hydrate Single-Crystal Structure Analyses. J Am Chem Soc 2004;126:9407–12.

[40] Kutzner C, Páll S, Fechner M, Esztermann A, de Groot BL, Grubmüller H. More bang for your buck: Improved use of GPU nodes for GROMACS 2018. J Comput Chem 2019;40:2418–31.

[41] Hansen J-P, McDonald IR. Theory of simple liquids. Elsevier; 1990.

[42] Allen MP, Tildesley DJ. Computer simulation of liquids. Oxford university press; 2017.

[43] Zhang Z, Guo GJ. The effects of ice on methane hydrate nucleation: A microcanonical molecular dynamics study. Phys Chem Chem Phys 2017;19:19496–505.

6 Concluding remarks and future work

6.1 Summary of conclusions

Chapter 2 provides an overview of the NGH investigation from fundamental theory to applications and related mechanisms. Two primary NGH production technologies were described and compared. Laboratory research exploring the mechanisms of different technologies was reviewed. In addition, studies on methane hydrate recovery kinetics from different aspects were described.

Chapter 3 presents the experimental results on the production behavior of hydrate spheres below the freezing point of ice. Three groups of hydrate samples with synthesized spherical methane hydrates in different sizes, varying from 11 to 22 mm, were employed by depressurization from 1.6 MPa to 2.4 MPa. From this work, the following conclusions can be drawn:

- The gas production process can be divided into three main periods: The first period is the excess gas release process. As a result of depressurization, excess gas is released initially, while gas production increases sharply until it reaches a maximum, which is influenced by the area-to-mass ratio of spherical hydrates. Then CH_4 is released from the hydrate during the second period and, once the pressure falls to equilibrium, the hydrate decomposition is initiated with the production rate fluctuating for short time followed by a decrease. The third period is a slow hydrate production process, and gas production changes almost imperceptibly during this period. The curve of the cumulative gas production and production percentages tends to flatten for a long period.

- The driving force of pressure differences and gas diffusion jointly govern the decomposition reaction. The extent of influence is consistent, depending on production pressure and pellet size. At a low pressure of 1.6 MPa, production rates are 0.83 SCC/min and 4.93 SCC/min for GMD are 11mm and 22mm, respectively. Fast production implies that the driving force of pressure difference control prevails initially, whereas with gas under pressure of 2.4 MPa, diffusion with ice coverage according to pellet size becomes more dominant.
- The experimental results indicate that hydrate decomposition is time dominant, and initial ice nucleation and conglomeration play an important role in the initial hydrate decomposition rate. An inhomogeneous ice rind along with a gas layer exists between the solid hydrate surface and vapor phase. This sandwiched structure should be taken into account when simulating the production of gas hydrate below freezing point.

Chapter 4 presents an experimental study on gas recovery and CO_2 storage behavior with a novel method that combinates depressurization and air/CO_2-enriched air replacement. Based on the experimental observations, a novel multilayer hydrate cap mechanism and an improved recovery method for gas from hydrate layers were proposed. The main conclusions from this investigation are:

- Under operating conditions of 8.5 MPa, 10.2 MPa, 18.7 MPa, the improvement in CO_2 storage performance is not as marked as that of CH_4 recovery.
- The chapter proposed gas production behavior via depressurization with CO_2-enriched air behavior for the first time, which explained the behavior well during the production process. The multilayer hydrate cap and its composition largely depend on the initial condition of injected gas, thereby causing limited recovery efficiency.
- The introduction of three stages of depressurization can prolong this production process and, most importantly, enhance the recovery ratio via attenuating the multilayer cap. For air injection, 51.7% CH_4 was recovered from 23.2% under a pressure of 18.7 MPa. A maximum of 74.4% recovery of CH_4 was achieved when 20 mol % CO_2 is added to the air. The results obtained from this study provide important insights into optimizing operating conditions to maximize efficiency and prolong the

production period for field hydrate production. A good balance with CO_2 storage was also evaluated.

- A novel multilayer hydrate cap attenuation mechanism was proposed for gas production behavior via depressurization with CO2-enriched air.

Chapter 5 summarizes the results of an MD investigation into methane decomposition under one-step and multi-step depressurization. The influence of temperature was additionally examined from 265 K to 285 K. In the analysis of decomposition quantities, structural properties, including configuration, potential energy, the radial distribution function (RDF), the F_4 order parameter, mean square displacement (MSD), and the diffusion coefficient were utilized. The main conclusions from this study are:

- MSDs and RDFs showed similar behaviors in line with increasing temperature from 265 K to 285 K, which can reduce hydrate stability. The diffusion coefficient was improved from 0.603×10^{-5} cm^2/s to 1.205×10^{-5} cm^2/s by an increase in temperature from 265 K to 285 K.

The F_4 order parameter confirmed the tendency for the regeneration of hydrates during depressurization. Multi-step depressurization compensates for energy loss simulation ranging from 1.5 ns to 3 ns by including the released methane molecules dissolved in the liquid water phase, thus breaking the trend for hydrate reformation during decomposition.

6.2 Suggestions for future work

The results in this work provide an improved understanding of the methane hydrate production driven by depressurization, CO_2 replacement, and its combined performance. However, additional work could be performed in this field to further improve the understanding mechanism and thereby aid in CH_4 production and CO_2 emission control. A few suggestions are described below.

Additional experiments with local gas composition measurement

Current understanding of gas exchange through different cages during gas replacement of natural gas hydrates at phase interface is still not widely get an agreement, and it needs more attention as an important control mechanism of CH_4 sequestration of CO_2 by replacement. Natural gas hydrate decomposition and gas exchange process interface and hole gas exchange interaction still exist great discrepancy in the world, which need to get more and deeper understand.

Influence of confined space for hydrate decomposition and replacement

The formation of hydrate near the solid-liquid-gas interface shows different characteristics from the previous liquid-water/gas interface, and the porous media surface also has a significant effect on the latticing of hydrogen bonds and the establishment of cage structures. The porous mesoporous surface which represent sediments also has a significant influence on the lattice of hydrogen bonds and the cage structure. This part can be studied by molecular dynamics simulations and quantum chemistry to investigate, that can be compared with experiments with the support of microscopic experiments such as Raman and nuclear magnetic resonance.

Publications

Shi, Meng, John M. Woodley, and Nicolas von Solms. “Macroscopic study on the production of hydrate spheres below the freezing point of ice energy:” *The Journal of Physical Chemistry B,* 2021, In preparation.

Shi, Meng, John M. Woodley, and Nicolas von Solms. “A molecular-scale approach to the multi-step depressurization of methane hydrate”, *Energy conversion and management*, 2021, In preparation.

Shi, Meng, John M. Woodley, and Nicolas von Solms. “An Experimental Study on Improved Production Performance by Depressurization Combined with CO_2-Enriched Air Injection.” *Energy & Fuels* 34.6 (2020): 7329-7339.

Shi, Meng, Xuemei Lang, Yanhong Wang, Nicolas von Solms, and Shuanshi Fan. “Investigation of the Growth Kinetics of Tetra-n-butylammonium Bromide Hydrate Formation in Small Spaces.” *Energy & Fuels* 33, no. 4 (2019): 3473-3482.